Argonne National Laboratory

REACTOR DEVELOPMENT PROGRAM

PROGRESS REPORT

March 1967

The facilities of Argonne National Laboratory are owned by the United States Government. Under the terms of a contract (W-31-109-Eng-38) between the U. S. Atomic Energy Commission, Argonne Universities Association and The University of Chicago, the University employs the staff and operates the Laboratory in accordance with policies and programs formulated, approved and reviewed by the Association.

MEMBERS OF ARGONNE UNIVERSITIES ASSOCIATION

The University of Arizona
Carnegie Institute of Technology
Case Institute of Technology
The University of Chicago
University of Cincinnati
Illinois Institute of Technology
University of Illinois
Indiana University
Iowa State University
The University of Iowa
Kansas State University
The University of Kansas
Loyola University
Marquette University
Michigan State University
The University of Michigan
University of Minnesota
University of Missouri
Northwestern University
University of Notre Dame
The Ohio State University
Purdue University
Saint Louis University
Washington University
Wayne State University
The University of Wisconsin

Printed in the United States of America
Available from
Clearinghouse for Federal Scientific and Technical Information
National Bureau of Standards, U. S. Department of Commerce
Springfield, Virginia 22151
Price: Printed Copy $3.00; Microfiche $0.65

ANL-7317
Reactor Technology
(TID-4500)
AEC Research and
Development Report

ARGONNE NATIONAL LABORATORY
9700 South Cass Avenue
Argonne, Illinois 60439

REACTOR DEVELOPMENT PROGRAM PROGRESS REPORT

March 1967

Albert V. Crewe, Laboratory Director
Stephen Lawroski, Associate Laboratory Director

Division	Director
Chemical Engineering	R. C. Vogel
Idaho	M. Novick
Metallurgy	M. V. Nevitt
Reactor Engineering	L. J. Koch
Reactor Physics	R. Avery
Remote Control	D. P. Mingesz (Acting)

Report coordinated by
R. M. Adams and A. Glassner

Issued April 28, 1967

FOREWORD

The Reactor Development Program Progress Report, issued monthly, is intended to be a means of reporting those items of significant technical progress which have occurred in both the specific reactor projects and the general engineering research and development programs. The report is organized in a way which, it is hoped, gives the clearest, most logical overall view of progress. The budget classification is followed only in broad outline, and no attempt is made to report separately on each sub-activity number. Further, since the intent is to report only items of significant progress, not all activities are reported each month. In order to issue this report as soon as possible after the end of the month editorial work must necessarily be limited. Also, since this is an informal progress report, the results and data presented should be understood to be preliminary and subject to change unless otherwise stated.

The issuance of these reports is not intended to constitute publication in any sense of the word. Final results either will be submitted for publication in regular professional journals or will be published in the form of ANL topical reports.

The last six reports issued in this series are:

September 1966	ANL-7255
October 1966	ANL-7267
November 1966	ANL-7279
December 1966	ANL-7286
January 1967	ANL-7302
February 1967	ANL-7308

REACTOR DEVELOPMENT PROGRAM

Highlights of Project Activities for March 1967

EBWR Plutonium Recycle Program

The EBWR has been operated at the maximum permissible power level of 70 MW. During the approach to power, pile-oscillator measurements of the reactor transfer function were made at 28, 38, 49 and 57 MW.

EBR-II

In preparation for Run No. 25, several zero-power reactor runs were made to obtain measurements of reactivity worth of the stainless steel subassemblies in Rows 7 and 8, which have replaced subassemblies of depleted uranium.

An extensive program of analysis has been initiated to determine the sources and extent of copper found in the reactor primary sodium system this month. The presence of copper was first revealed when normal flow was restricted in the primary plugging-meter loop, resulting in removal of the plugging and throttle valves in this system. Removal of the copper electrodes associated with the auxiliary primary pump confirmed that the exposed copper ends were severely pitted and eroded and had indeed lost copper to the primary sodium. The exposed copper ends of the electrodes have been sheathed in stainless steel and the electrodes have been reinstalled. The pump has been checked out and is operating satisfactorily. Analysis for further sources of copper in the primary system is continuing and results are being evaluated. The extended shutdown is being used to advantage for reactor modifications and improvements that had been scheduled for a later date, and for physics studies associated with the substitution of stainless steel for depleted uranium in blanket Rows 7 and 8.

Postirradiation examination of radial-blanket subassemblies from the 7th, 8th, 9th, and 12th rows of the reactor has been completed. As would be expected, length, diametral, and density increases were greatest for the innermost rows, decreasing along the radius away from the core, with no significant increases noted for the 9th or 12th row subassemblies. In addition to maintaining current levels of fuel production, a large effort is being devoted to design work on a cold fabrication line to increase fuel production by the end of FY 1967.

ZPPR

The construction contractor has enlarged his working force in an attempt to get back on schedule in the reactor cell area. Concrete for the

reactor cell floor and pit and for the blanket storage room floor has been poured. A procedure was approved for storing the bed and tables on-site. The long and short sections of the bed and two tables have been placed on a storage support structure in the reactor pit and a 2-in.-thick weatherproofed wooden roof was placed over the units. Side protection will be placed after a wooden impact shield is formed over each unit.

ZPR-3

Experiments are in progress with Assembly 48B, a reactor with a two-zoned plutonium core and with a 12 x 15-in. central region that contains plutonium with 22% Pu^{240} substituted for 4.5% Pu^{240}. Critical mass was determined after control-rod calibrations were made as well as measurements of the worth of core-edge material and of fuel spiking of the safety rods. In the high-plutonium-content central region, measurements were made of sodium substitutions, fission ratios, perturbation reactivity measurements with small samples, and of fine flux variations across the cell. U^{235} fission ratios were measured versus U^{233}, U^{234}, U^{236}, U^{238}, Pu^{239}, and Pu^{240}. Reaction rate traverses have been made in a radial direction at the core midplane and reactivity traverses have been made in the radial direction using stainless steel, tantalum, boron 10, U^{235}, Pu^{239}, and U^{238}. Work on an improved proton recoil neutron spectrometer is also reported this month. A report is given on work done to define more narrowly the limits of precision of ZPR-3 experiments by refinement of measurements related to the ZPR-3 gap interface.

AARR

A preliminary report on the geology of the site for AARR is available.

Specifications for the primary heat exchangers and for the control-rod guide assembly have been released for bids.

TABLE OF CONTENTS

TABLE OF CONTENTS

TABLE OF CONTENTS

I. PLUTONIUM UTILIZATION

A. Research and Development

1. Plutonium-fueled EBWR

a. Transfer Functions. During the approach to 70-MW(th) operation, transfer functions were measured at 28, 38, 49, and 57 MW(th). A preliminary comparison of the transfer functions measured at 28 and 38 MW(th) with those measured previously (see Progress Report for November 1966, ANL-7279, p. 1) indicates a stabilizing change has occurred in the resonance region from ~3 to 18 radians/sec. The transfer function measured at 49 and 57 MW(th) indicates the presence of a second resonance region in the frequency range from 0.5 to 0.8 radians/sec. Extrapolations of the transfer-function measurements indicate the reactor would be stable at powers greater than 150 MW(th).

b. 70-MW Operation. The EBWR was shut down in mid-February as scheduled to remove certain fuel pins for isotopic analysis at Pacific Northwest Laboratory. Power operation resumed on March 2.

The reactor operation was interrupted on March 11 through March 14 for the removal of one set of Pu^{239} and Pu^{241} foils from the Plutonium Zone and to install a riser on the vessel steam exhaust duct. The riser is an aid in the reduction of moisture carry-over at high power levels. For 70-MW operation, the steam quality has been measured and found to be 99.6%.

At the month's end, the reactor was operating at 70 MW with essentially zero boric acid and the control rods 1 through 9 banked at 31.5 in. Seventy-megawatt operation is expected to continue through late April. At this time, the reactor will be shut down for the removal of additional fuel pins.

The power generated by the plant is as follows:

	Thermal Power	Electrical Power
During March 1967	27,051.3 MWh	2,822 MWh
Total since start of Plutonium Recycle Program	117,350.9 MWh	12,866 MWh

c. Pressure-vessel Surveillance. In a routine hydrostatic test at 250 psig, water leaked from around one (of the five) instrument nozzles in the flat cover plate. Investigation of the stainless-steel-clad interior surface of the cover plate revealed several cracks in the arc-deposited cladding.

Grinding explorations showed that the surface cracks extended through the cladding to the interface with the A105-II carbon-steel forged cover plate, but not into the carbon steel itself. Dye-penetrant examination of the seal-welds and cladding areas around the other four nozzles revealed minor cracks around three of them. Grinding into these three regions showed that the cracks were shallow, with a maximum depth of 1/16 in. It was concluded that the cracks had started at the surface of the cladding.

Because the leaking flange connection was not needed during the scheduled EBWR program, it was replaced with a solid threaded rod of Type 304 stainless steel machined to the same dimensions as the nozzle. The rod was screwed into the threaded hole and seal-welded to the carbon-steel cover plate with Type 309 stainless steel welding electrodes. The bare steel plate was then reclad with a 2-pass weld using a Type 309 stainless steel electrode for the first pass and Type 308L stainless steel electrode for the finish pass. Other than a fairing operation, the other three instrument-nozzle crack regions needed no additional conditioning. The entire clad surface of the cover plate was examined with dye penetrant; no other evidence of cladding distress was found.

This was the second time that the cladding around the leaking connection had cracked. The first time that the cover-plate cladding was discovered to have cracked was during the 1965 examination of the EBWR vessel and primary piping. At that time, the cracking was ascribed to the use of Type 310 stainless steel electrodes to sealweld the nozzle to the cladding. But this new discovery of cracking indicates the probable existence of a delayed fracture mechanism associated with localized residual welding stresses.

II. LIQUID-METAL FAST BREEDER REACTORS

A. EBR-II

1. Operations

Several one-hour-long, zero-power reactor runs were made to obtain reactivity worths of the stainless steel subassemblies in Rows 7 and 8 (see Sect. II.A.4.a). Two flux wire irradiations were conducted to obtain fission-rate distribution information related to changes in the blanket loading (see Sect. II.A.4.b).

Substitution of stainless steel for depleted uranium in Row 7 produced an increase of 219 Ih of reactivity. The data for substitution of stainless steel in Row 8 have not yet been fully analyzed. The first 23 changes in the flats of Row 8 produced an increase of approximately 180 Ih, and the final 18 an increase of approximately 50 Ih.

Two control rods that had been period calibrated showed some small changes (see Sect. II.A.4.d). Additional rod calibrations will be performed after the core configuration is fixed for Run No. 25.

Early in this report period, a flow decrease was noted in the primary plugging-meter loop. Operational efforts to restore normal flow were unsuccessful. The loop was removed from service, and the plugging and throttle valves removed for cleaning and inspection. When the valves were cleaned in alcohol it was noted that a thin plating of copper was present on the inner surface of both valves and copper was deposited in the flutes of the plugging valve. The valves were cleaned and reinstalled, and the loop was returned to service. Normal flow could not be re-established, presumably due to the presence of copper. The loop was shut down and removed; the entire system, including the economizer, was removed for further inspection. The secondary-sodium-system plugging meter was removed and installed in the place of the primary unit, since it was known that it was operating satisfactorily. A program of sodium sampling and a system study to determine the possible sources of copper were immediately started (see Sect. II.A.2).

Investigation indicated the most likely sources of copper to be the copper electrodes associated with the auxiliary primary pump. Therefore, the pump was shut down, after lifting the reactor cover to improve thermal convection flow within the reactor, and the electrodes were removed.

Examination revealed severe pitting and erosion of the negative electrode and some pitting of the positive electrode. Measurements made by water displacement indicated that approximately 10 lb of copper was missing from the two electrodes.

The electrodes were repaired and modified by the installation of a stainless steel sleeve over the copper; this sleeve provides a continuous covering over the conductors and electrodes. The bus bars were reinstalled in the primary tank and the auxiliary pump restored to operation. Tests indicated satisfactory operation after the series resistance in the circuit was adjusted to compensate for the addition of the stainless steel sleeve.

Sampling has continued on a three-shift basis to improve the sampling statistics and to observe, if possible, any reduction in copper concentration attributable to cold-trap operation.

A total of 269 individual transfers, either to or from the reactor grid or the storage basket, were made during the month. Row 7 inner blanket subassemblies and Row 8 outer blanket subassemblies were transferred to the Fuel Cycle Facility for disposal. Forty-one stainless steel outer blanket subassemblies were transferred to the storage basket and thence to the reactor grid. Nine special flux wire subassemblies were loaded and unloaded in connection with measurements of fission-rate distribution.

After removal from the primary tank, the Mark-II oscillator rod drive was disassembled for inspection. The sensing-rod bellows was ruptured, as was expected (see Progress Report for February 1967, ANL-7308, p. 2), and sodium oxide was preventing operation of the gripper. No obvious reason for the bellows failure has been found. The Stellite-Colmonoy journal bearings on the drive shaft and the bearing carrier were inspected. The bearing that ran in the argon atmosphere was highly polished and in perfect condition. The two sodium-lubricated bearings were also in good condition, with only slight wear marks evident. The bearing-carrier tube has been cleaned and is ready for reassembly.

The fabrication work done by Idaho Nuclear Corporation on the Mark-III Fuel Unloading Machine (FUM) gripper was completed. The gripper has been received and final assembly work is underway. Design of the prototype manual jaw actuator was completed and fabrication is about to start.

Assembly of the new bulk-sodium-level transmitter is complete except for lead filling. A comprehensive test of the load cell and electronics was done before assembly, and preparations are being made to test the completed assembly in water before installation in the primary tank. Selection of a nozzle in the primary tank for this unit is in progress.

2. Copper in Primary Sodium

In late February and early March, difficulty was experienced in obtaining satisfactory flowrates in the EBR-II primary sodium plugging loop

upstream of the cold trap (designated PI-A) preparatory to making plugging-temperature determinations. The plugging valve and the throttle valve in this loop were removed and disassembled on March 2. After removal of sodium by dissolution in ethanol, copper, identified by qualitative chemical analysis, was found deposited on the stems and within the bodies.

In an effort to restore the primary plugging loop to operability and to permit plugging temperature measurements and the taking of sodium samples for analysis, the valve stems and bodies were cleaned and the valves were reassembled and installed. The loop was put into operation on March 3 and plugging runs were attempted. The apparent plugging temperature was 230°F. However, only a very low flowrate through the loop could be attained during hot operation. Operating behavior of the loop indicated that a flow restriction might exist in the loop economizer (regenerative heat exchanger).

On March 4, a small sodium leak was found at a weld just upstream of the loop throttle valve. The loop was secured and cooled. Work was initiated on this date to remove the entire primary plugging loop, PI-A, and to replace it with the plugging loop from the secondary sodium system. The installation was completed on March 8. This permitted continued measurement of primary plugging temperatures and taking of sodium samples for chemical analyses of copper content.

Concurrently, the valves were removed from PI-B, the plugging loop downstream of the cold trap. These valves were made available for installation, with a newly fabricated economizer, in the secondary system. It was found impossible to remove the PI-B economizer because of severely limited accessibility.

A "dip sampler" was fabricated to permit taking of samples from the bulk primary sodium through the Fuel Transfer Port and the PI-A loop for comparative purposes. Relatively large sodium samples (100 to 300 g each) were taken initially. A series of samples was taken with the cold trap secured, as it had been during the prior work in March.

The primary cold trap was put in service on March 10 and maintained in operation at flowrates, mostly in the range of 15 to 30 gpm for the remainder of the month. Initially, plugging temperatures were about 280 to 300°F. They showed a continuing decrease with cold-trap operation until, during the last half of March, they were consistently less than 250°F.

Sampling from PI-A and the Fuel Transfer Port was continued to discover whether cold-trap operation would reduce the copper concentration in the primary sodium. The variations observed in the analyses for copper in portions of sodium taken from the large samples indicated that nonhomogeneity of copper concentration probably exists in such samples. Since

these variations were of about the same order as the expected real changes of copper concentration in the primary sodium, it was recognized that improved sampling methods were required. To obviate the effects of possible segregation of copper in the cooled sodium sample, smaller samples (10 to 15 g) were taken and the entire sample was analyzed.

Initial plans called for the use of nickel sample cups because it was expected that the copper content of the nickel would be low. However, because only a few nickel cups were available and material for fabrication of more could not be obtained readily, sample cups were fabricated of Type 304 stainless steel.

Subsequent chemical analyses for copper content of material in nickel and stainless steel cups indicated that the nickel contained 109 ppm of copper, and the stainless steel 200 to 600 ppm. Tests demonstrated that the nickel readily yields copper to the nitric acid solution used for dissolution of copper in the sodium samples. Stainless steel cups yielded no copper under the same conditions. Hence, stainless steel cups were used for sampling. Some information was obtained to the effect that higher copper concentrations might be found in sodium samples taken in stainless steel than in samples taken in Pyrex glass. Thereafter, Pyrex beakers were used for sampling from the bulk sodium (Fuel Transfer Port). However, because glass beakers could not be used in the sodium sampling system, use of stainless steel cups for the PI-A samples was continued.

Chemical analyses for copper were performed in the Idaho Division Chemistry Laboratory during the first half of the month by the neo-cuproin colorimetric method. Samples taken on, and after, March 15 were analyzed in the chemistry laboratory of the Idaho Chemical Processing Plant (ICPP), by the same colorimetric method. Occasional check analyses were performed in the Idaho Division Laboratory.

Starting on March 20, a very intensive sampling program was conducted to check analytical precision and to define better the copper concentration in the primary sodium. Initially, the primary coolant pumps were operated only intermittently, between fuel-handling periods. Starting on March 26, the pumps were maintained in operation at full reactor flow-rate to provide maximum mixing of the primary sodium. Full flow was continued for the remainder of the month.

The throttle valve and the plugging valve were removed from the PI-A loop on March 28 to permit inspection for copper deposition. The valves had been in service since March 8. The valves were disassembled and sodium was dissolved from the stems and bodies by ethanol. There was no visual evidence of copper deposition on the valve surfaces. The PI-A loop was then returned to service.

A sampling valve was installed at the PI-B location downstream of the primary cold trap, to permit sampling and analysis for copper in the cold trap effluent.

During attempts to sample from the PI-A loop on March 31, it was found that the sampling valve leaked in the closed position. Also, difficulties were encountered with the sampling-system components.

A temporary sampling system was devised and constructed, comprising an ambient pressure sampling chamber, argon purged, and a large waste vessel for collecting overflow sodium. The sampler was designed to accommodate 10-ml Pyrex beakers of the same type as used for the dip samples from the Fuel Transfer Port. This sampling system was put into operation successfully for taking samples from cold trap influent and effluent.

Sampling from the Fuel Transfer Port was continued in conjunction with these samples.

By the end of the month, nearly 150 samples had been taken for analysis at ICPP and about 90 values had been reported. About 40 chemical analyses had been performed at EBR-II in connection with various aspects of the "copper problem." These analytical data are being evaluated in terms of primary system operation. Results and conclusions will be reported in the April Progress Report.

a. Check for Copper Deposition on Reactor Components. A blanket subassembly removed from Row 8 of the reactor was "leached" in nitric acid. Great care was taken to eliminate spurious sources of copper and to measure copper contributions from sources which could not be eliminated. For comparative purposes, a newly fabricated stainless steel reflector subassembly, having about the same exposed stainless surface as the standard blanket subassembly, was also "leached." The copper concentration in the acid wash solution from the blanket subassembly contained 625 μg of copper, whereas the solution from the new stainless steel subassembly contained 1969 μg. These results indicate that copper deposition on the blanket subassembly, if any, was insignificant.

The stainless steel strainers from experimental subassemblies XO09 and XO13 were separately leached in nitric acid and the solutions were analyzed for copper. These subassemblies had not been washed for sodium removal prior to disassembly. The surface area of the strainer is 220 cm^2. Pertinent data are tabulated below:

Strainer from Subassembly	Time in Reactor	Cu (μg)	Cu (μg/cm^2)
XO09	3/20/66-12/21/66	120	0.55
XO13	7/17/66-9/7/66	109	0.49

3. Anomalous Swelling of Mark-IA Fuel

In the EBR-II Mark-I fuel-element design, the plenum size was such that, beyond 9% swelling of the fuel pin, the plenum gas pressure increased very rapidly. The maximum permissible burnup was therefore limited to a value (1.2 a/o) which would not produce fuel swelling in excess of ~8%. In the Mark-IA design the plenum space is enlarged by shortening the fuel pin so that the fuel could swell to a greater extent (~14%) before unduly high jacket stresses develop. The Mark-IA fuel is also of higher enrichment than the Mark-I (52.5% compared to 48.4%) to compensate for the decrease in amount of fuel alloy per fuel element and the expected increase in the number of experimental irradiations.

As reported previously (see Progress Report for May 1966, ANL-7219, and in more detail in the Progress Report for June 1966, ANL-7230), early surveillance measurements on the Mark-IA fuel showed that it was swelling at a greater rate than the Mark-I fuel. Subsequent monthly reports (e.g., Progress Report for August 1966, ANL-7249) noted additional observations that the origin of the fuel-casting batches and the impurity content in the fuel alloy were also evidently influencing the swelling rate of the Mark-IA fuel.

It appears that unexpected changes in the swelling characteristics of the fuel alloy itself accompanied the design change. The situation can be summarized as follows:

a. The original Mark-I fuel was cast at Lemont in Building 6 in a prototype furnace similar to the production furnace later installed in the Fuel Cycle Facility (FCF) at Idaho. Virgin metals were used for making the alloys. This fuel swells about 6 to 7% at 1.2 a/o burnup of heavy atoms.

b. About 3000 pins of the Mark-IA fuel were cast at Lemont in Building 350 in a smaller furnace of the same type fitted into a plutonium glovebox. The fuel alloy was also made from virgin metals and is designated as Type SL. This fuel swells about 14 to 15% at 1.2 a/o burnup, approximately twice as much as the Mark-I fuel.

c. The Mark-IA fuel pins cast at Idaho in the FCF furnace are made from melt-refined irradiated pins. This fuel alloy is designated as Type MR. This material swells about 14% at 1.2 a/o burnup, about the same as the Lemont Building 350 fuel.

d. Some of the fuel pins, cast in FCF at Idaho, are made from melt-refining runs in which the furnace charge contains considerable amounts of reject pins and pin ends from previous castings. The alloy produced from these melts is designated as Type MCS. This material swells only about 8% at 1.2 a/o burnup, about the same as the Mark-I fuel cast in Lemont in the Building 6 furnace, or the Mark-I fuel cast in the FCF at Idaho.

In order to identify and correct the causes of the anomalous swelling, an extensive series of experiments were designed in October and November 1966. The succeeding months have been primarily occupied with producing the large amount of experimental fuel elements required and placing them under irradiation in EBR-II. These EBR-II irradiation experiments, as well as more recent experimental studies, are summarized below with preliminary observations to date. Table I lists the status of the EBR-II irradiations.

TABLE I. Status of Test Irradiations of EBR-II Driver Fuel

Test No.	Description	Status	Subassembly No.	Reactor Grid Position	Irradiation Start Run No.
1	MC-S Type Fuel	In Reactor	C-291	3-C-2	25
		In Reactor	C-292	2-C-1	25
		In Reactor	C-296	3-E-1	25
		In Reactor	C-2036	4-A-1	25
		In Reactor	C-2027	4-E-1	25
		In Reactor	B-362	6-B-2	25
		In Reactor	B-364	6-D-5	25
		In Reactor	B-367	6-F-5	25
2	Design Change I versus IA	In Reactor	C-297	2-E-1	25
		In Reactor	C-298	2-A-1	25
3	Enrichment Change	In Reactor	C-283	1-A-1	24
		In Reactor	C-293	3-E-2	25
		In Reactor	C-295	5-D-4	25
4	Cooling Rate	In Reactor	C-2035	3-B-1	25
5	Trace-element Impurities	Pins Prepared			

Note: For Run No. 25, 18½% of driver fuel positions are occupied by test subassemblies.

a. Characterization of Microstructures. Optical metallography and electron microscopy are being performed on both irradiated and unirradiated fuel alloy. Assistance has been obtained from LASL because of the large number of specimens to be examined. Negotiations have been started with PNWL for a subcontract for additional electron microscopy.

Light and electron micros of two cross sections from Pin 71 (EBR-II Subassembly C-180) located 2 and 6 in. from the cooler end of the pin were examined during a visit to Los Alamos Scientific Laboratory where the pin had been prepared for metallurgical examination. No unique structural features associated with swelling could be seen in either the as-polished or etched condition when examined optically to 1500X.

Electron replicas were also prepared from both sections, and data for the calculated temperature and the calculated swelling values at these locations are as follows:

Location, Distance from Cool End of Pin 71 (in.)	Calculated Temperature at 0.707 R from Pin Centerline (°C)	Percent ΔV per a/o Burnup
2	437	3.6
6	478	5.0

The electron micros taken at these two sections showed a nonrandom distribution of very fine bubbles in both sections. The measured bubble diameter (after electrolytic etching) varied from 400 to 600 Å (0.04 to 0.06 μ). In the section located 2 in. from the cooler end the bubbles appeared to be nonrandomly distributed on a grid network having dimensions of approximately 2 μ. Micros taken at higher magnifications (to 89,000X) showed a tendency for the bubbles to be aligned along features which were not revealed by the etchant. Microtears were revealed in some areas at high magnification that occasionally served as trapping sites for the bubbles.

b. Hot Cell Measurements on Bare Fuel Pins. Examination of the average behavior of four to six Mark-I and Mark-IA pins shows that the Mark-I pins have a relatively symmetrical diameter profile; the swelling profile is evidently more sensitive to burnup than to temperature. On the other hand, the Mark-IA fuel swelling is sensitive to both burnup and temperature. This is shown by enhanced swelling rates of the hotter upper ends of the fuel pins. The swelling of the SL material produced at Illinois appears to be especially temperature sensitive.

Furnace heating tests have been completed on two Mark-IA elements containing SL material with 1.2 a/o burnup. Both elements showed little significant diameter or volume changes in successive 10-min heatings at 550, 600, 650, and 700°C. At 750°C, the elements increased in diameter 0.1 and 0.4%, and in volume 1.2 and 1.4%. The jackets on both elements failed on heating to 775°C. The average volume change in the two Mark-IA elements after heating to 750°C is 60% greater than the average volume change reported previously (see Progress Report for September 1965, ANL-7105) in three Mark-I elements from C-104 after similar heating to 750°C. In other respects, the behavior of the Mark-IA elements was similar to that shown by the Mark-I elements.

c. High-burnup Irradiations of Mark-IA Fuel Elements. Approval in principle has been obtained for irradiations in EBR-II of encapsulated Mark-IA fuel elements to burnups of 1.8 a/o or more. Seven encapsulated elements were subsequently placed in the reactor in experimental subassemblies XO15 and XO17, and irradiation was started. Irradiation of these encapsulated elements to burnups substantially higher than that presently allowed for Mark-IA driver subassemblies will enable assessment of (i) the possible effect of higher pressures in the Mark-IA fuel element in reducing fuel-swelling rates, and (ii) the mode of failure of fuel elements irradiated beyond the point of jacket rupture.

In addition to the above encapsulated elements, three driver subassemblies containing only the lowest swelling type of U-5 w/o Fs alloy (Type MCS) have been placed in the reactor in position 3-C-2, 4-E-1, and 6-D-5 for irradiation to a burnup higher than 1.2 a/o. The burnup level selected will be based on the condition of identical fuel examined at 1.2 a/o.

d. Effect of Mark-IA Fuel-element Design Change. Irradiation started on two driver subassemblies in positions 2-A-1 and 2-E-1 that were both loaded with identical fuel material in Mark-I and Mark-IA fuel-element designs. These irradiations are intended to determine the effect of the design change alone on the swelling rate of U-5 w/o Fs alloy fuel pins.

e. Effect of Increased Enrichment. Irradiation started on three driver subassemblies in positions 1-A-1, 3-E-2, and 5-D-4, containing fuel elements enriched both to 48 and 52%. These irradiations are intended to determine possible temperature effects associated with increasing the 48% enrichment of the Mark-I fuel to 52% in the Mark-IA design.

f. Effect of Cooling Rate of Injection Castings. The cooling rate of U-5 w/o Fs alloy is known to affect its microstructure. In order to determine the possible effects of differences in cooling rates on the swelling rate of this alloy, elements in the experimental driver fuel subassemblies being irradiated for the anomalous Mark-IA fuel-swelling program have been carefully identified with respect to top and bottom orientation as originally cast, and also with respect to their original position in the injection-casting bundle. Irradiation also started on one driver subassembly in position 3-B-1 containing identified fuel pins.

g. Effect of Trace-element Impurities. There is increasing evidence that the Mark-I and Mark-IA fuel pins showing lowest swelling contained larger than normal contents of C, Al, Si, and Fe, or some combination thereof. In order to determine whether or not deliberate trace additions of those elements are beneficial, two castings were prepared and cast into fuel pins. One casting duplicated as closely as possible the SL material that is known to swell excessively; the other was made from the same base stock but contains several hundred ppm each of C, Al, and Si. Elements containing both types of material will be loaded into the same subassembly so that they will experience identical reactor conditions. As the interrelationship between swelling and composition become clearer (see Sect. II.A.3.j), additional test melts will be made.

h. Effect of Pressure. The study of the effect of pressures greater than those obtainable in the Mark-I and -IA elements is being done on small specimens (1 to 2 in. long) irradiated in instrumented capsules in the CP-5 reactor. The initial experiment is in preparation. It is intended to determine

the swelling rate of U-5 w/o Fs alloy at normal EBR-II temperature and under pressures ranging from 50 to 2000 psi. Most of the pressures to be used are well beyond the maximum 330 psi pressure presently permitted in the Mark-IA fuel element.

i. Effect of Heat Treatment. Although the 500°C sodium-bonding treatment used with U-Fs alloy fuel pins transforms any gamma phase which might have been retained in the alloy, experiments on related alloys (such as U-4 w/o Mo-0.1 w/o Si) have shown that solution-treated material can be relatively resistant to high-temperature swelling. Accordingly, specimens are being prepared for instrumented capsule irradiations in CP-5 with both solution-quenched and aged structures, and with and without additions of beneficial additives.

j. Statistical Analyses. The anomalous-swelling study involves a large number of variables and large quantities of data. The experimental observations on fuel swelling (the dependent variable of primary interest) are characterized by a high level of scatter. Preliminary analyses have shown that the interrelationships between the variables are not easily defined. Clearly, statistical analyses are required. A considerable effort was made in preparing the preliminary data in a form that is suitable for statistical treatment. The services of the Applied Mathematics Division have been engaged to conduct the analyses.

4. Reactor Improvements

a. Irradiated-fuel Monitor. Approximately 40% of the fabrication (see Progress Report for January 1967, ANL-7302, pp. 11-12) is complete. Chemical analyses of the stainless steel used in these parts show that it is acceptable.

b. Rotating Plug Seal Cleaning System. The special pump for circulating the tin-bismuth eutectic alloy has continued to operate successfully in the laboratory mockup of the cleaning system (see Progress Report for February 1967, ANL-7308, pp. 4-5).

A motorized skimmer for removing the floating oxides is being tested to evaluate its effectiveness in a continuously circulating cleanup system. The full-scale system mockup utilizes the special pump to circulate molten alloy through electrically heated piping to a shallow tray in which the skimming device is mounted. A motor-driven 4-in.-wide endless belt passes across the surface of the flowing alloy in the tray to sweep the

floating oxide into a debris collector. Basically, the system functions as intended and does remove surface oxide, but modifications are needed to improve effectiveness.

Other oxide-removing devices are being investigated as alternates.

c. Irradiation Subassembly Mark-C37. Photographic studies involving ink injections in a water loop determined the mixing patterns where the bypass coolant joins coolant flowing from the experiment specimens near the top of a subassembly (see Progress Report for February 1967, ANL-7308, p. 3). A Plexiglas test section simulated the outer hexagonal can at the mixing section; the ink was injected near the top of the flow channels between the elements. Test runs were made at full 140-gal/min flow and at half-flow. Although a channel between the wall of the inner hexagonal can and the outer row of elements gave the most adverse mixing, the test results satisfactorily confirmed the theoretical evaluation that the bypass flow effectively dilutes the higher-temperature coolant before it emerges from the mixing section. A velocity effect was apparent but, at both flowrates, the pattern indicated proper dilution.

A final series of tests will be performed to establish the subassembly orifice size required to regulate the total flow through the subassembly. The orifice plate near the bottom of the subassembly permits adjusting the pressure drop to accommodate test specimens of various heat-generating characteristics. Flowrates and pressure drops will be determined for several orifice-hole sizes. Similar calibration measurements on the orifices for the bypass flow divider were reported previously (see Progress Report for February 1967, ANL-7308, p. 3).

d. Control-rod Model-IHE. The Model-IHE control rod (see Progress Report for October 1966, ANL-7267, p. 8) is being designed to increase the hydraulic holddown forces on the control rods. A full-scale prototype Model-IHE control rod was tested in a water loop to confirm the computations predicting the seating or holddown force (see Progress Report for January 1967, ANL-7302, p. 13). Figure 1 shows the seating forces for the actual EBR-II application. As is shown by the top curve, the Model-IHE rod will provide positive downward seating or holddown forces during the fuel-handling period when the control-rod drives are not connected to the control rods; no rod rise will occur even if upward flow of primary coolant is inadvertently increased to the maximum capability of both main coolant pumps in the primary system. As the second curve shows, the seating force of the Model-IHE control rod when disconnected from its drive is positive (downward) at all flows within the flow capability of the two pumps (that is, up to 100% flow). The seating force in the raised, or operating, position for both the Model-IHE and the present design is

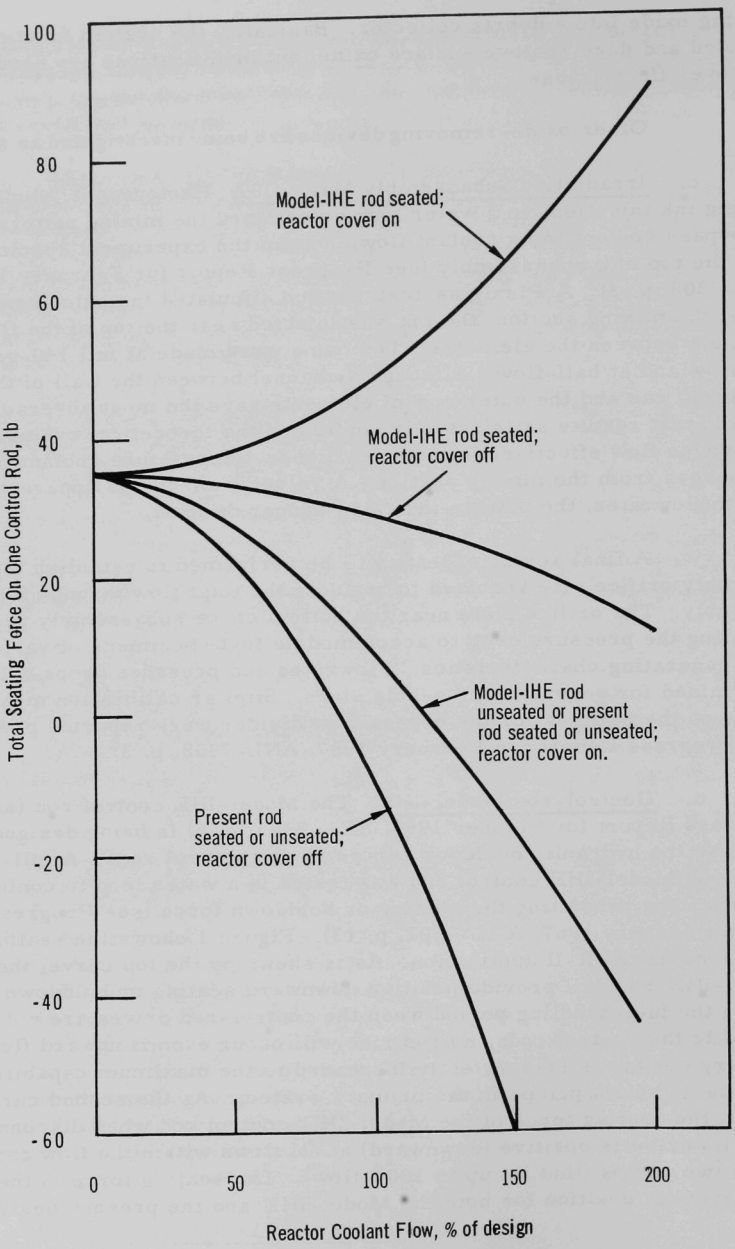

Fig. 1. EBR-II Control-rod Seating Force

shown by the third curve; the seating force is positive for the range of design reactor flow (0-100%), which tends to reduce relative movement between the control rod and the drive should there be any vertical play. The lowest curve is for the rods that are now in the reactor.

Maximum flow with both pumps full on is estimated to be 122% of full reactor design flow when the reactor cover is on and 131% when the reactor cover is off.

e. Instrumented-subassembly System. Development of the instrumented-subassembly system is continuing (see Progress Report for November 1966, ANL-7299, pp. 5-6 for description of the general concept and see Progress Report for January 1967, ANL-7302, pp. 15-18, and Progress Report for February 1967, ANL-7308, p. 5 for further details). A preliminary concept has been devised for the instrumented subassembly itself. In addition, emphasis continues on the design of a suitable coupling between the instrumented subassembly and the extension tube.

(i) Instrumented Subassembly. A preliminary reference concept has been devised for the instrumented subassembly and the associated guide thimble that will locate the subassembly in the reactor (see Fig. 2). The guide thimble would be inserted and locked in the reactor grid in the same manner as the control-rod guide thimble. No changes are anticipated in the installation and removal procedures for the new guide thimble; the standard reactor fuel-handling system will be used. The guide thimble will be reusable, so it will not have to be removed when instrumented subassemblies are changed.

The subassembly consists of a hexagonal tube that contains the fuel elements and the instrument sensors, a bottom adapter, and a standard EBR-II cone-tipped upper adapter that couples to the extension tube. A typical arrangement of instrument sensors is shown in Fig. 2. The fuel elements and sensors are housed in the subassembly. Immediately above the bottom adapter is a coolant flowmeter. Above it is a T-bar grid for supporting the fuel elements. The 17 elements and two conduits shown, which are ~5/16 in. in diameter and 45 in. long, are separated by helically-wound spacer wires. The conduits provide straight passages through the fuel bundle for the sheathed electrical conductors originating at the flowmeter and for the tubing that houses a neutron-flux monitor. Six fuel elements are fitted with thermocouples at the center of the fuel pins at various elevations. The sheathed thermocouple leads emerge from the top of the fuel elements. A fission-gas pressure transducer is fitted at the upper end of a fuel element. The remaining 11 fuel elements in Fig. 2 are not equipped with sensors. Six coolant thermocouples are shown.

(ii) Subassembly Attachment and Lead Severance. Design and evaluation work continues on various concepts for coupling and decoupling the top of the instrumented subassembly to the extension tube and for

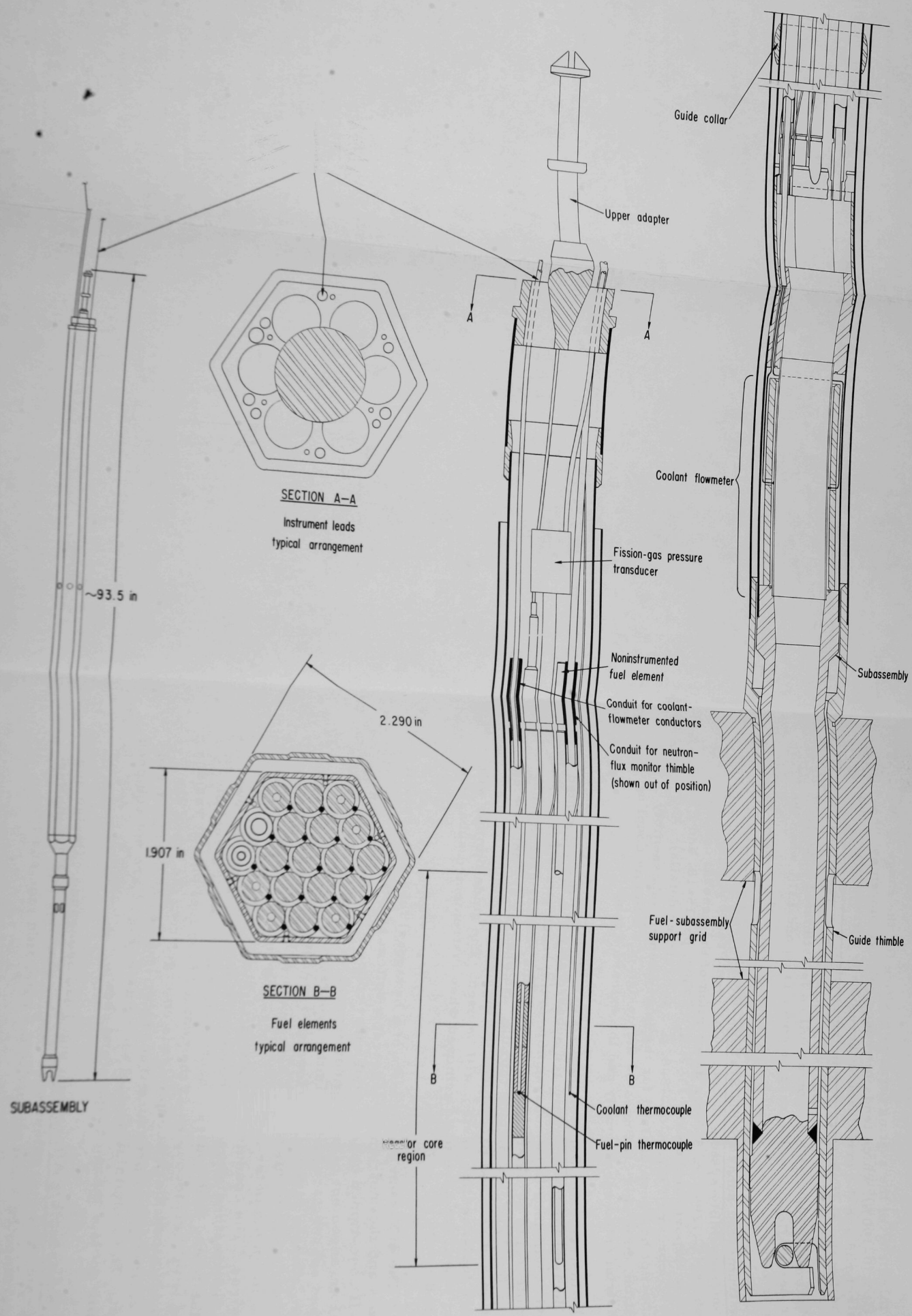

Fig. 2. Typical Arrangement of Sensors and Leads in Instrumented Subassembly

severing the instrument leads so the subassembly can be removed from the core. In addition to conducting tests on the gripper, welded and threaded coupling concepts that were designed earlier (see Progress Report for January 1967, ANL-7302, pp. 15-18), three new attachment methods have been devised: a top-end-fixture coupling, a hexagonal-support coupling, and an internal-bayonet coupling (see Fig. 3).

With the top-end-fixture coupling, the subassembly attaches to four jaws of a support tube. To disconnect, the sleeve that locks the jaws in place is raised and then a release rod spreads the four jaws. Although this coupling scheme provides reliable connection during fuel-handling operations, it has a disadvantage in that the coupling must be disconnected before the lead cut-off tool can be inserted. A preliminary mockup of this coupling has been fabricated.

The hexagonal-support coupling consists of an interlocking support sleeve and collar. The hexagonal support sleeve on the extension tube slides over the collar on the subassembly; when the extension tube is turned 30°, the corners of the hexagonal collar project onto the shoulder of the support sleeve. To lock the subassembly to the extension tube, two to six lock pins are inserted into the triangular corner spaces of the support sleeve. A preliminary mockup is being fabricated.

The internal-bayonet coupling is somewhat similar to the hexagonal-support coupling. It consists of a bayonet sleeve, attached to a bayonet tube, and a bayonet collar integral with the top end fixture of the instrumented subassembly. The sleeve and collar are machined so that one can slide over the other in one relative position. Then, by rotating the sleeve (by the bayonet tube) 90°, the mating parts interlock. This scheme has the same drawback as the top-end-fixture scheme: the sleeve must be withdrawn before the lead cutter can be inserted. Efforts are being made to redesign this coupling so that the subassembly will be supported axially as well as restrained radially by the extension tube while the leads are being cut. A preliminary mockup is being fabricated.

A preliminary mockup of the gripper coupling has been fabricated. A severance test has been conducted in which sheathed leads were cut within the coupled section. The coupling twist caused by the cutting torque was measured; ~1° of coupling twist was observed in cutting two 1/16-in.-dia leads and ~3° of twist were caused by cutting two 1/8-in.-dia leads. These twists correspond to cutting torques of ~10 ft-lb for the 1/16-in.-dia leads and ~40 ft-lb for the 1/8-in.-dia leads. Although these torques and twists seem acceptable, an improved, simplified, and more rigid version of this coupling is being pursued. Attempts also are being made to extend the retaining sleeve so that it will not be necessary to use a sleeve-lifting tool for decoupling.

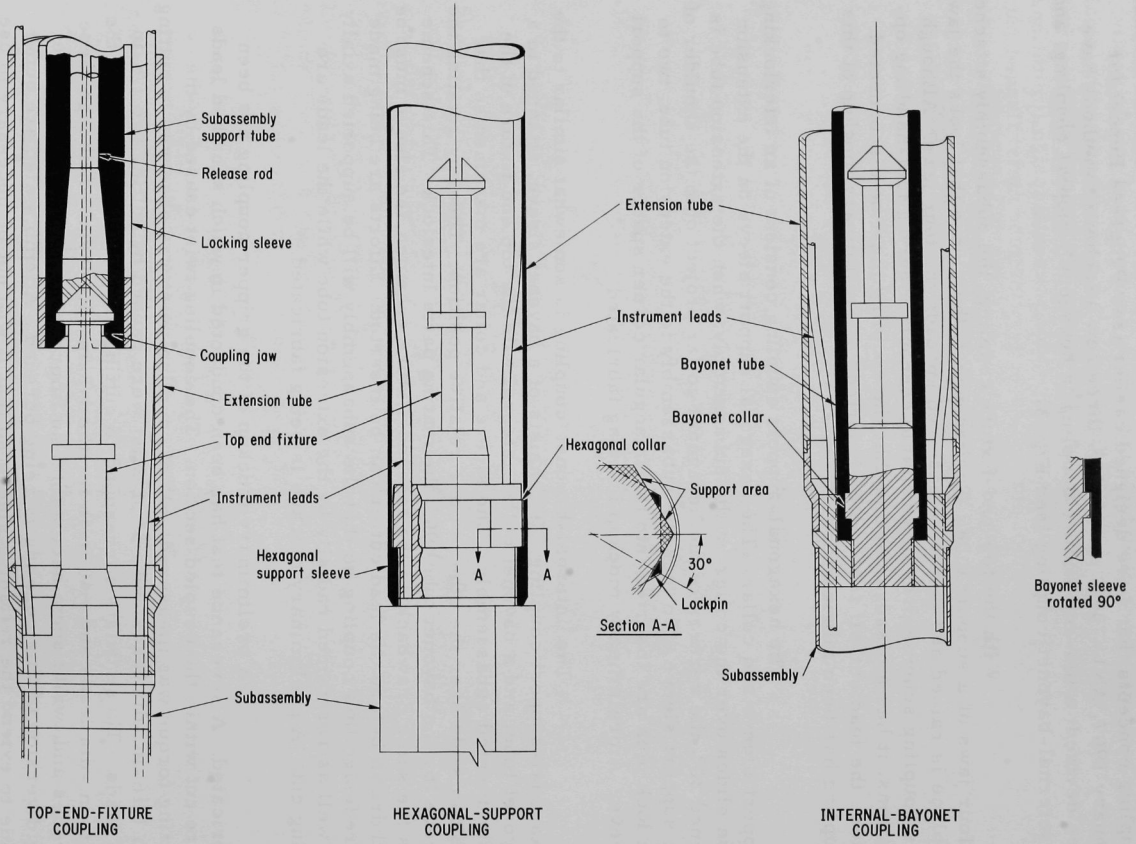

Fig. 3. Three Additional Methods for Coupling and Decoupling Instrumented Irradiation Subassembly and Extension Tube in EBR-II

For the welded coupling, tube-cutting operations with a rotary cutter and knife-action cutter have been simulated in ambient bench tests. The cutting operation could not always be completed satisfactorily. One test was conducted in 600°F sodium using new rotary cutters; the small shafts that support the cutters broke. The rotary-disc-cutter shaft design could be improved to avert breakage, but space presents design limitations. Although the knife-action tool performed better, the tube metal flanged out more. For these reasons the welded coupling is being dropped from consideration.

The threaded coupling is contemplated for use with axial cutting of the instrument leads. Fabrication of a mockup will be considered if acceptable lead-cutting forces can be obtained. A vertical cutoff assembly has been constructed to simulate the arrangement described previously for the threaded coupling (see Progress Report for January 1967, ANL-7302, pp. 16-17). Several tests were conducted in which 1/16-in.-dia solid stainless steel wires as well as 1/8-in.-dia copper-clad mineral-insulated leads were sheared sequentially by the stepped cutting edge. The cutting force for each 1/16-in.-dia stainless wire was only ~90 lb, but the bending of wires and compression of the remaining stubs raised the total measured cutting force to ~1800 lb. Although the subassembly system will be designed to withstand forces of this magnitude, improvements are being studied for reducing the peak forces.

Reference dimensions and intended uses for sheathed leads are shown in Table II. To simulate the lead-cutting operations to be performed at the top region of the test subassembly, numerous preliminary rotary cuts have been made on 1/16-in.-dia leads, which require a force of ~100 to 150 lb (~10 to 15 ft-lb torque). Since 0.125-in.-dia leads require cut-off forces of ~500 lb (~50 ft-lb torque), tests are being conducted on these heavier leads. To establish lead-cutter performance, tests also have been initiated on heavy-wall tubing (more readily obtainable than sheathed leads), which requires ~90 ft-lb cutting torque. In addition to these cutting tests in a dry atmosphere, three tests have been conducted in 700°F sodium; in these, two, four, and twelve 0.125-in. leads, respectively, were cut. The torque required was 35 to 45 ft-lb.

TABLE II. Preliminary Data on Sheathed Leads for Various Sensors

Sensors	Conductor			Sheath		
				Dimension (in.)		
	Max No.	Size	Material	OD	Thickness	Material
Flowmeter, permanent-magnet type	4	24 AWG	304 SS	0.125	0.020	304 SS
Flowmeter, other type	4	24 AWG	Nickel	0.125	0.020	304 SS
Fission-gas-pressure transducer	4	24 AWG	Nickel	0.125	0.020	304 SS
Coolant thermocouples, 1/16 in.	2	0.010 in.	Chromel-alumel	0.062	0.009	304 SS
Coolant thermocouples, 0.040 in.	2	0.0065 in.	Chromel-alumel	0.040	0.006	304 SS
Fuel thermocouple, 0.062 in.	2	0.010 in.	W-3% Re--W-25% Re	0.090[a]	0.009	a
Flux monitor[b]	3	-	-	0.125	-	-

[a]Cover sheath of Type 304 SS over an 0.062-in.-OD x 0.007-in. tantalum sheath.
[b]Inserted in a dry tube (Type 304 SS) of 3/16-in.-OD x 0.010-in. wall.

f. Fuel Element Mark II. Burnups achievable with the Mark-I and Mark-IA driver fuel elements have been limited to ~1.2 a/o by fuel-pin swelling and pressure increase from fission-product gas release that could lead to jacket rupture. To raise burnup to ~2% with the same alloys and overall fuel-subassembly dimensions, a reference design has been established for the Mark-II fuel element (see Table III). The Mark-II design permits fission-product gases to escape to a larger gas plenum within the fuel element, where both the gases and further fuel swelling are restrained by a thicker jacket. Like the Mark-I and Mark-IA designs, the Mark-II fuel element uses fuel of U-5% Fs alloy, Type 304ELC stainless steel as the jacket material. The end fittings, spirally wrapped spacer wires, and jacket outer diameter stay the same. The smaller fuel diameter and thicker sodium bond will allow the fuel to swell enough (up to 33%) that voids formed in the fuel alloy by the fission-product gases will interconnect, enabling the gases to escape from the fuel alloy. (Experiments indicate that gas release starts at 20 to 25% swelling and becomes very significant by 30%.) The gases that escape from the alloy are accommodated in the larger volume formed by the longer jacket, restrainer, and plenum. The fuel alloy is slightly longer to compensate partly for the fuel-diameter decrease, but enrichment also will have to be increased. To allow for the longer fuel element and the resultant increase in pressure drop, the upper and lower axial shields will be modified.

TABLE III. Dimensions of EBR-II Driver Fuel Elements

Part	Dimension (in.)		
	Mark I	Mark IA	Mark II
Fuel-element length	18	18	24
Plenum length	2.2	2.9	8.3
Fuel restrainer gap	0.40	0.40	0.70
Fuel length	14.2	13.5	14.2
Fuel diameter	0.144	0.144	0.130
Sodium-bond radial thickness	0.006	0.006	0.010
Jacket ID	0.156	0.156	0.150
Jacket wall	0.009	0.009	0.012
Jacket OD	0.174	0.174	0.174
Spiral spacer wire diameter	0.049	0.049	0.049

Work remaining to be accomplished includes axial-shield design, heat-transfer analyses, evaluation of designs for the fuel axial restrainer, hydraulic testing, safety analyses, irradiations in EBR-II, and final adjustments to the design.

Several designs for the fuel axial restrainer are being evaluated for their performance and effect on element fabrication and assembly.

So that proper distribution of coolant flow through the reactor will not require that the entire present EBR-II core loading be changed when the first Mark-II subassembly is inserted, hydraulic analyses and tests will determine how proposed fuel-element dimensional changes affect coolant pressure drop through the fuel region of the core. With the fuel-element dimensions established, the total pressure-drop characteristics through the new subassembly design will be matched to those of the present subassemblies (38 psi at design flow in Rows 1 and 2) so that both types can be used interchangeably without disturbing the proper distribution of coolant flow through the reactor. A series of representative arrangements have been analyzed preliminarily to define the relation between fuel-element dimensions and pressure drop and to illustrate possible compensating changes in other parts of the subassembly. Although the longer fuel element increases pressure drop through the fuel section of the subassembly, changes to the axial-shield sections to reduce pressure drop through them can keep total pressure drop through the subassembly the same as in the present designs. Hardware is being fabricated to make available an additional hydraulic test loop for the extensive testing needed.

The changes made to reduce coolant pressure drop through the stainless steel axial-shield section tend to decrease its shielding effectiveness and result in greater neutron dosage to the grid plate and reactor-vessel cover. Preliminary studies indicate that proper redesign can minimize the effect. Investigations of radiation intensities, heating distribution, and stresses in the reactor cover and grid continue.

Heat-transfer calculations indicate that, at core center and with 65-MW(th) operation with newly loaded pins, the thicker cladding and bond in the Mark-II design will raise the temperature drop across the bond from 7 to 12°C and across the cladding from 34 to 45°C, for a total increase of 16°C in the temperature difference from fuel surface to jacket exterior.

The final selection of Mark-II subassembly design will involve an optimization that considers pressure drop, physics, safety, shielding, and materials performance. The fuel burnup achievable with the Mark-II design will depend primarily on the in-reactor behavior of the fuel alloy, which will be determined by surveillance of the performance of production fuel.

g. Nuclear Instrumentation. The equipment specifications have been prepared, purchase orders written, bids obtained and evaluated, and the equipment orders placed. The delivery schedule quoted by the manufacturer is as follows:

Linear Channel	June 20, 1967
Source Range Channels	July 14, 1967
Power Range Channels	August 4, 1967
Power Supplies	August 4, 1967

Detailed wiring changes necessary for installation of one source range channel have been completed. Work is continuing on the remaining two channels. Completion percentage is 2%.

h. Reactor Systems Instrumentation

(i) Temperature-monitoring Devices. The equipment specifications have been prepared, purchase orders written, bids obtained and evaluated, and the equipment orders placed. The delivery schedules quoted are as follows:

MV/I Converters	May 15, 1967
Monitor Switches	May 10, 1967

Preparation of engineering package scheduled to begin 4/3/67. Completion percentage is 2%.

(ii) Multipoint Recorders. The equipment orders have been placed, and delivery has been quoted by the manufacturer for May 15, 1967. Completion percentage is 40%.

(iii) Miniature Recorders. The equipment orders have been placed, and delivery has been quoted by the manufacturer for May 15, 1967. Work on alarm functions and engineering package is scheduled to begin on April 15, 1967.

(iv) Selected-parameter Data-processing System

(a) 100-point Scanning System. The equipment specification has been prepared, the purchase order written, bid obtained and evaluated, and the equipment order placed. The delivery schedule quoted by manufacturer is May 8, 1967. Progress reports from the manufacturer indicate that they may meet their scheduled date.

(b) 50-point Scanner and Alarm System. The 50-point scanner and alarm system has been assembled and shop tests have been completed. The unit has been moved out of the shop area and has been placed into position for interconnection into the system. Terminal boards have been mounted in the control-room panels for intermediate terminations. The 21 thermocouples for the core subassembly have been disconnected from the existing system and reconnected for use in the new system and on the Automatic Data Logger. This has been completed so that reactor downtime is not a requirement for task continuation. The master patch panel for both systems has been assembled and mounted. Wiring of the master patch panel has been in progress for 1.5 days. Completion percentage is 60%.

i. Modifications for Increased Fuel Production

(i) Bonder. The bonder-control equipment and associated panels have been fabricated; shop testing is complete. Operational checks with the equipment connected to the system are scheduled for the first week of April 1967. Work continues on "as-built" prints and on operations manual. Completion percentage is 90%.

(ii) Skull-oxidation Furnace. The skull-oxidation furnace controls and associated panels have been fabricated, and shop testing is complete. The control has been connected to a furnace, and operational testing is in progress. The fabrication sketches have been updated and sent to the drafting group for system drawings. Completion percentage is 90%.

(iii) Bond Tester. The fabrication and assembling of readout and control circuits is in progress. The readout panel has been completed and shop tests are in progress. Work on the control-circuit cabinet is approximately 50% complete. The completion percentage is approximately 65% for the overall project.

j. Modification for Cold Fuel Production

(i) Leak Detectors. The panel cutouts have been made for the recorders and the panel painted. The solenoid racks have been fabricated and are now awaiting solenoid delivery for continuation of work. The electrical-control sketches for panel interconnections have been completed for each of the five systems. Continued effort is dependent on component delivery. Overall completion percentage is 10%.

(ii) Sodium Extruder and Settler in Glovebox. The control prints for motor and pressure control are complete. Work is in progress on the balance of prints necessary for system fabrication. The necessary equipment is on order, with deliveries scheduled for the first two weeks in April 1967. Overall completion percentage is 2%.

(iii) Bonder. The electrical-circuit prints have been completed for the system control. In-panel wiring is approximately 40% complete. All necessary components are now on hand for system completion. Overall completion percentage is 30%.

(iv) Injection-casting Furnace. Work is in progress on the electrical-control prints necessary for system fabrication. The prints are approximately 60% complete. Equipment deliveries are approximately 90% complete on the control components.

The prototype induction heater has not been operated successfully and will require circuit and component changes to satisfy system

requirements. Design and test of prototype are in progress. Once a coil design can be proved it will be necessary to order a capacitor to match the coil for maximum power transfer. An alternate power supply now available will be temporarily connected to the system for the initial operating period. Provisions for use of the alternate supply are now in the package design. Overall completion percentage is 2%.

(v) Pin Processor. Remaining to be delivered are the Digital Voltmeter and the cabinets for housing the equipment. The electrical drawings necessary for fabricating and assembling of the equipment are completed. Internal interconnections within the equipment drawers has started and is approximately 40% complete. Overall task completion is 30% complete.

(vi) Welder. Work on a spare welder is about 90% complete. Should a spare be required, it will be fabricated after the Cold Fuel Line has been placed into operation.

(vii) Alloy Furnace. The electrical-control prints have been completed, and the necessary equipment and components have been delivered with the exception of the cabinets. The cabinets are scheduled for delivery on or before April 10, 1967. Layout work on the panels was started and has been in progress for two days. Overall task completion percentage is approximately 10%.

5. Reactor Physics

a. Reactivity Worth of Stainless Steel in Rows 7 and 8. The reactivity worth of the stainless steel reflector in Rows 7 and 8 has been assessed. Because it was necessary to interrupt loading sequences to run criticals, only two measurements of the stainless steel reactivity worth have been obtained. Final values must await additional measurements of the reactivity worth of a fueled versus stainless steel subassembly in Row 6. Thirty-one stainless steel reflector subassemblies were loaded into Row 7 in three steps of 10, 11, and 10 each. A clean measurement of the incremental worth of the second loading (11) was made and found to be 85 Ih (0.20% $\Delta k/k$). By extrapolating these results to the rest of the loading and taking into account the relative position of the subassemblies, the total worth of the Row 7 reflector is estimated to be 219 Ih (0.53% $\Delta k/k$). The incremental reactivity worth of the addition of 23 stainless steel reflectors in Row 8 has also been measured as 180 Ih (0.43% $\Delta k/k$). These subassemblies were all loaded on the four central locations of each flat of Row 8. The final determination of the worth of the remaining 18 stainless steel subassemblies in Row 8 is not yet available, but the indications are that the total worth of two rows of stainless steel will be about +1% $\Delta k/k$.

b. Measurements of Fission Rate. During the shutdown prior to Run No. 25, four low-power runs were made to measure flux distributions.

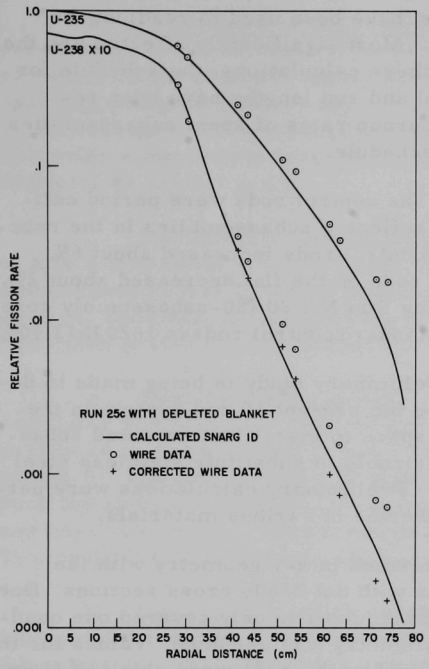

Fig. 4. Fission Rate Distribution in EBR-II

These are designated Runs No. 25A, B, C, and D. The sequence has been run with the following respective configurations: (a) the core with depleted uranium blanket; (b) the same as (a), but with the wire subassemblies in different locations than for (a); (c) with wire subassemblies distributed for measurement of the depleted uranium blanket; and (d) for measurement of the core and blanket with stainless steel blanket subassemblies in Rows 7 and 8.

Before any stainless steel was introduced into Rows 7 and 8, fission and capture rate measurements were made in the uranium blanket, Rows 7 through 15. The exposure was split into two runs, one of 50 kWh and another of 500 kWh. The results of these measurements are given in Fig. 4 along with the calculated values obtained by use of the SNARG code. The data for the depleted uranium wire (containing 0.22% U^{235}) were corrected for U^{235} content; the resulting data are in good agreement with the calculations. The uncorrected data give the actual fission rate distribution in the blanket, since the wire detectors and blanket material have the same isotopic composition. The slight relative increase in fission rate at the outer edge of the blanket is undoubtedly due to the moderating effect of the graphite neutron shield.

In conjunction with the stainless substitutions, fission rate distributions have been measured, using the special wire subassemblies, at selected positions from the core center out through Row 11, using both U^{235} and U^{238} detectors. The irradiation time was 50 MWh. The data are presently being analyzed and will be important in ascribing final burnup rates in the driver and experimental subassemblies, determining the effects of stainless steel on the flux distribution, and determining the appropriate burnup rate for uranium blanket material in Rows 9 and 10.

c. Adjustment of Burnup Rates in the Driver Fuel. The enlargement of the core to 91 subassemblies along with the use of the partially fueled driver has significantly changed the burnup rate as a function of position in the core subassemblies. Calculations, substantiated by fission-rate measurements made with the uranium blanket and present measurements

made with the stainless steel reflector, have been used to readjust the burnup rate in all core subassemblies. Most significantly affected are the Row 6 subassemblies. As a result of these calculations, the schedule for subassembly removal has been revised and run lengths have been re-estimated. As in the past, measured burnup rates of spent subassemblies will be used to confirm the unloading schedule.

d. Control-rod Calibration. The control rods were period calibrated with one row of stainless steel reflector subassemblies in the reactor. The average worth of the corner control rods increased about 6% while the average worth of the control rods on the flat decreased about 2%, compared with the worth obtained during Run No. 20 (80-subassembly core). The total reactivity held in the eleven standard control rods is 1620 Ih (3.90%).

e. Control-rod Worths. A preliminary study is being made to design an 8 rod control system to replace the present 10 rod system in the EBR-II Reactor and provide the extra space to insert instrumented subassemblies for irradiation. It is also desirable to substitute stainless steel for the natural uranium in the blanket. Preliminary calculations were performed to investigate the control-rod worths of various materials.

The calculations were performed in x-y geometry with the SNARG-2D code in an S2 approximation with Set 23606 cross sections. Due to limitations of computer storage, the calculations only covered one quadrant of the reactor, that is, fourfold symmetry was assumed. Values for the transverse buckling (z-direction) required by the code were obtained from a one-dimensional diffusion calculation and resulted in a value of k = 0.99889 for the reference case. The reference reactor consisted of a 91-subassembly core (6 full rings), surrounded by a natural uranium blanket. The modified reactor was made by substituting two rows (Rows 7 and 8) of stainless steel for natural uranium subassemblies. This assembly yielded a value of k = 1.0048. Various materials, of typical design compositions, were placed in control-rod positions for an 8- and 10-rod control system in the modified assembly. The corresponding values of k for the control-rod materials were calculated for two spectrum-averaged stainless steel cross sections. The stainless steel cross sections were only used for the stainless steel in Rows 7 and 8.

Referring to Table IV, the computations indicate that the control-rod worths are somewhat insensitive to the averaging method. The rod worths were all determined with respect to fuel replacement.

TABLE IV. Control Rod Worths for Various Materials in EBR-II (Run 25) with Stainless Steel Subassemblies in Rows 7 and 8

Material in Control Rod Positions	Stainless Steel Cross Sections Weighted for an All Natural Uranium Blanket				Stainless Steel Cross Sections Weighted for a Stainless Steel Blanket			
	8 Control Rods		10 Control Rods		8 Control Rods		10 Control Rods	
	$-\Delta k/k$ (%)	$\frac{-\Delta k/k}{\text{Rod}}$ (%)	$-\Delta k/k$ (%)	$\frac{-\Delta k/k}{\text{Rod}}$ (%)	$-\Delta k/k$ (%)	$\frac{-\Delta k/k}{\text{Rod}}$ (%)	$-\Delta k/k$ (%)	$\frac{-\Delta k/k}{\text{Rod}}$ (%)
50% Na, 50% SS, 100% Na	2.148	0.2685	2.725	0.2725	-	-	-	-
					2.407	0.3009	3.029	0.3029
80% Ta, 10% Na, 10% SS	5.571	0.6964	7.011	0.7011	5.540	0.6925	-	-
55% B_4C, 25% Na, 20% SS	5.972	0.7465	7.507	0.7507	5.937	0.7421	-	-
55% B_4C (69% enrich), 25% Na, 20% SS	11.737	1.4671	14.382	1.4382	11.681	1.4601	-	-

f. Experiment-relocation Studies. The anticipated increase in power of EBR-II will require the relocation of some of the experiments presently in the reactor. Such changes will be accompanied by a corresponding change in fission-rate distribution and a different critical condition of the reactor. The computer has been used to calculate the overall effects of moving experiments from Row 4 to Rows 5 or 6, with the stainless steel reflector in Rows 7 and 8.

Preliminary results indicate that movement of 12 experiments to Row 6 will cause a rather large change in fission-rate distribution, while a movement to Row 5 is less drastic. At the time the power change is planned, such calculations will have to be repeated for the loading conditions then prevailing in the reactor.

g. New Oscillator Design. Several new designs for the rotating oscillator rod have been proposed to eliminate the problem of rubbing experienced by the previous design. One such design is to balance a single poison B^{10} rod on one side with a UO_2 rod on the opposite side, and to reduce the radius of rotation. Calculations of the worth of such an oscillator rod have been made. These calculations indicate that 57 g of U^{235} opposite 75 g of $B_4^{10}C$ will provide an adequate oscillator signal of 15-20 Ih.

h. Gamma Heating Calculations. With the substitution of stainless steel for depleted uranium in the inner blanket, questions arose about the extent of gamma heating in the stainless steel blanket and, beyond that, in the depleted uranium blanket. Two configurations of interest are the single row of stainless steel elements in Row 7 followed by depleted uranium, and the double row of stainless steel in Rows 7 and 8 followed by depleted uranium. A crude calculation of gamma heating in these arrangements was made as follows:

An estimate of the gamma flux emanating from the core was based on the central gamma production and the previously estimated core gamma-distribution pattern. The pattern was appropriately adjusted for a 91-element core at 45 MW. The energy spectrum of this gamma flux was assumed to be a mixture of the spectra attributed to prompt fissions and to equilibrium concentration of fission products.

A slab model of the inner rows of the blanket was visualized and attenuations calculated through the various rows of material. Volume fractions were taken as 60/20/20 in a uranium/stainless steel/sodium subassembly, and 80/20 in a stainless steel/sodium subassembly. Attenuations were calculated for each group and the resulting fluxes summed to estimate the total energy absorption.

Gamma fluxes directly impinging on the blanket were thus calculated to be 140 watts/cm^2 at the midplane. These are attenuated to about 40% in passing through a row of stainless steel subassemblies, or to about 8% in passing through a row of depleted uranium subassemblies. There results an energy absorption due to this direct gamma flux of about 35 watts/cc in the inner edge of a depleted uranium element in the 8th row after a single row of stainless steel, or 14 watts/cc in the ninth row depleted uranium after two rows of stainless steel subassemblies. Energy absorption in the inner edge of a stainless steel subassembly in Row 7 is about 23 watts/cc.

A significant correction to the absorption of direct core gammas is the buildup due to (n,γ) reactions occurring in the blanket. It is estimated that this could amount to as much as a 60% augmentation of gamma energy absorption in the depleted uranium blanket subassemblies.

6. Surveillance

a. Irradiation Stability of Mark-I Fuels. Recent information resulting from surveillance of EBR-II Mark-I fuels has indicated a variation of stability under irradiation. Investigation of probable causes of behavioral differences has resulted in consideration of two variables: (a) the level of purity and (b) the cooling rates of cast pins. To test these hypotheses, two groups of fuel pins have been made during this reporting period.

Two melts under identical conditions were made for injection-cast irradiation specimens for EBR-II. Each melt contained enough metal to fill 78 molds, which was the maximum capacity of the injection-casting furnace. One melt was U-5 w/o Fs and the second was the same alloy with additions by weight of 600 to 900 ppm Al, 350 to 550 ppm Si, and 200 to 300 ppm C. Both melts contained the same Mark-IA enrichment (52.4 to 52.5% U^{235}). The ANL Chemical Engineering Division alloyed the casting billets for these melts. The ingots from both batches were analyzed and major constituents found to be within specifications. The minor alloy additions were low and were compensated for in the injection casting melts.

Preliminary results on the two casting melts indicate that approximately 120 to 136 acceptable castings should be available for irradiation testing or metallographic examination. This includes 70 to 78 pins without the alloy additions and 50 to 58 pins with the additions. All the pins are being carefully handled to retain complete identification as to position in casting pallet, which is related to cooling rate and thereby microstructure.

7. Experimental Irradiations

The status of all experimental irradiations in the reactor and the approximate exposure at month's end is shown below:

Sub	Date Loaded	Capsule Content and Number of Capsules( )		Experimenter	Approximate Accumulated Exposure (MWd)	Goal Exposure (MWd)
XG02	7/16/65	UO_2-20 w/o PuO_2	(1)	GE	9,744	13,600
		Stainless Dummies	(18)			
XG03	7/16/65	UO_2-20 w/o PuO_2	(2)	GE	9,744	19,450
		Stainless Dummies	(17)			
XG04	7/16/65	UO_2-20 w/o PuO_2	(2)	GE	9,744	39,000
		Stainless Dummies	(17)			
XG05	9/3/65	UO_2-20 w/o PuO_2	(9)	GE	9,317	14,750
		U-15 w/o Pu-10 w/o Zr	(1)	ANL		
		U-15 w/o Pu-10 w/o Ti	(1)	ANL		
		UC-20 w/o PuC	(3)	ANL		
		Structural	(5)	GE		
XA08	12/13/65	UC-20 w/o PuC	(8)	ANL	7,495	19,800
		Structural	(11)			
XO10	3/24/66	UO_2-20 w/o PuO_2	(4)	GE	6,675	19,600
		Structural	(11)	ANL		
		Structural	(4)	PNWL		
XO11	5/9/66	UO_2-20 w/o PuO_2	(7)	ANL	5,104	8,300
		UO_2-20 w/o PuO_2	(9)	GE		
		304 SS-30 w/o PuO_2	(1)	PNWL		
		304 SS-20 w/o PuO_2	(1)	PNWL		
		304 SS-20 w/o UO_2	(1)	PNWL		
XO12	8/10/66	UO_2-20 w/o PuO_2	(19)	NUMEC	2,975	20,600
XO14	7/17/66	Structural	(5)	PNWL	3,674	a
		Graphite	(2)	PNWL		
		Structural	(7)	GE		
		Structural	(5)	NRL		
XO15	11/15/66	PuO_2-UO_2	(11)	NUMEC	1,320	11,000
		PuO_2-UO_2	(2)	GE		
		(Pu,U)C	(4)	ANL		
		MK-IA (Metal)	(2)	ANL		
XO16	1/13/67	Structural	(9)	ANL	0	3,000
		Structural	(10)	GE		
XO17	11/15/66	PuO_2-UO_2	(11)	NUMEC	1,320	6,500
		(Pu,U)C	(3)	UNC		
		MK-IA (Metal)	(5)	ANL		
XO18	12/6/66	Structural	(3)	GE	630	21,300
		Structural	(1)	PNWL		
		Structural	(2)	ANL		
		Structural and Heavy Metal Fission Yield Samples	(1)	ANL		
XO19	1/13/67	UO_2-20 w/o PuO_2	(7)	GE	0	7,500[b]
		$(U_{0.8}\ Pu_{0.2})C$	(3)	UNC		
		Structural	(8)	PNWL		
		Graphite	(1)	PNWL		
XO20	1/13/67	UO_2-20 w/o PuO_2	(9)	GE	0	7,500[b]
		$(U_{0.8}\ Pu_{0.2})C$	(3)	UNC		
		Structural	(4)	PNWL		
		Structural	(2)	ANL		
		Graphite	(1)	PNWL		
XO21	2/27/67	Structural	(7)	PNWL	0	21,500

[a]Maximum attainable before reaching experimental subassembly capacity.
[b]Are being considered for further exposure.

8. Vertical Assembler-Disassembler (VAD)

Assembly of the VAD is now approximately 80% complete; further assembly is dependent on the delivery of a number of components now past due.

Work is now under way on:

1. the operational testing of the drives used to position the subassemblies vertically using prototype control systems;
2. the assembly and wiring of the control console;
3. the operational testing of the partially completed machine and subsystems;
4. the preparation of some installation drawings and instructions.

The correction and adjustment of a number of out-of-tolerance components, discovered during inspection and functional checkouts, has been completed. Calibration of the load-monitoring system, operational tests on the Miller ES welding power supply, routing of the pneumatic and electrical lines, and the locating of service line junction points has also been completed.

9. Fuel Cycle Facility (FCF)

a. Examination of Irradiated Radial Blanket Rods. Postirradiation examination of radial blanket subassemblies from the 7th, 8th, 9th, and 12th rows of the reactor has been completed. The 7th row subassembly (A752) showed a maximum diameter increase of the declad uranium slug of 24 mils (0.457 measured versus 0.433 in. nominal). Lenth increases up to 1/8 in. for an 11-in.-long slug were measured. Density measurements showed a minimum density of 17.3 g/cc as compared to a nominal density of 18.96 g/cc. The 8th row subassembly (U-1049) showed a maximum diameter increase of 17 mils (0.450 in. measured). Length increases of the order of 1/16 in. were measured. The lowest density measured in the 8th row was 18.0 g/cc. No significant dimensional changes were measured in the 9th row (U-1339) or 12th row (U-1124) subassemblies. A decrease in density of less than 1% was measured for slugs of U-1339; however, this may not be significant because it is within the extremes of manufacturing tolerances. No density changes were noted for U-1124. Additional postirradiation examination of other blanket subassemblies (including Row 10) are scheduled.

b. Fabrication of Unirradiated Fuel in the FCF. To increase the production capabilities of the fuel cycle, a cold fabrication line is being established. Equipment design was based on the following: (1) The line must operate in the shortest possible time. (2) The line should be capable

of producing 16 subassemblies per month in case of a major shutdown of the in-cell process, but it would probably be operated at about half this rate, as required to supplement the in-cell process. (3) The line must be capable of manufacturing Mark-IA, Mark-IB, or Mark-II fuel pins and elements.

To reduce the design effort, existing equipment drawings were modified to improve remote-handling features. The final Mark-II fuel-element specifications have not been determined, but a maximum length of 29 in. has been fixed. Therefore all equipment that has to handle fuel elements has designed into it the capability of working 18-in. elements (Mark IA or B) or, with minor modifications, any other length up to 29 in.

The only equipment undergoing major redesign is the injection-casting furnaces. The in-cell furnace would have required too much time to duplicate, even without remote features. The design of the new furnace has been completed and fabrication is proceeding.

Completion and installation of all equipment (except assembly machine) is expected to be finished in FY 1967. Checkout of all equipment with depleted uranium should be finished during July, with test operation using enriched fuel to begin thereafter.

c. Operating Manipulators. As a result of the failure of the retainers, the ball bearings that guide the telescoping tubes on one manipulator were released. The carriage was removed from the cell, and the telescoping-tube assembly was replaced with an assembly of a new design which incorporates rollers rather than recycling ball bearings as tube guides. If this concept proves acceptable it will be used for all future telescoping-tube replacements. It is felt that this design will eliminate the problem of sticking tubes.

d. FCF Operations. Operations were continued on the receiving of radial blanket subassemblies from the reactor, removal of the sodium, and transfer of these subassemblies to interim storage in the waste burial ground. Seven runs were made with unirradiated uranium to produce additional fuel for fabrication into subassemblies. These EUF runs produced 75 kg of alloy. Process operations are summarized in Table V.

TABLE V. Production Summary for March 1967

	March	Total This Year
Subassemblies received:		
Core Control, Safety (for processing)	0	20
Other (56 blanket; 5 flux wire S/A)	61	92
Subassemblies dismantled (for processing):	4	24
Subassemblies dismantled (for examination, etc.):	8	28
Subassemblies fabricated: reprocessed	15	44
unirradiated	0	4
Reprocessed subassemblies transferred to reactor:	16	36
Elements decanned:		
From irradiated subassemblies	563	
Rejects	58	
Total Decanned:	621	

Melt Refining

	Irradiated Fuel	Recycle Material	New Fuel
No. of runs	4	10	8
Average pour yield, %	92.5	92.6	96.8

Processing

Injection-casting runs (total number):	17	
Elements processed:		
Accepted:	1242	
Rejects:	106	
Elements welded:	1330	Rewelded: 0
Elements leak tested:		
Accepted:	744	
Rejects:	11	
Elements bonded (including recycle):	1299	
Elements bond tested:		
Accepted	1097	
Rejects:	202	
Elements to surveillance:	18 from 7 subassemblies	

Waste Shipments

Cans to burial ground:	10
Oxide and glass scrap to ICPP (No. of shipments):	11

B. Physics Development

1. ZPR-3

a. Assembly 48B. Assembly 48B, a reactor with a two-zoned core, is a variation of Assembly 48, for which experiments have recently been completed. Both are plutonium assemblies with well-degraded spectra; physics studies with this type of core have been in progress since June 1966. Assembly 48B is identical in core and blanket loading to Assembly 48, except for a central core region, 12 in. high by approximately 15 in. in diameter, inserted into the 30 x 30-in. core area. In the central core region, plutonium with 22% Pu^{240} has been substituted for plutonium with 4.5% Pu^{240}, changing the average Pu^{240} content of the fuel from 6.0 to 17.1%.

After loading the central region with the high-Pu^{240} plutonium and reducing the core size, preliminary measurements were made with a proton-recoil spectrometer placed at the center of the core. Background gammas and spontaneous neutrons from the plutonium were too high for good measurements, so count rates were checked to help determine the design of a spectrometer suitable for accurate measurements in this type of core. Reduction in counter sensitivity and improvements in electronics were indicated, and both developments are being pursued. The proton recoil spectrometer development is discussed in Sect. II.B.1.c.

The control rods were calibrated by both inverse kinetics and a rod-bump method. Measurements of the worth of materials at the core edge and of fuel spiking of the safety rods were made, and the critical mass was derived.

Measurements were concentrated in the central region with the high Pu^{240} content, and these included sodium substitutions, fission ratios, perturbation reactivity measurements with small samples, and foil irradiations to determine fine flux variations across a reactor cell. The ratios of fission in U^{233}, U^{234}, U^{236}, U^{238}, Pu^{239}, and Pu^{240} relative to that in U^{235} were measured.

Following this, reaction-rate traverses were made in the radial direction at the core midplane. U^{235}-, U^{238}-, plutonium-fission counters, and a BF_3 proportional counter were used. Reactivity traverses in the radial direction have also been made using stainless steel, tantalum, B^{10}, U^{235}, Pu^{239}, and U^{238} samples.

It is interesting to note that the average plutonium-240 content in the central zone is 17%, which is the highest yet used in a fast reactor experiment and is approaching that expected in fast power reactor fuel. The previous highest plutonium-240 content in a fast reactor experiment was 10%, attained in ZEBRA Core VI. Measurements in the cental zone,

therefore, are directly useful to investigate the effects of change of fuel composition in a power reactor. In particular, significant changes in the reactivity worth of sodium are expected. These data will be of great value in establishing the sodium-void coefficient in fast power breeder reactors.

b. Assembly 48A. Assembly 48A (see Progress Report for February 1967, ANL-7308, pp. 12-15) is the critical experiment which was run in support of the FFTF reactor being designed by Pacific Northwest Laboratory. The results of the axial traverses are shown in Fig. 5 for measurements at the center of an Inconel reflector drawer mockup adjacent to the core (approximately 1.09 in. from the core-reflector interface). The reaction rates were determined with an enriched BF_3 fission counter, and with depleted uranium (80 ppm U^{235}), and plutonium (4.75% Pu^{240}) fission counters.

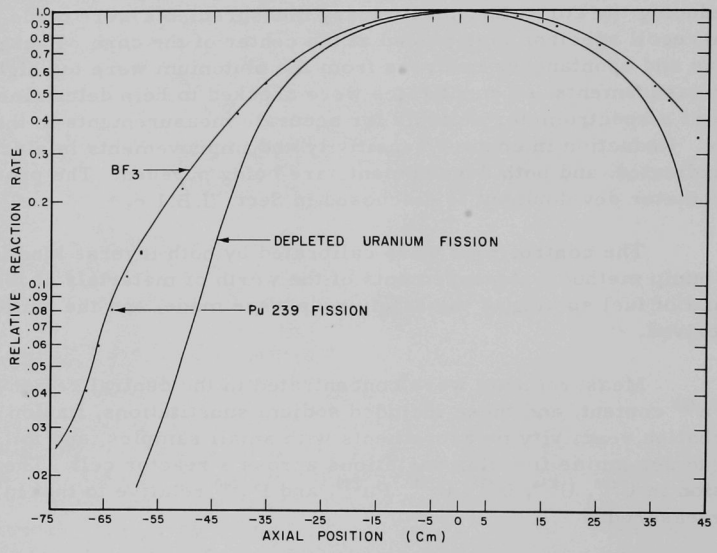

Fig. 5. Reaction Rates at the Reflector-Core Boundary in Assembly 48A

The reactivity traverses of various materials through the core will be reported as soon as the analysis is completed.

(i) Cross-section Set. Further progress has been made on the preparation of a six-group cross-section set (see Progress Report for February 1967, ANL-7308, p. 15) for FFTF computations using the 2D SNARG code. In Table VI are compared the measured central worths of the materials in Assembly 48 with the computed worth. Set 22001, cross section for

B^{10}, Al, Ta, and Mo were obtained from the ANL-224 set. The cross sections for the remaining isotopes were derived using the MC^2 code from its cross-section library tape and averaged over the fundamental-mode spectrum of the Assembly-48 core composition. In addition MC^2 cross sections were derived for the same materials averaged with zero buckling in the composition of the Assembly-48 blanket and in the composition of the Assembly-48A reflector.

TABLE VI. Experimental and Computed Central Worth (Ih/kg) in Assembly 48

Material	Measured	Set 22001 (22 Groups)	Set 22611 (6 Groups)	Set 22612 (6 Groups)	Set 22614 (6 Groups)
U^{235}	+339 ± 4	+330	+370.4	+362.9	+337.4
U^{238}	-24.8 ± 0.5	-22.2	-23.0	-23.1	-23.1
Pu^{239}	+445 ± 4	+424.2	+457.3	+455.8	+467.5
Pu^{240}	81 ± 20	+46	+28.5	+36.1	+23.8
B^{10}	-8926 ± 80	-7694	-9227	-8802	-9940
SS(304)	-14.1 ± 0.2	-15.5	-15.4	-15.6	-15.3
Fe	-12.3 ± 0.4	-15	-14.5	-14.8	-14.1
Cr	-9.4 ± 0.4	-16	-15.1	-15.3	-16.4
Ni	-18.2 ± 0.2	-20	-4.5	-22.3	-22.4
Al	-15.7 ± 0.8	-20.1	-18.8	-19.2	-18.3
Na	-6.3 ± 0.3	-11.33	-8.96	-8.96	-10.63
C	-4.6 ± 1.2	-8	-9.7	-9.7	+0.7
O	-6.8 ± 0.9	-12.0	-13.6	-13.5	-8.6
Ta	-164 ± 5	-135	-147	-144	-157
Mo	-43.4 ± 0.4	-55	-59.1	-58.3	-60.3

Using these cross-sections and the MACH 1 diffusion code, the critical radius was found for a spherical reactor of Assembly-48 composition in both the core and a 30-cm blanket having a small sample-holding region in the center. The change in k_{eff} was then computed for samples of the same mass and density as the actual samples used in the experiment. A solid cylindrical or cubical experimental sample was replaced in the computation by a solid sphere, and a cylindrical annular sample was replaced by a spherical shell of the same thickness.

The experimental worths of materials and those calculated by set 22001 agree to within about 30% except for Pu^{240}, Cr, O, C, and Na.

The 22-group set 22001 is collapsed into six groups using the MACH 1 code with the group structures given in Table VII. The worths of the materials using these sets are shown in columns 3, 4 and 5. Comparison of the worths of materials computed with sets 22614 and 22001

show agreement to within 20% except for Pu^{240}, B^{10}, C, and O. Set 22611 compares to within 20% except for Pu^{240}, Ni, and Na. Finally, set 22612 gives material worths all of which agree with those of set 22001 to within 20%.

TABLE VII. Description of 6-group Set Structures

Set	Distribution of 22 Groups among 6 Groups	Lower Energy Limit (eV)
22611	1-3	1.35×10^6
	4-7	1.83×10^5
	8-10	4.09×10^4
	11-14	4.31×10^3
	15-20	2.75×10^2
	21-22	2.90×10^1
22612	1-3	1.35×10^6
	4-7	1.83×10^5
	8-11	2.48×10^4
	12-14	4.31×10^3
	15-20	2.75×10^2
	21-22	2.90×10^1
22614	1-3	1.35×10^6
	4-7	1.83×10^5
	8-11	2.48×10^4
	12-14	4.31×10^3
	15-18	9.61×10^2
	19-22	2.90×10^1

In constructing the 6-group set the perturbed worths were computed with the 22-group set in three regions of the spherical core. Region 1 was a centrally located sphere 7 cm in radius. Region 2 was taken to be a spherical shell 5 cm thick and having an outer radius of 30 cm. Region 3 was a spherical shell 5 cm thick having an outer radius coincident with the core boundary at 47 cm. The object was to define a coarse structure which best simulates the overall capture, fission, scattering, and leakage components of reactivity when compared with the 22-group components. Results for the group structures of Table VII have been computed. They corroborate the information noted in Table VI but give a more detailed view of the competing processes.

The set 22612 will be used in the SNARG-2D code for the preliminary analysis of the FFTR control-rod critical experiments. It is planned that the choice of this cross-section set will be re-evaluated when the ENDFB cross sections in MC^2 format becomes available.

At that time finer structured sets (seven or eight groups) will be explored in an attempt to improve agreement between experimental and computed reactivity change.

c. Proton Recoil Spectrometer. An improved proton-recoil neutron spectrometer is being constructed for use in ZPR-3. The system is basically similar to that of Bennett,[1] but utilizes improved amplifiers and a computer that replaces a conventional two-parameter, pulse-height analyzer.

[1] Bennett, E. F., Fast Neutron Spectroscopy by Proton-recoil Proportional Counting, Nucl. Sci. Eng. 27, 16 (1967).

The preamplifier[2] is a pole-zero-corrected, charge-sensitive device that uses two field-effect transitors in parallel for the input stage. The linear amplifier is a delay-line type which is matched to the preamp so as to allow recovery from 1000 times overload in 35 μsec or less. The fast amplifier, differentiator, and stretcher will be essentially those used by Bennett.

A dual, 4096-channel analog digital computer (ADC) interfaced to an on-line computer will be used as a two-parameter analyzer. The computer will have an 18-bit word length and a memory capacity of 8192 words. The signals from the ADC's will be sorted and divided on-line before being stored, and a Tektronix memory scope will be used to monitor the computer memory.

Spectrum measurements in plutonium-fueled cores have presented great difficulties due to the high gamma background. It is believed that this electronic system will improve spectrum measurements for these cores.

d. ZPR-3 Interface Correction. To define the limits of precision of ZPR-3 experiments more narrowly, a re-examination has been made of many corrections and assumptions applied in the past. Within the last few months, several experiments have been done to define precisely the interface correction for Assembly 48.

The drawers most commonly used in ZPR-3 are made of perforated stainless steel, 1/32-in. (0.79 mm) thick. Thus with the halves closed, the fuel in half No. 1 is separated from that in half No. 2 by 2/32 in. of about 53%, Type 304 stainless steel. There are other gaps in the fuel columns, but in a large core these are likely to be fairly well distributed throughout the length of the columns.

For these experiments, a dial gage was mounted at the top of the assembly, where it would measure the last 1/2 in. of separation. The assembly was loaded to be slightly supercritical with the halves together, and the reduction in reactivity due to various gaps was measured, mostly by subcritical-multiplication techniques. The gaps included air spaces, a solid stainless steel sheet, and several thicknesses of stainless steel, perforated with 1/4-in. holes spaced such that their average density was 4.49 gm/cc, or 57.2% of normal.

The experimental data are given in Table VIII. Here both the measured (dial gage) and the expected (sheet thickness) separations are tabulated. Figure 6 illustrates the results for the measured separations

[2] Larson, J. M., Electronic Components for a Proton-recoil Spectrometer, USAEC IDO Report in preparation.

plotted against reactivity loss. If the thicknesses inserted had been used as abscissa, the slope of the four points using perforated inserts would be slightly steeper. All the experimental separations listed in the table are in addition to the normal 1/16-in. interface gap.

TABLE VIII. ZPR-3 Gap Worths

Dial Gage Separation (in.)	Gap Medium	Measured Thickness of Insert (in.)	Reactivity Loss with Respect to Normal Closure ($\Delta k/k$, %)
	Measured Values		
0.0009	Air		0.0016
0.0248	Air		0.0634
0.0415	57.2% SS	0.031	0.0577
0.0448	Air		0.0933
0.0696	57.2% SS	0.0575	0.1051
0.0960	Air		0.1727
0.1363	100% SS	0.1220	0.1986
0.1373	57.2% SS	0.1263	0.2114
0.1450	Air		0.2854
0.1947	Air		0.3703
0.2935	Air		0.5319
	Calculated Values		
0.060	60% SS		0.120
0.180	60% SS		0.360
0.060	(homogenized)		0.070

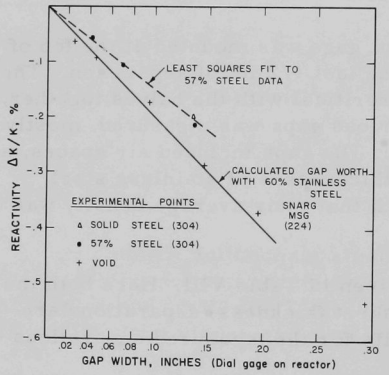

Fig. 6.

Worth of ZPR-3 Interface Steel. (The origin represents normal closure, with the drawer front material filling the interfacial gap. It is a point in each experimental series. The calculated curve is also normalized at this point.)

Also given in Table VIII are calculated values of gap worth. The SNARG-ID transport code in slab geometry was used in S8 approximation, using the Modified Single Gaussian (MSG) quadrature parameters suggested by Meneghetti.[3] This quadrature emphasizes detail in the transverse direction and is applicable to problems involving thin transverse slabs. Argonne cross-section set 224 was used. The differences between the reference problems and the two gap problems are shown in the table. The last calculation tabulated is the case for which the materials of the 0.060-in. gap are spread homogeneously through the core materials and the whole mixture is expanded inward to fill the gap. This corresponds to the manner in which ZPR-3 compositions are normally reported, and is seen to differ by only +0.05% from the corresponding heterogeneous gap.

The 0.05% figure can be reduced even further if one takes into account the fact that the calculations in general have overestimated the effect of the gap. Comparison of the calculated with the experimental line in Fig. 6 shows that the calculated slope is perhaps as much as 30% too steep. Thus the difference between the homogenized gap and the corresponding interface is closer to 0.02 to 0.05% $\Delta k/k$.

The experimental points yield about 1.50 ± 0.05% $\Delta k/k$-in. for gaps filled with perforated stainless steel. Calculations made as described yield about 2% $\Delta k/k$-in.

The criticality correction to eliminate the gap and reduce core length in Assembly 48 to 30 in. is +0.1% $\Delta k/k$.

The correction to homogenize the gap materials throughout a uniform 30.06-in. core is between +0.02 and +0.04% $\Delta k/k$ (after making some allowance for the fact that the calculations seem to overestimate the gap worth by about 30%).

Comparison with an earlier study (EBR-II mockup) shows that the correction decreases with increasing size of assembly. The ZPR-9 Assembly-4 experiments[4] produced a smaller gap effect than the EBR-II experiments, indicating that composition of core and reflector are also important factors.

2. ZPR-6

The series of Doppler measurements planned for Assembly 5 of ZPR-6 has been completed. The results, which have an experimental precision of 0.001 Ih/kg U or Pu, are shown in Table IX. These measurements are of the single-sample reactivity type previously made on the ZPR-6

[3]Meneghetti, David, Discrete Ordinate Quadratures for Thin Slab Cells, Nucl. Sci. Eng. 14, 295 (1962).

[4]The Progress Reports for February 1965, ANL-7016, and for August 1964, ANL-6936, contain reports of measurements of ZPR-9 gap worth.

and -9 assemblies. The measurements with the expanding natural UO_2 sample and with the expanding and nonexpanding enriched UO_2 samples were made to compare with the previous results obtained in the small zoned versions of Assembly 5, Assemblies 4Z (of ZPR-6), 11, and 12 (of ZPR-9). These results confirm the sufficiency of the spectral matching in these zoned assemblies to that of the full-size Assembly 5, in that adjustment of the zoned results for differences in the perturbation denominator predict the full-size results. The plutonium measurement is tentatively interpreted as indicating a negative Pu^{239} Doppler effect in this spectrum. However, the reactivity effect of expansion is quite large in this sample, so that final interpretation must be delayed until reproducibility checks are made and a systematic intercomparison of expanding and nonexpanding sample measurements is carried out.

TABLE IX. Results of ZPR-6 Assembly-5 Doppler Measurements

Date of Measurement	Sample No.	Nominal Dia and Length (in.)	Material	Enrichment (%)	Total Mass (kg)	Sample Type[a]	Measured Reactivity Change versus Temperature (464 Ih = 1% Δk/k) Temp (°K, Ih/kg U or Pu) — Data normalized to 0.000 Ih/kg at nominal room temperature and uncorrected for expansion.				
2/16/67	N1	1 x 12	UO_2	Natural	1.116	FE	293	492	687	293	878
							0.000	-0.109	-0.184	+0.001	-0.241
							1061				
							-0.291				
2/24/67	HE8	1 x 12	UO_2	97.7	0.9133	FE	293	428	612	839	1058
							0.000	+0.021	+0.039	+0.048	+0.049
2/27/67	HE10	1 x 12	UO_2	97.7	0.8071	NNE	293	339	370	395	428
							0.000	+0.010	+0.014	+0.020	+0.025
							469	486	578	774	958
							+0.029	+0.034	+0.040	+0.053	+0.060
3/6/67	PuINV2	1 x 12	PuO_2	88.6 w/o 239 11.4 w/o 240	0.9347	NNE	311	353	398	426	457
							+0.000	-0.016	-0.021	-0.030	-0.028
							483	522	595	717	857
							-0.034	-0.039	-0.050	-0.066	-0.086

[a]FE--freely expanding; NNE--constrained axially and radially.

3. ZPR-9

Assembly 16, the third of four softened-spectrum assemblies proposed to investigate the systematics of the U^{235} Doppler coefficient, is now installed. This assembly has the same volume fraction of polyethylene as Assemblies 13 and 14 (see Progress Report for January 1967, ANL-7302, pp. 34-35, and for February 1967, ANL-7308, pp. 17-18) but 5.3 v/o of the depleted uranium in Assembly 13 has been replaced with carbon. Table X shows the central material worths in Assembly 16. Doppler measurements are currently being made.

TABLE X. Assembly 16 Central Worths

(1% Δk = 428.074 Ih)

Sample	Weight (g)	SS Can Weight (g)	Net Worth (Ih)	Experimental (Ih/kg)	Calculated (Ih/kg)
Mo	598.8	-	-12.834 ± 0.02	-21.43 ± 0.04	-28.27
Ni	546.1	-	-6.985 ± 0.02	-12.79 ± 0.04	-11.30
Fe	484.3	-	-2.925 ± 0.02	-6.040 ± 0.05	-5.055
Be	114.3	-	+6.502 ± 0.02	+56.9 ± 0.2	+72.15
C	102.0	-	+1.809 ± 0.02	+17.7 ± 0.2	+14.80
Al	167.1	-	+0.166 ± 0.02	+1.0 ± 0.12	+2.247
Na	51.38	56.42	+0.087 ± 0.02	+1.7 ± 0.3	+5.021
W	1108	-	-33.25 ± 0.35	-30.01 ± 0.32	-
Ta	924.7	27.54	-57.48 ± 0.35	-62.16 ± 0.38	-
B	75.2	20.6	-82.05 ± 0.35	-1090 ± 5	-5625
Poly	58.988	-	+28.80 ± 0.23	+488.2 ± 3.9	+580.4
Poly	13.70	72.32	+7.536 ± 0.02	+550.1 ± 1.4	+580.4
Depleted Uranium	1155	-	-10.616 ± 0.02	-9.191 ± 0.02	-15.918
Enriched Uranium	18.17 total	-	-	+143.6 ± 0.0	+112.5[a]
	16.93 U^{235}	72.32	+2.610 ± 0.02	+154.2 ± 1.1	+121.5
SS	481.0	-	-3.983 ± 0.02	-8.28 ± 0.04	-6.073
SS Can	72.38	-	-0.712 ± 0.02	-9.8 ± 0.3	-
B_4C	59.62	64.70	-49.91 ± 0.35	-837.1 ± 5.9	-4399
Al Can	26.36	-	+0.035 ± 0.02	+1.3 ± 0.8	-
Pu^{239}	115.53	19.77 SS 7.05 Al	+22.99 ± 0.23	+199.0 ± 2.0	+178.6

[a]Adjusted for U^{238} in sample.

4. Plutonium Conversion for ZPR-6 and -9

An Architect-Engineer, Sverdrup & Parcel and Assoc., Inc., of St. Louis, Missouri, was selected in December 1966 to prepare Title I (conceptual design) and Title II (detailed design) for a confinement shell to go over both the ZPR-6 and -9 reactor cells. The conceptual design includes the design of the confinement shell around both reactor cells, the addition of a new plutonium and uranium storage vault, modifications to the air-conditioning system, and an emergency sand filter system. The final Title I report has been completed and received by the Laboratory, and the A-E was authorized to proceed on Title II (detailed design).

A Preliminary Safety Analysis Report (PSAR) for the utilization of plutonium and U^{233} fuels with ZPR-6 and -9 was submitted to the Commission

for review in August 1966. Commission reviewers requested formal answers to a series of questions on the PSAR. A supplement to the PSAR entitled "Answers to Questions on the PSAR on the Use of Plutonium and U^{233} on ZPR-6 and -9" has been prepared and submitted to the Commission. The detailed design of the modifications to the facility should be completed about June 1967. Construction of the modifications could start in early FY 1968, depending upon the date of approval of the PSAR.

5. ZPPR

a. General. The construction contractor has increased his working force in an attempt to get back on schedule of work in the reactor cell area. The concrete for the reactor cell floor and pit has been poured, as well as for the blanket storage room floor. The usual placing of backfill, wall finish, lighting fixtures, and ventilation ducts is continuing.

The contractor submitted his first proposal for storing the bed and tables on March 17. Informal meetings were held with the contractor on five succeeding days relative to his proposal for storage of the units. The handling procedure for the removal of the bed and tables from the low-bay trailers was received on March 27, and the large section of the bed was delivered to the contractor on that date. It was placed on the storage-support structure in the reactor pit the same day. The short section of bed and two tables were delivered the next day and placed on the storage-support structures. A 2-in.-thick, weather-proofed wooden roof was placed over the units. Side protection will be placed after a 7-in.-thick wooden impact shield is formed over each unit. Inspection, for moisture particularly, will be made periodically on the units.

The present status of the reactor components is as follows:

Matrix Drawers: The remaining 280 normal front drawers were received and accepted. The vendor scrapped the narrow drawers made for the poison safety blade locations and has started refabrication.

Poison Rod Drives: The vendor has all material for the poison rod drives and is now assembling the units. An ANL representative visited the vendor to review his progress on March 22.

Personnel Shields: All items for the personnel shields have been received by the vendor except the ball screws, boron paint, and the tractor drives. The ball screws and paint were to be shipped by the manufacturers on March 31. Delivery of the tractors was scheduled for the middle of June. The vendor's progress was reviewed at his plant by an ANL representative on March 22.

Matrix Alignment: The casting patterns are made and are ready to be poured.

Source Drives: Preliminary tests at the vendor's plant on the mechanisms of the drives were satisfactory. Preparations are being made to fill the neutron shield with borated paraffin.

Rod Drive Mounting Plates: During the rough machining of the repoured plate, three large gas pockets were uncovered. Discussions with the vendor indicated that the pour was made at too low a temperature. An ANL representative visited the plant on March 29 while a new casting pour at high temperature was made.

Fuel, Control and Safety Rod Drawers and Ball Joint Assemblies: The reworked machined parts of the drawer assemblies have been received. An ANL representative visited the vendor on March 22 to discuss rework of the sheet metal drawers. The vendor stated he could not rework the drawers to the required specifications and asked to be relieved of supplying these particular items, with no cost to ANL. Bids have been sent out and have been received from other manufacturers. These bids are now being reviewed.

Poison Safety Blades and Sheaths: The blades and sheaths have been received, checked, and accepted. The clevis used for connecting the blades was not within specifications and was returned to the vendor for rework.

Boron Fabrication: The order for preparing the boron carbide plates has been placed with Cerac Hot-Pressing Inc., Menomonee Falls, Wisconsin.

Stack Gamma Monitor: The stack gamma monitor has been shipped without the alarm bell, which is on backorder.

Stack Particulate Monitor: Checkout of the monitors indicates a faulty mechanical clutch on a sample pump. Repairs are being made and further checkout will be made.

b. Fuel Development. Two hundred and thirteen plate-type fuel elements were manufactured for zero-power reactor physics experiments. The plutonium fuel was obtained from highly irradiated material and contains 22% Pu^{240}. The elements consisted of Pu-1 w/o Al fuel cores in Type 304 stainless steel jackets.

During this reporting period, ninety-five 3 x 2 x 1/8-in. elements, seventy-eight 2 x 2 x 1/8-in. elements, and forty 1 x 2 x 1/8-in. elements were shipped to the Idaho Division to complete the fabrication program.

Concern existed that residual fuel core cleaning liquid in the elements would cause element pressurization and jacket bulging during extended use. During the reporting period, heating tests were conducted on five 3 x 2 x 1/8-in. elements to determine whether any liquids were present. The elements were heated to 100°C and held at temperature from 10 to 40 hr. Distortion of the element side panels occurred. After cooling, the elements did not pass through the parallel-plane inspection gage.

Two of these elements were heated to 300°C and held for 30 min. Excessive jacket bulging was observed during heating, but near 300°C the bulges began to decrease rapidly. One element decreased 0.028 in. in thickness while at temperature. After cooling, both elements passed through the inspection gage. A leak test was made and indicated that the elements were leak tight. A second 300°C heating cycle was applied and an insignificant amount of bulging was observed.

It was concluded that stresses were induced in the element jackets during welding. Partial stress relief occurred when elements were heated to 100°C, causing jacket panel distortion. Additional stress relief at 300°C caused the jacket panels to return to an undistorted geometry. Pressure calculations were made which indicate that liquids were not present in the elements in more than submilligram quantities.

(i) Programmatic Requirements. Experiments in ZPPR and other zero-power reactors require fabrication of 10,300 kg of stainless steel-jacketed, U-28.3 w/o Pu-2.5 w/o Mo fuel elements containing 2900 kg plutonium. The plutonium in these elements will be approximately 88% fissile. An additional 500 kg of 88% fissile plutonium will also be fabricated as uranium-plutonium oxide to study the effects of oxide dilution on reactor physics. Approximately 190 kg of plutonium containing 30% Pu^{240} will be fabricated as uranium-plutonium molybdenum alloy to study the effects of plutonium isotopic concentration.

Ideally the concentration of fissile plutonium and alloying elements should be held constant in the fuel elements of different isotopic composition. In order to do this, the 30% Pu^{240} alloy will be of U-36 w/o Pu-2.5 w/o Mo composition. Experimental determination of the fabricating and physical properties are required to ascertain that this alloy is suitable for fabrication and use in ZPPR fuel elements. The preparation of specifications for fabrication of the special isotopic composition elements will be based upon these experimental determinations.

The oxide elements present additional problems. The composition, form, and design of the oxide elements is influenced by experimental conditions. It presently appears that part of the oxide should be fabricated as high-density plates and part as oxide-fueled rods to allow

greater experimental flexibility. The experimentalists also require a close control, or precise knowledge of, the oxide-metal ratio, the uranium-plutonium ratio, and density and weight of the oxide elements. The effects of fuel-element composition and design and the variations that can be tolerated in the oxide-fuel elements are presently under study.

(ii) Ingoting of Plutonium. Because of the large quantity of plutonium required for the ZPPR program, it must be obtained from different sources, and it varies widely in isotopic composition. Isochem Incorporated, Richland, Wash., has received a contract to blend the plutonium to an 11.5% ± 0.5% Pu^{240} composition, to cast it into ingots weighing approximately one kg each, and to supply analytical information on each melt of the plutonium cast. The fuel-element fabricators will further reduce the compositional variations by making up the alloy to a uniform 25 w/o of Pu^{239} + Pu^{241}. As of March 28, Isochem had blended approximately 455 kg of plutonium, of a total 1400 kg to be produced as blended ingots by June 30, 1967. About 50 kg of this material has been shipped to the Rocky Flats Division of Dow Chemical Company.

(iii) Fuel-element Fabrication. Experiments in FY 68 require that 4000 kg of the U-28.3 w/o Pu-2.5 w/o Mo fuel elements, containing 1100 kg of plutonium, be fabricated by March 1, 1968. In order to assure that the fuel elements will be available, arrangements have been made for fabrication of 700 kg of plutonium into alloy fuel elements by the Rocky Flats Division of the Dow Chemical Company by methods developed at ANL. This plant has previously fabricated zero-power reactor elements for ANL and has most of the facilities that are required. As of March 23 the casting line for the preparation of a uranium-molybdenum alloy was essentially ready to operate. The glovebox line was nearly ready for the casting of fuel plates. A machining glovebox line was under design, and milling machines for this line were scheduled for delivery in April. Preliminary designs were ready for ANL review of fixtures, gages, and tooling. A proof-of-process run was scheduled for May and June, and production fabrication of the fuels is scheduled to begin in July 1967, and proceed through January 1968 at a rate of 100 kg Pu per month. If a commerical fabricator cannot be obtained by the start of the Rocky Flats production, a second shift can be activated there for the full March 1, 1968 programmatic requirement.

Negotiations are continuing with Nuclear Materials and Equipment Corporation to deliver fuel elements containing 555 kg of plutonium by March 1968 with options for additional fabrication, and bids have been solicited by the AEC for the second commercial source of the ZPPR fuel elements, for the period following 1968.

(iv) Fuel-element Jackets. The fuel-element jackets consist of rectangular stainless steel sleeves, of 0.015-in. wall thickness, formed to precise cross-sectional dimensions. The manufacturers of formed tubing

were unable to bid this item because the conventional drawing and Turk's-head forming methods do not provide the uniformity of wall thickness required. Argonne National Laboratory developed a method of stretch forming the tubing into a precision die box by means of a wedge expended mandrel which produced the required cross-sectional precision but did not result in thinned or over-worked corners that were produced by conventional drawing operations.

A contract for precision-welded and drawn, Type 304L stainless steel, round tubing with a 0.016-in. wall was let to Pacific Tube Company. The first deliveries of this tubing are scheduled for April 1967. Production tooling for stretch forming the round tubing into the jacket-sleeve shape has been made in ANL shops and orders have been placed with ANL shops for an initial run of jacket sleeves. Process and product specifications have been prepared for the forming process of the jacket sleeves and it is hoped that commercial fabricators can be obtained that will perform this jacket sleeve forming operation. The initial order being formed in ANL shops will be used for demonstration of the process to the prospective fabricators. ANL production can continue if the commercial fabricators do not show interest. Deliveries of jacket sleeves are scheduled to begin in May and to continue through December for the March 1, 1968 fuel-element requirements.

(v) Doppler Specimen Manufacture. The Doppler effect of reactor fuels are being investigated. Thirty-two elements containing PuO_2, PuO_2-UO_2, and UO_2 in capsules of 0.5- and 1-in. nominal diameters for use in the above program are being fabricated. The specimens consist of columns of oxide granules vibratorily compacted into Invar or Inconel jackets.

A furnace used for sintering oxide granules malfunctioned in such a manner that it was out of service during the entire reporting period. In the meantime, work continued on the tableting and granulation of oxides. To date the following weights of -40 +80 mesh granules have been made and stored preparatory to firing: 11 kg of PuO_2, 4 kg of PuO_2-50 w/o UO_2, and 3.5 kg $U^{233}O_2$. This represents about 80% of the material required to complete the task.

A set of contact plates required to correct the furnace malfunction has been made by Central Shops and delivered. Preparations are now under way to install the plates in the furnace and reassemble the heater, which rests on the plates.

C. Other Fast Reactor Physics

1. Burnup Measurements for Fast Reactors

The program for the development of analytical methods for the determination of burnup of fast reactor fuels and for the measurement of fast fission yields continues. The status of the investigation of a method that uses an EDTA titration of the total rare earth group to monitor burnup was reported in the Progress Report for September 1966, ANL-7255, p. 19. A combined separation-titration procedure in which lanthanum was used as a stand-in for the rare earth group gave very satisfactory results.

Attempts to apply this procedure to a mixture of rare earths having the composition expected in a nuclear fuel yielded results as much as 20% low. Since it has been reported that under certain conditions cerium (IV) can polymerize in acid solution, the various steps of the procedure were reviewed to see if at some point(s) cerium polymerization might have occurred. It was concluded that conditions in the procedure were conducive to polymer formation. Subsequent experiments have confirmed this conclusion.

By altering several steps in the procedure, the results have been improved markedly. Further elucidation of the behavior of cerium will be necessary before the procedure can be modified to insure that cerium will be separated with the other rare earths and will behave like the other rare earths in the titration.

D. Component Development

1. Sodium Technology and Development

a. In-core Flowmeter. So that sodium flow through individual subassemblies or process tubes can be measured, technology will be established to assure that small magnetic, turbine, or other types of flowmeters can be obtained for use in severe temperature and radiation environments. To demonstrate performance and reliability, prototype flowmeters will be tested out-of-pile and in-pile.

The report on the initial evaluation of in-core flowmeters has been drafted.

(i) Thermal and Mechanical Tests of Magnet Materials. Thermal tests of Alnico-V magnetic material continue. A second rod magnet having a length-to-diameter ratio (L/D) of 6 was thermally stabilized by subjecting it to five thermal cycles to 1300°F instead of the specified three. Within experiment accuracy, this magnet behaved exactly as did the first during the first three thermal cycles (see Progress Report for February 1967, ANL-7308, pp. 24-25), that is, noticeable changes in remanence were still occurring--but on the fourth and fifth thermal cycles, the residual flux did not change from that after the third cycle.

This second rod magnet has accumulated 270 hr operation at 1200°F and has performed exactly as the first magnet did; the first magnet has now accumulated 440 hr operation at 1200°F and is still producing the initial stabilized flux at room temperature within the accuracy of the gaussmeter. There is again an indication of random flux changes less than +2% of the full-scale reading or ±20 gauss.

Rod magnets of Alnico-V, -VI, and -VIII for both the out-of-pile and in-pile tests have been ordered directly from the manufacturers.

(ii) Magnetic Flowmeter Prototype. The internal impedance and magnetic-flux density of the preliminary prototype flowmeter were checked before the flowmeter was installed in the calibration loop.

(iii) Magnet Irradiation Tests. Calculations have been completed for estimating the radioactivities and dose rates from rod-type magnets to be irradiated in EBR-II. With EBR-II operating at 45 MW(th), total neutron doses of 2×10^{21} to 2×10^{22} n/cm^2, and the normal 10-day sample postirradiation cooling time, only the Co^{58} [from $Ni^{59}(n,p)Co^{58}$], Co^{60}, and Fe^{59} activities are important for Alnico materials. The gamma heating rates in the Alnico during irradiation were also estimated.

b. Fuel-pin Thermocouple. A preliminary report on previous experience with fuel-pin thermocouples has been drafted.

The vendor has not supplied the spectrochemical analysis of the 99.9%-vitrified-thoria insulators, so measurements of the electrical properties have not begun.

For study of the compatibility of tantalum and W-25% Re with UO_2, a tantalum capsule was assembled with UO_2 fuel and dry stagnant helium at slightly less than 1 atm pressure. After the capsule was kept at 2000°C for ~33 hr, it was both visually and hermetically intact, and no gross reaction was visible externally. Sectioning revealed no gross reaction; metallographic examination is being made. An identical capsule will be tested at 2400°C.

All needed information has been received on the reactors being considered for the initial in-pile tests of the thermocouples; evaluation is underway and a recommendation as to which reactor to use is imminent.

E. Fuel Development

1. Metal Fuels

a. Studies of Uranium-Plutonium Alloy Fuel Performance. Transverse macrosections of the U-Pu-Zr fuel of elements irradiated in EBR-II to about 5 a/o burnup of the U + Pu at a maximum jacket temperature of 630°C were reported (see Progress Report for February 1967, ANL-7308, p. 27) to show bands thought to be correlated with phase transformations. A fuel pin of U-Pu-Zr and one of U-Pu-Ti, each in V-20 w/o Ti tubes and irradiated at maximum jacket temperatures of 540°C to estimated burnups of 5.0 a/o, were then being prepared for shipment to ANL, Illinois. Irradiations of two similar elements were to be continued to an estimated burnup of 7.5 a/o.

Of 16 experimental fuel elements with U-Pu-Zr pins (U-15 w/o Pu-9 w/o Zr or U-15 w/o Pu-12 w/o Zr) severally jacketed in V-20 w/o Ti, Types 304 and 316 stainless steel, and Hastelloys -X and -X-280 (see Progress Report for December 1966, ANL-7286, p.23), two have been removed from Subassembly XA07 of EBR-II; some are still undergoing postirradiation examination. All fuel elements were intact, though somewhat bowed, but the fuel pins had increased in length about 1.9%, had become elevated about 0.20 in. above the bottom closures, and most had sustained one or two separations (see Progress Report for January 1967, ANL-7302, p. 47). Fission gas sampling was completed in March, and six elements remain to be destructively examined.

Neutron radiographic examinations have been completed on a U-15 w/o Pu-10 w/o Zr element and on a U-15 w/o Pu-10 w/o Ti element removed from EBR-II Subassembly XG06. Both elements had been irradiated to approximately 5 a/o burnup at linear heat ratings near 10 kW/ft, and with maximum jacket temperatures of 540°C. The radiographs show that the U-Pu-Zr alloy fuel pin elongated 3.60% within the V-20 w/o Ti alloy jacket. Part of the total elongation (~0.7%) resulted from an axial fuel separation near the mid-length of the element. The U-Pu-Ti alloy fuel pin elongated a total of 8.80%, including an elongation of 2.35% around and above the upper fuel restrainer. The jackets on both fuel elements appeared to be intact. Similar differences in the axial elongation of U-Pu-Zr and U-Pu-Ti alloy under irradiation were previously noted in capsule irradiations of the two alloys (see Progress Report for October 1966, ANL-7267, p. 35).

Encapsulation is largely completed on the M-3 group of experimental fuel elements, preparatory to insertion in EBR-II. These elements consist of U-15 w/o Pu-10 w/o Zr alloy in jackets of Types 304 and 316 stainless steel, and V-20 w/o Ti alloy. They are similar to the XA07 group but are scheduled for irradiation to higher burnups than those reached by the XA07 group.

The status of the alloy fuel elements in EBR-II remains unchanged from last month, owing to shutdown of the reactor.

b. Modifications of Injection-casting Furnace. An injection casting furnace has been modified to permit operation at higher temperature and to increase furnace capacity. This was done by replacing a copper coil with a tungsten induction-coil assembly. The copper-coil assembly, which has been successfully used for five or six years, is temperature limited. Gradual increases in casting temperature over the last few years have been met by placing thicker insulation layers between coil and melt. When casting temperatures of about 1500°C became necessary to process U-Pu-Zr alloys, the insulation required reduced the furnace capacity to about 12 pins per melt. Despite the efforts at insulating the coil from the melt, copper vaporized from the coil and deposited on cold surfaces necessitates continuous maintenance to prevent short circuits.

The basic features of the tungsten-coil assembly have been tested in other D-350 furnaces. The geometry is reversed from that of the copper-coil assembly, i.e., the coil is situated inside the heat shields. This orientation produces two advantages: (a) the burden of insulation is between the heat shields and the furnace shell where space is available and (b) better electrical coupling between coil and melt is realized. The heater assembly was constructed outside the hoodlines and installed in the furnace as a unit. The coil is now being tested prior to use.

c. Crucible Development. The demands for increasing alloying and casting temperatures in the fabrication of fuel alloys has limited the selection of crucible and mold materials. Crucible materials, mold materials, and washes for most lower melting alloys have been developed over the last few years. In general, the alloys of uranium and/or plutonium which can be alloyed below 1400°C are made in graphite, alumina, magnesia, zirconia, or thoria. For certain alloys special refractory coatings have been developed for crucible and mold protection. Some of these coatings include magnesium zirconate, thoria, beryllia, and yttria. Higher melting alloys of U-Pu-Zr and U-Pu-Ti have extended the use of developed crucible and mold materials beyond their capabilities and presented fabrication problems. Severe erosion of ZrO_2, Al_2O_3, and coated MgO and graphite crucibles results from their use for the alloying of U-Pu-Zr and U-Pu-Ti at temperatures of 1600 to 1700°C. Oxygen contamination of 1800 to 2000 wt. ppm is common. Injection-casting molds of Vycor glass are being used beyond their softening point, causing a reduction in casting efficiency.

Some special alloying techniques are used to reduce oxygen contamination. One method is to alloy in a series of binary melts to reduce the alloying temperature. Another method is to use arc melting for alloy preparation. The latter method is the most common with commercial fabricators in the production of zirconium and titanium alloys. The major disadvantages of these two special alloying methods is their adaptability to remote fabrication. Part of our program includes the development of fuel alloys for remote fabrication in the EBR-II Fuel Cycle Facility. At the present time this facility is equipped with induction-heated furnaces and uses the injection-casting method for pin fabrication.

During this reporting period work was initiated in cooperation with the Engineering Ceramics Group to solve the imminent problem of crucible materials. Upon search of the literature, we have concluded that a ZrO_2-15 a/o Zr crucible offers promise of success. Tablets of ZrO_2-15 a/o Zr were pressed, sintered, and examined. Small test crucibles were made, and U-10 w/o Zr was melted at 1650 to 1700°C in these containers. Back-up systems of hydrogen-reduced zirconia, gadolinia-stabilized urania, and gadolinia crucibles are included in this work.

The ZrO_2-Zr crucibles were made from ZrO_2 and ZrH powders. The mixture was milled in alcohol with a small quantity of Carbowax 4000 and vacuum dried. The crucibles were formed by dry pressing in a 1-in.-dia die.

Two sintering temperatures were used. The first set of samples was vacuum sintered at 2000°C for 2.5-3 hr. The microstructure showed ZrO_2 grains surrounded with a metal phase. The second set was vacuum sintered at 1800°C. The metal phase in this material appeared as discrete particles dispersed through the matrix. The density of the sintered material was 5.43 g/cc.

The UO_2 and Gd_2O_3 crucibles were formed in a manner similar to that described above. They were fired in hydrogen at 1700 to 1750°C for 4 hr. Their densities were 7.86 and 6.75 g/cc, respectively. These were lower than expected and shall require further study; however, the crucibles were adequate for the present tests.

The preliminary screening tests in the compatibility between crucible materials and U-Pu-Zr alloys was conducted by melting a U-10 w/o Zr alloy. This alloy was selected so that the tests could be made outside a glovebox system. As the tests progress the most promising crucibles shall be tested with a U-15 w/o Pu-10 to 15 w/o Zr alloy. The U-10 w/o Zr alloy was produced by arc melting depleted uranium with crystal-bar zirconium. The uranium and zirconium were chemically cleaned and washed in acetone. The material was remelted several times to produce four homogeneous ingots of 200 g each. All four ingots were sliced into five or more sections. Oxygen analyses showed 280 wt. ppm.

The first compatibility test run with U-10 w/o Zr was made with ZrO_2, ZrO_2-Zr, Gd_2O_3, and UO_2 crucibles. The ZrO_2 crucible was a lime-stabilized insulation brick which was shaped into a small container. The alloy was taken to 1650 to 1700°C in a vacuum of 10^{-5} to 10^{-6} mm Hg and held for 10 min. The total time of the run was one hour.

Visual observations of the four crucibles indicated that the ZrO_2 and the UO_2 material were not wetted by the alloy. The ZrO_2-Zr showed a small amount of wetting, whereas the Gd_2O_3 was completely wet. Oxygen analyses on the alloy melted in ZrO_2, UO_2, Gd_2O_3 and ZrO_2 + Zr revealed 1825, 1300, 1700, and 785 wt. ppm, respectively. Metallographic examination of the alloy material from each crucible is being carried out.

A second test of the same crucible has also been made. In this test larger quantities of material were used and temperature was held for one hour. The results from the two melts are now being assessed.

2. Oxide and Carbide Fuels

a. Studies of Mixed-oxide Fuel Performance. Two fuel elements of stainless steel-jacketed, vibratorily-compacted powders from hypostoichiometric Dynapak UO_2-20 w/o PuO_2 had been irradiated in EBR-II to burnups of 2.7 and 2.9 a/o (U + Pu) at maximum jacket temperatures reported as being 555 and 565°C, respectively (see Progress Report for February 1967, ANL-7308, p.28). The jackets were still intact. The fuel columns were also reported to have elongated about 0.54%, and 65% of the fission gas, corresponding to 224 psi, was found to haye been released from the higher-burnup specimen. Fuel densification and grain growth had occurred in a zone next to the axial cavity, but there was no evidence of plutonium migration. Random metallic inclusions were observed. Use of a more recently

accepted parameter indicates that the maximum jacket temperature was 605°C for the element, SOV-6, being examined. The maximum heat rating was 19.8 kW/ft, as shown in Table XI. (The other element, SOV-5, is being held intact for transient irradiation.)

TABLE XI. ANL Ceramic-fuel Irradiations Removed from EBR-II Experimental Subassembly X009 for Examination

Specimen Number	Design Parameters					Operating Conditions			
	Fuel Composition (w/o)	Effective Density (%)	Cladding Composition	Cladding OD (in.)	Cladding Thickness (in.)	Max kW/ft	Max Cladding Temp (°C)	Estimated Burnup	
								a/o (U + Pu)	fiss/cc x 10^{-20}[a]
SOV-5	UO_2-20 PuO_2	83.4	304 SS	0.296	0.021	19.0	595	2.7	5.6
SOV-6	UO_2-20 PuO_2	83.3	304 SS	0.296	0.021	19.8	605	2.9	6.0
SMV-1	UC-20 PuC	80.0	316 SS	0.306	0.025	25.3	675	2.7	7.2
SMP-1	UC-20 PuC	81.4	316 SS	0.306	0.024	18.9	600	2.1	5.6
VMV-1	UC-20 PuC	85.9	Vanadium	0.301	0.024	29.5	680	3.1	8.9

[a]Based on effective density.

Alpha autoradiographs of metallographic specimens representing the full length of the fuel column failed to show evidence of plutonium migration at any location along the length of the fuel. Some localized areas of low alpha emission, however, indicated that clumping of the UO_2 fraction occurred during preparation of the mixed oxide powder.

Etching the metallographic samples revealed grain boundaries of the coarse columnar grains, as well as those of the finer equiaxed grains. The metallic inclusions previously reported were not attacked by the etching reagent but were shown to be located in the grain boundaries.

The stainless steel upper end closure in contact with the hot fuel at the top of the column showed evidence of surface melting. Stringers of steel were plainly visible penetrating down through cracks in the uppermost part of the fuel column. Globules of steel in this area were similar in appearance to the metallic inclusions noted throughout the structure.

Etching reagents darkened the steel inclusions in the top of the fuel without affecting inclusions elsewhere, indicating a difference in chemical behavior. Preparations are being made to remove fuel samples for electron microprobe examination of the metallic inclusions.

The status of the elements in EBR-II did not change during March, for the reactor was not in operation.

b. Pilot-scale Process Equipment. Development of oxide and carbide fuel includes fabrication capability in the form of vibratory compaction. To achieve this end, development of a process and determination of the effect of process variables have been carried out. The next logical step, that of obtaining pilot-scale fabrication capability, has been started. Process equipment such as a jaw crusher, screens, and a gamma absorptometer have been purchased or constructed. The final step toward

realization of small-scale production is the installation of the process equipment into a suitable glovebox enclosure. This work is now under way.

During the reporting period the fabrications to construct a vibratory-compaction processing line, PF-16, were received from Union Carbide Corporation, Paducah, Kentucky. A contract has been let for the erection of the hoodline and the electrical, piping, and millwright work necessary to provide a completed facility. The hoodline has been erected, and piping and electrical work has started. At this time the installation work is about 10% complete.

c. Performance Studies of Mixed-carbide Fuel. Fission-gas release from pelletized UC-20 w/o PuC solid-solution powder in Type 316 stainless steel was reported (see ANL-7308, p.30) to have been only 2% after irradiation at a maximum jacket temperature of 640°C to a burnup of 2.1 a/o (U+Pu). This element, and one with a similar jacket consisting of vibratorily compacted physically mixed UC-20 w/o PuC irradiated at a maximum jacket temperature of 570°C to 2.7 a/o burnup, did not change significantly in dimensions. An element consisting of vibratorily compacted solid-solution UC-20 w/o PuC powder irradiated in a vanadium jacket at 640°C to 3.1 a/o burnup elongated 0.31% and increased 0.83% in diameter, and the restrainer rod of the element had deflected. Fifteen additional elements, which were under irradiation during February, remained in EBR-II for continued irradiation when operation of the reactor is resumed.

Three elements, listed in Table XI, were subjected to further postirradiation examination in the Metallurgy Alpha-Gamma Hot Cell.

Measurements of fission-product gas release gave the following preliminary results:

Specimen Number	Fuel Description	Gas Release (% of Theoretical)	Max Est (kW/ft)	Estimated Burnup (a/o)
SMP-1	Solid-solution Pellets	2.9	18.9	2.1
VMV-1	Solid Solution, Vib. Compacted	9.0	29.5	3.1
SMV-1	Phys. Mixed Vib. Compacted	13.2	25.3	2.7

An instrument for plotting surface contour was prepared for introduction into the hot cell for use on the pellet rod SMP-1. This instrument will enable determination of possible ridges on the fuel jacket from enclosed fuel pellets.

Rod VMV-1 was sectioned and prepared for metallography. Figure 7 shows a cross section near the center of the fuel column where the cross-sectional area showing sintering is approximately 0.160 in. (65% of the diameter). At a location near the top end, the sintered diameter on the polished cross section was found to be only about 0.090 in. (35% of the diameter). Coring is still visible in original particles outside of the sintered diameter (see Fig. 7). The fact that this structure is visible in some particles but not in others may be due to nonuniformity of the surface as a result of the manner of preparation.

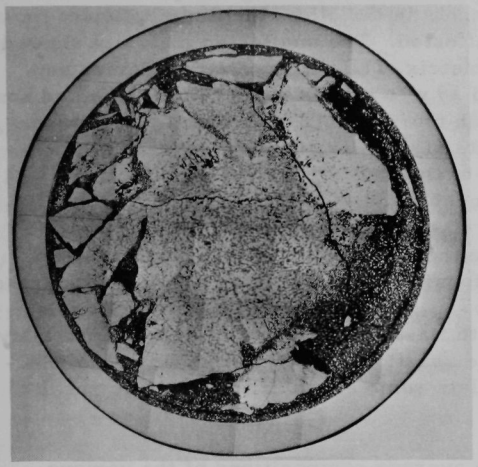

11X

Fig. 7. Cross Section near the Center of Rod No. VMV-1 after Irradiation. As Polished.

d. Compatibility of (U,Pu) Carbides with Potential Jacket Materials

(i) 16-25-6 Alloy Compared with Previous Work.

The stoichiometric (4.83 w/o equivalent C) carbide of U-20 w/o Pu in contact with V-20 w/o Ti at 700°C for 1000 hr was reported (see ANL-7302, pp. 50-51) to form a reaction zone of 10 μ average (35 μ maximum) depth, but one that penetrates the material at grain boundaries an average distance of 50 μ (80 μ maximum). A nonstoichiometric (5.25 w/o equivalent C) carbide of the same alloy formed a reaction zone of 18 μ (55 μ maximum) depth, but one that penetrated the material at grain boundaries an average distance of 65 μ (100 μ maximum).

Earlier compatibility results (see Progress Report for April 1966, ANL-7204, p. 17) on testing (U,Pu) carbide with alloy 16-25-6 (w/o Cr, Ni, and Mo, respectively) had shown a slightly greater affected zone in the jacket material when tested at 800°C for 1000 hr with the hyperstoichiometric composition [~20% $(U,Pu)_2C_3$] compared to the stoichiometric composition. A test of this alloy under the same conditions with a (U,Pu) carbide composition containing 6.75 w/o equivalent carbon [~90% $(U,Pu)_2C_3$] has resulted in a zone identical in appearance with those of the previous tests, but with no significant increase in depth. The average depth of the zone, 28 μ, was, in fact, less than that obtained when tested with the 5.25 w/o equivalent carbon composition. (It should be noted, however, that although both compositions have overall uranium to plutonium ratios of four to one, the plutonium content of the sesquicarbide phase of the two compositions is not equal. The plutonium content of the sesquicarbide phase in the 5.25 w/o C composition has been found to be almost twice that of the monocarbide matrix.)

The affected zone, when etched, appeared to contain a large number of very small precipitates and grain boundaries were absent. A recent electron-microprobe study of the composition of this material showed that among the major elements in the alloy, the distribution of molybdenum was most significantly affected. The unaffected material showed about 3.5 w/o molybdenum in the matrix, while the grain boundaries and spots within grains contained 14 to 19 w/o molybdenum. In the affected zone the molybdenum content was a much more evenly distributed 5 to 7 w/o. The overall iron and nickel contents of the affected zone appeared to be 1 to 2 w/o lower than the contents of the unaffected material, while the relative chromium contents were unchanged.

(ii) Inconel 625. Since the reaction between Inconel 625 and (U,Pu)C at 800°C for 1000 hr was found to be fairly extensive (see Progress Report for October 1966, ANL-7267, p. 38) and appeared to be the same general type of reaction as that with Hastelloy-X, another nickel-base alloy, an attempt was made to analyze the reaction products by means of an electron microprobe in order to correlate some of the metallographic results with compositions.

Table XII lists the average compositions of the various adjacent zones after corrections for matrix absorption and/or enhancement. Percentages of niobium and tantalum (4 w/o total in the jacket material) and carbon (4.8 w/o in the fuel) were not determined. Nickel was the only element from the jacket material that diffused into the fuel side of the original interface but was the major element (54 w/o) in the zone. The mottled reaction zone observed by metallography appeared to be made up of two bands of rather complex composition containing a high percentage (43 to 52 w/o) of chromium. Although no uranium was found beyond the nickel-rich zone in the fuel, an average of 5 w/o plutonium was observed in a portion of the

TABLE XII. Composition of Zones of Reaction for Hyperstoichiometric[a] (U,Pu)C versus Inconel at 625-800°C for 1000 hours

		Zones Identified Metallographically						
		Reaction Zone in Direction of Fuel (36 μ)	Mottled Reaction Zone in Direction of Cladding (26 μ)		Inconel 625 Containing Precipitates (120 μ)			Unaffected Inconel 625 (w/o)
		Average Size of Zones Identified with Microprobe						
Element	(U,Pu)C (w/o)	36 μ	8 μ	18 μ	12 μ	Precipitates	108 μ	
U	76	34	-	-	-	-	-	-
Pu	19	12	1	5	-	-	-	-
Ni	-	54	10	21	61	24	70 → 61	61
Cr	-	-	52	43	20	61	15 → 22	22
Mo	-	-	13	16	7	14	7 → 9	9
Fe	-	-	1	0.5	8	1	4 → 3	3

[a] 5.25 w/o equivalent carbon.

chromium-rich mottled zone. The composition of this mottled zone was not well established, as the elements analyzed totaled only 77 and 86%. Some of the remaining composition can be accounted for by carbon, which was shown by photographs of the carbon X-ray intensity to be relatively high.

In the area of the cladding containing precipitates, three observations were made: (1) a 12 μ band immediately adjacent to the mottled zone was richer in iron than any other portion of the cladding, (2) nickel and iron contents continuously decreased throughout this area from the iron-enriched band to the unaffected cladding matrix, while the chromium and molybdenum contents continuously increased, and (3) the precipitates, which were numerous and very small in size close to the original interface, become less frequent but larger in size as the distance from the interface increased.

(iii) Hastelloy-X. Hastelloy-X has been tested at 800°C for 1000 hr with a (U,Pu) carbide composition containing 6.75 w/o equivalent carbon [~90% $(U,Pu)_2C_3$]. Five zones were found to be associated with the reaction.

On each side of the original interface there were zones identical in appearance to those previously observed in nickel-base alloys: an 8 μ zone on the fuel side, identified as having a high nickel content, and a 6 μ zone on the jacket side, identified as having a high chromium content. In addition, beyond the nickel-rich zone, there was a 5 μ gray layer and beyond this a 25 μ zone, which appears to be monocarbide resulting from reduction of the sesquicarbide phase. The gray layer is probably a uranium-plutonium oxide. The jacket itself was undoubtedly the source of the oxygen; no other surface of the fuel pellet exhibited any oxide formation. The formation of a visible oxide layer as part of the overall interaction in the case of the sesquicarbide phase can be related to the insolubility of oxygen in sesquicarbide.[5] This layer was not found when Hastelloy-X was tested with (U,Pu)C (which has a rather high solubility for oxygen) under the same time-temperature conditions.

On the jacket side, fine precipitates were observed in the Hastelloy-X grains and grain-boundaries to an average depth of 125 μ.

3. Fuel Cladding and Structure

a. Fabricability of V-15 w/o Cr-5 w/o Ti. The preliminary fabricability evaluation of the V-15 w/o Cr-5 w/o Ti alloy (see Progress Report for January 1967, ANL-7302, p. 53) has been completed. Working extruded V-15 w/o Cr-5 w/o Ti and V-10 w/o Cr at room temperature was then reported to require a prior one-hour anneal at 1200°C, but the resulting grain

[5] Storms, E. K., A Critical Review of Refractories, LA-2942, p. 185 (March 1964).

growth of the V-10 w/o Cr was quite pronounced, whereas that for V-15 w/o Cr-5 w/o Ti was slight. Knowledge gained is being applied to the processing of a production-size ingot (AM-101) that has since been consolidated.

The V-15 w/o Cr-5 w/o Ti alloy is more difficult to process than the V-15 w/o Ti-7.5 w/o Cr alloy, probably because of a more segregated or cored ingot structure. The extrusion operation transforms the ingot coring into a banded or stringered structure that hampers further fabrication. The alloy can be processed by conventional means after the extruded structure is sufficiently broken up. Generally, all traces of banding have been eliminated and the precipitate is uniformly dispersed by the time the final product size is reached. The results of homogenization of thermal treatments are being analyzed, both on the as-cast ingot and the extruded products, in an effort to improve the structures and improve subsequent processing.

b. Development of Refractory-Metal Alloys for Service in Oxygen-contaminated Sodium. As reported in ANL-7308, pp. 32-33, vanadium and the alloys V-5 w/o Cr, V-20 w/o Ti, and V-15 w/o Ti-7.5 w/o Cr had been exposed to flowing (6.1-m/sec) sodium containing 8 to 10 wt. ppm oxygen at 550°C for 54 days in continuing tests. All alloys showed small weight gains, but the difference between alloys was much less than at 650°C.

A dynamic test at 550°C (6.1-m/sec velocity) was next interrupted for examination of specimens at 88 days. The samples continued to exhibit small weight gains, the amounts, in mg/cm^2, being: V, 0.16; V-5 w/o Cr, 0.08; V-15 w/o Ti-7.5 w/o Cr, 0.30; and V-20 w/o Ti, 0.30. The specimen surfaces appear metallic with slight darkening. The oxygen concentration was 6.5 wt. ppm by mercury amalgamation and nitrogen was less than 1 wt. ppm in a sodium sample taken at this time.

Samples of a stronger alloy, V-15 w/o Cr-5 w/o Ti, were added to the continuing test.

c. In-reactor Corrosion of Jacket and Structural Materials by Sodium. As reported in ANL-7308, pp. 33-34, the weight losses of V-20 w/o Ti and V-40 w/o Ti samples exposed to EBR-II core sodium for four months are equivalent to removal of about 0.5 mil of surface. Of potential significance is the fact that no hardened layer was formed on the surfaces of these samples.

More recently, specimens of V-20 w/o Ti were nitrided in a dry nitrogen atmosphere at 590°C for periods up to 64 hr and then exposed to sodium at 550°C (cold trap at 170°C) for one week in order to determine if the nitride film would inhibit the formation of the usual subsurface hardened layer. After the sodium exposure, the layer on the 64-hr nitrided

specimen was significantly thinner than on the controls (not prenitrided), but the nitrided sample had nearly twice the weight loss of the control. Further experimentation is planned in an effort to learn why V-20 w/o Ti samples exposed in the EBR-II reactor did not develop a hardened subsurface layer.

4. Fuel Reprocessing

a. Processes for Fast Reactor Fuels. Pyrochemical processing of fast reactor fuels of the ceramic type (e.g., oxide or carbide) clad with stainless steel is being investigated. A conceptual flowsheet currently under investigation has been described previously (see Progress Report for September 1966, ANL-7255, pp. 30-31). The process utilizes liquid metal-molten salt extractions and salt-transport separations[6] for the separation of fissile and fertile constituents of the fuel from the fission products. Recent laboratory investigations of the current flowsheet are discussed below.

The first step after the decladding of mixed oxide (PuO_2-UO_2) fuels is the reduction of the oxide to metal (plutonium and uranium) by a liquid Cu-33 w/o Mg alloy in contact with a molten salt. The alkali, alkaline earth, and rare earth fission products and the solid MgO formed as a byproduct of the reduction reaction remain in the waste salt. The plutonium, uranium, and noble and refractory-metal fission products are transferred into the Cu-Mg alloy; the plutonium is in solution and the uranium is present as a precipitated metal phase. Spent fuel will contain neptunium, presumably as the oxide, which will also be reduced by the liquid Cu-Mg alloy. Therefore, two laboratory experiments were carried out to determine the extent to which neptunium might coprecipitate with uranium.

In the first experiment, U_3O_8 in the form of salt sticks[7] was suspended in a 50 m/o $MgCl_2$-30 m/o NaCl-20 m/o KCl salt mixture. The U_3O_8 was reduced using a liquid Cu-31 w/o Mg alloy which contained about 0.7 w/o neptunium. The system was equilibrated by stirring for 24.5 hr at 700°C. Filtered metal and salt samples were taken periodically following 15-min settling periods. Analyses of these samples indicate that there was a reduction of neptunium concentration in the salt and metal phases with time (from about 0.67 w/o to about 0.48 w/o in the metal phase). If the neptunium was lost because of solid-solution formation with uranium, then small amounts of neptunium in an alloy used to reduce U_3O_8 would be precipitated with the uranium.

---

[6] Salt-transport separations are based upon the selective transfer of fissile and fertile materials from one liquid-metal solution (donor) to another (acceptor) by cycling a molten salt phase which acts as a carrier between the two metal solutions. Noble and refractory-metal fission products remain in the donor alloy.

[7] The salt sticks were cast from U_3O_8 which had been prewetted with the 50 m/o $MgCl_2$-30 m/o NaCl-20 m/o KCl salt mixture.

A second experiment was conducted to observe the behavior of neptunium, using a U_3O_8-NpO_2 mixture containing about 0.4 w/o neptunium. The mixture of oxides was reduced using a Cu-33 w/o Mg alloy and a 16 m/o $MgCl_2$-42 m/o NaCl-42 m/o $CaCl_2$ salt mixture. The oxide mixture was held in a 1/2-in.-dia tantalum cup which was completely submerged in the salt phase. The system was equilibrated at 700°C for 96 hr with no stirring. Analyses of the salt and the Cu-Mg alloy, and of the material remaining in the cup at the end of the run, showed that only 25 w/o of the total neptunium reduced was in the salt and Cu-Mg alloy. Apparently 75 w/o of the neptunium reduced precipitated with the uranium metal. The results of both experiments show that small amounts of neptunium will coprecipitate with uranium.

A third laboratory experiment was carried out to study the reduction of NpO_2 with a liquid Zn-10 w/o Mg alloy, and the distribution of neptunium between a 50 m/o $MgCl_2$-30 m/o NaCl-20 m/o KCl molten salt mixture and the alloy. Data on the solubility of neptunium in the liquid Zn-10 w/o Mg alloy were also obtained. Neptunium oxide, which had been mixed with some of the powdered salt mixture and pressed into pellets, was added to the metal-salt melt which was being mixed at 800°C. The reduction was carried out for 2 hr, after which filtered metal and salt samples were taken at various temperatures ranging from 550 to 750°C to determine distribution coefficients and solubilities of neptunium at each temperature. Figure 8 presents the neptunium contents of the salt and neptunium solubilities in the metal alloy at the various temperatures during the experiment. Figure 9 gives a comparison of neptunium distribution coefficients (K_d = w/o Np in salt/w/o Np in metal) with those of plutonium in a similar system. The distribution coefficient of neptunium varied from 2.3×10^{-3} at 800°C to 7.8×10^{-3} at 574°C. The portions of the lines represented by a broken line are extrapolations to 450°C in all of the figures. The divergence of the distribution coefficients of neptunium and plutonium at low temperatures may provide the basis for a neptunium-plutonium separation. The neptunium-plutonium separation factors as a function of temperature are presented in Fig. 10.

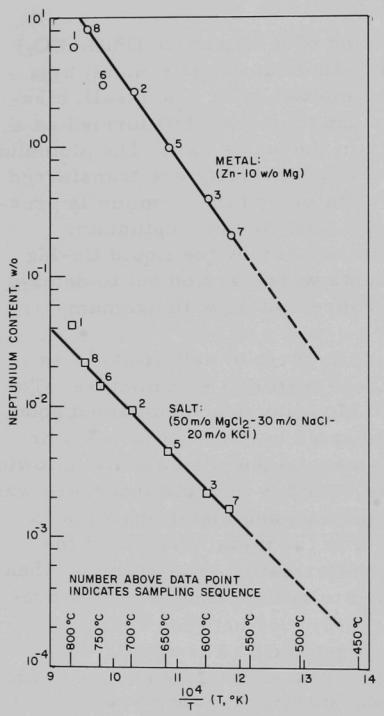

Fig. 8. Neptunium Solubility in Zn-10 w/o Mg Metal Phase and Corresponding Neptunium Content of 50 m/o $MgCl_2$-30 m/o NaCl-20 m/o KCl Salt Phase

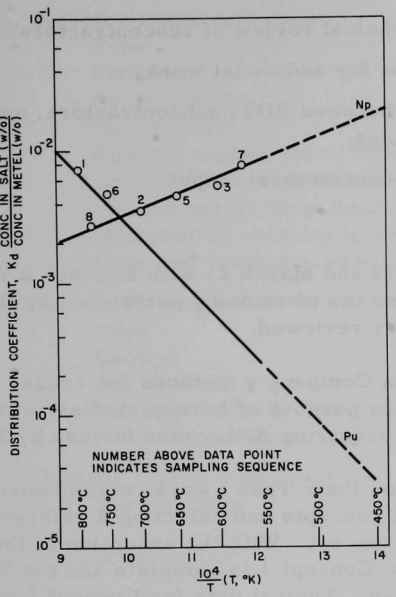

Fig. 9. Distribution of Neptunium and Plutonium between 50 m/o $MgCl_2$-30 m/o NaCl-20 m/o KCl Salt and Zn-10 w/o Mg

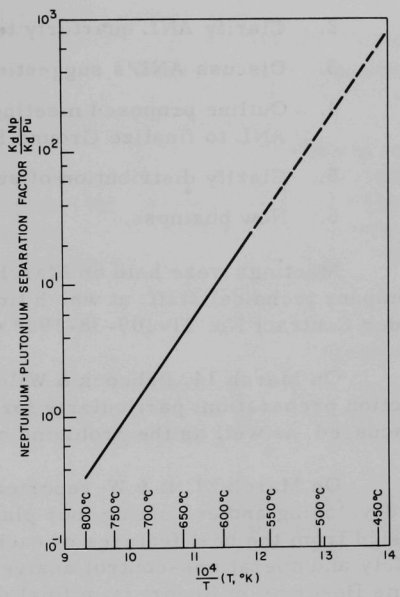

Fig. 10. Neptunium-Plutonium Separation Factor for Neptunium and Plutonium Distributing between 50 m/o $MgCl_2$-30 m/o NaCl-20 m/o KCl Salt and Zn-10 w/o Mg

The experiment demonstrated that neptunium oxide can be effectively reduced by a Zn-Mg alloy, with the reduction limited by the equilibrium distribution of neptunium between the respective salt and metal phases. Neptunium solubility in a Zn-10 w/o Mg alloy is fairly high, varying from 8.1 w/o at 800°C to 0.2 w/o at 574°C, and is comparable to plutonium solubility in a similar alloy. The neptunium-plutonium separation suggested by the divergence of their distribution coefficients at low temperatures would have application in pyrochemical processes currently being investigated.

F. Design Concept Analysis and Advanced Systems Evaluation

1. 1000-MWe Study

A meeting was held at ANL on March 8, 1967 between representatives of AEC-RDT and members of the ANL Project staff. The agenda was as follows:

1. Review ANL proposed procedures for technical surveillance of subcontractors' studies.

2. Clarify ANL quarterly technical review of subcontractors' studies.
3. Discuss ANL's suggestions for additional work.
4. Outline proposed meeting between RDT, subcontractors, and ANL to finalize Ground Rules.
5. Clarify distribution of subcontractors' output.
6. New business.

Meetings were held on March 14 and March 21 with Babcock & Wilcox Company technical staff, at which times the work being performed by them under Contract No. 31-109-38-1998 was reviewed.

On March 14, Babcock & Wilcox Company's methods for cross-section preparation, particularly for the purpose of burnup studies, were discussed, as well as the problems of acquiring ANL codes for use by B & W.

On March 21, B & W reported on their Task I work, which consists of developing and evaluating four plant concepts and selecting a reference design from the best features of each concept. With the exception of the safety and operations-control analysis, Concept 1 is complete and the Systems Description Report is in final draft. Typical data for Concept 1 is as follows:

General	
Reactor Power, Electrical (Net), MWe	1033
Thermal (Total), MWt	2649
Breeding Ratio, integrated (EOL)	1.39
Doubling Time, yr	11.8
Reactor Core System	
Geometry	pancake
Core height, in.	20
Core diameter, in.	149
Average core power density (BOL), kW/ℓ	464
Specific power (kW/kJ fissile material)	859
Max linear heat rate @ 105% power, kW/ft	18.9
Max fuel temp @ 105% power, °F	4500
Max cladding temp @ 105% power, °F	1296
Fuel-pin dia, in.	0.300
Average core burnup, MWd/tonne (U+Pu)	55,200
Core lifetime, full power days	550
Fuel type	vibratory compacted UO_2-PUO_2
Enrichment, w/o fissile plutonium	12
Density, % theoretical	85

Reactor Coolant System	
Type	Pot
Coolant	Sodium
No. of pumps	6
No. of IHXs	6
Reactor coolant flow, lb/hr	100.4×10^6
Coolant inlet temp to reactor, °F	800
Coolant outlet temp from reactor, °F	1100
Max coolant velocity in core, fps	18.8
Core and blanket pressure drop, psi	42
Intermediate Coolant System	
Type	Loop
Coolant	Sodium
No. of loops	6
No. of pumps (36,000 gpm each)	6
No. of steam generators (once-through type)	3
Energy Conversion System	
Turbine type	tandem-compound four flow turbine
Steam cycle	1450 psig/1000°F/NRH

Concept 2 and its Systems Description Report is essentially complete. Concept 3 design work is approximately 75% complete, with the Systems Description Report about 50% complete. Concept 4 has been defined in general terms. It will be of higher performance and of a more advanced design than any of the first three concepts.

The B & W work has been reviewed by the ANL staff for adequacy of techniques and procedures employed in the performance of the work, particularly in the physics area.

On March 15 a meeting was held with representatives of the LMFBR Program Office to discuss the possible ANL suggestions for future work within the general scope of the 1000-MWe Follow-on Studies.

ANL Project Staff visited Westinghouse Advanced Reactors Division (WARD) to discuss detail Program Planning and to cooperate in the establishment of the WARD initial working PERT network. This network has been made available to ANL prior to full contractual agreement.

ANL Project Staff has been increased by one full-time Engineer and by the assignment of specific liaison personnel from Metallurgy, Chemical Engineering, and Reactor Physics Divisions.

During the month a final draft of "Procedures for Project Control and Reporting--1000 MWe Follow-on Studies" was prepared. The objective of

this document is to establish the internal procedures that ANL will follow in the overall planning, organizing, coordinating, technical evaluation, directing, and controlling required to meet successfully the objective of the Project within given technical, schedule, and cost constraints. Rough drafts were prepared of (i) "Commentary on the ANL Summary Report," the objective of which is to define the contents of the ANL Summary Report and to delineate the controls and methodology necessary to achieve, with a minimum of normalization, standardization in reviewing the various subcontractors' Final Reports, and (ii) the outline of "Summary and Evaluation of Research and Development Proposals," the objective of which is to review and establish the merit of the research, development and testing programs recommended by the subcontractors.

Agreement on contract terms has been reached with Combustion Engineering, Inc., and a contract has been prepared for signature. Other contracts are being held in abeyance pending clarification of nontechnical matters.

G. General Research and Development

1. Fast Reactor Core-parameter Study

Self-consistent diffusion-theory calculations were made with the MACH-I code and ANL cross-section set 224 to determine the effect of parametric variation of the thickness of the axial and radial blankets. In the first set of calculations, the radial blanket was held fixed at its reference thickness (38.10 cm) and the axial-blanket thickness was varied. In the second set, the axial blanket was held at its reference thickness (45.72 cm) and the radial-blanket thickness was varied. The observed trend of breeding ratio with core height-to-diameter ratio (H/D) and blanket thickness merely reflects the relative importance of a given blanket for a given core geometry. For example, the increase in breeding ratio with increasing axial blanket thickness becomes increasingly steep as the core H/D decreases.

Sodium-void calculations have been made using the Russian ABN cross-section set. In one set of calculations, σ_p^{238} = 100 b and σ_p^{239} = 100 b; in the other set, σ_p^{238} = 10 b and σ_p^{239} = 100 b. Here σ_p denotes the potential scattering cross section. In both cases, the void coefficient (for uniform removal of 40% of the core sodium) was found to decrease with decreasing core H/D. The coefficient for the σ_p^{238} = 10 b case was consistently below that for the σ_p^{238} = 100 b case. These calculations confirm that further consideration must be given to the effect of voiding upon σ_p^{238} to obtain meaningful coefficients.

A description of the details of the second phase of the neutronics calculations for the parameter study is being prepared.

2. Use of U^{235} in a Fast-reactor Era

Some neutronic thermal-design aspects of use of U^{235} in a fast converter reactor (FCR) during a fast-reactor era were described previously (see Progress Report for February 1967, ANL-7308, pp. 41-46). To indicate relative performance, the fuel-cycle costs, U_3O_8 requirements, and plutonium production were estimated and are described here. Note that one important way to use U^{235}, namely, as startup fuel in a fast breeder during an interim era, has not been investigated; this startup use will be calculated after the detailed neutronic fuel-cycle program portion of ARC (the Argonne Reactor Code) becomes operational. The characteristics of FCR plants can, however, illustrate a performance bound in fuel strategy studies.

a. Aspects of Fuel-cycle Cost. The fuel-cycle cost estimates were used in two ways: (1) to provide guidance in the selection of design values and (2) to indicate the relative performance of U^{235}-fueled FCRs to plutonium-fueled LMFBRs, and thus to aid in establishing the value of plutonium compared to the value of U^{235}. These two uses are not independent; some iteration is needed for proper investigations of reactor design. For first estimates involving thermal performance of the core, it is assumed that the U^{235} is worth \$12/g in FCRs and that fissile plutonium is worth \$17/g. In the more detailed fuel-cycle cost estimates, values were based on \$8/lb U_3O_8 and \$30/kg per unit separatory work.

(i) Fuel-cycle Costs for FCRs. The principal cost components for fast-converter-reactor fuel cycles are due to fuel fabrication, fissile inventory, U^{235} consumption, and plutonium production. This study assumes that an average core burnup of 100,000 MWd/tonne of heavy atoms will be attainable with reasonable clad thicknesses and fuel densities, and thus does not include burnup variation as a design parameter.

(ii) Fuel Fabrication. Based on previous work, it appears reasonable that combined core and axial-blanket fabrication costs, expressed on an average kilogram basis, might vary with fuel-pin diameter (unclad fuel) as shown in Table XIII. With plutonium losses and inventory

TABLE XIII. Partial Fuel-cycle Cost as a Function of Fuel-pin Diameter

Pin Diameter (in.)	Fabrication Cost		Inventory Cost for Core (mills/kWh)	Combined Cost (mills/kWh)
	(\$/kg)	(mills/kWh)		
0.18	235	0.65	0.29	0.94
0.20	200	0.55	0.36	0.91
0.25	150	0.41	0.56	0.97
0.30	120	0.33	0.81	1.14

charges during fabrication excluded, the costs shown are for oxide fuel with stainless steel cladding in a fast-reactor era that provides a large tonnage throughput for the fabrication facilities. For 100,000-MWd/tonne burnup, a blanket-to-core weight ratio of 2, 90% of the power from the core, and a 41% net efficiency for converting heat to electricity, the contribution of fabrication cost to power cost is as shown in the third column of Table XIII.

(iii) Fissile Inventory. Core, blanket, and external inventory are included in total costs; however, a reasonable core design can be roughly estimated separately. For an example of the magnitude of core inventory costs, assume U^{235} concentration of 0.13, fissile plutonium (Pu_f) concentration of 0.025, average linear power of 11 kW/ft, annual capacity factor of 0.80, and annual charge rate of 0.10 for fissile material; then the core inventory costs, using the previously mentioned U^{235} and Pu_f prices, for the various pin sizes are as shown in the fourth column of Table XIII. Thus, the core inventory costs vary appreciably with fuel-pin diameter and are of significant magnitude. Combination (last column of Table XIII) of the core fissile inventory charges and the fabrication costs indicates that a minimum cost would occur with a fuel-pin diameter of about 0.21 in. This, of course, is only an example, but it is indicative for the region of design interest.

(iv) U^{235} Consumption. The consumption of U^{235} over a fuel cycle is difficult to express functionally from the cases calculated; values are from 0.9 to 1.1 g/MWd of the reactor. In general, as the core becomes larger, the spectrum softens, the required U^{235} concentration decreases, and the Pu_f concentration increases. If the volume fraction of fuel and fertile material remains constant as size is increased, fewer grams of U^{235} are destroyed per megawatt-day. From a practical standpoint, however, the volume of sodium increases and fuel fraction decreases. As indicative of magnitudes, a value of 0.9 g/MWd corresponds to 1.1 mills/kWh cost for the fuel cycle.

(v) Fissile-plutonium Production. This value increases with increasing PDF ratio (fissile atoms produced/fissile atom destroyed on an instantaneous basis) and saturates as size is increased. In addition, the Pu_f burns out more readily as core conversion ratio increases. A Pu_f net production rate of 0.8 g/MWd corresponds to credit of 1.4 mills/kWh for the fuel cycle. Thus, the net difference between Pu_f produced and U^{235} destroyed in this idealized case is a credit of 0.3 mills/kWh.

b. Comparisons of Fuel-cycle Cost. Ideally, the cost comparisons of various concepts would include capital, fuel, and other production expenses on a year-by-year basis. In the case of the efforts with U^{235} use, the only readily available way of indicating relative performance is by means of fuel-cycle costs. These are limited to equilibrium fuel performance with certain cost adjustments for initial costs.

To provide a broad indication of relative performance, the fuel-cycle costs for the following systems were calculated:

1. LWR, a 1088-MW(e) light-water-reactor plant of assumed characteristics;
2. FBR-BeO, a 1075-MW(e) plant with an oxide-type plutonium-fueled fast breeder reactor and with BeO added to the core (design related to that of the General Electric Co.[8]);
3. FBR, the same general design as the FBR-BeO example, but with the BeO removed from the core and axial blankets;
4. FBR-U^{235}, which is similar to the FBR design, but with U^{235} fuel in place of plutonium;
5. FCR, a 1075-MW(e) plant with a fast converter reactor specifically designed for U^{235} fuel (core 60% higher than in the FBR design and fuel-pin diameter decreased slightly).

To provide a quick preliminary comparison, the characteristics of nuclear plants using each of these reactor systems were selected without the emphasis on details that would be required in a detailed study. In addition, no optimization procedures were used to adjust plant performance to changing factors of cost, such as plutonium price.

Fuel-cycle calculations were made with the use of a computer code which uses an accounting procedure that the utility industry might use in such survey studies. The cost of uranium for specified concentrations is estimated based on optimum tailing concentrations using the input U_3O_8, fluorination, and separatory work costs. A program option allows for U^{235} burnup costs to be estimated based on either the schedule of costs for various U^{235} concentrations or on mixing of 50 w/o U^{235} to reconstitute the burned fuel. For fast converter reactors there is no effective cost penalty by using the mixing of 50 w/o U^{235} option. Thus the problem of activity levels associated with reintroduction of spent fuel into the diffusion plant is obviated; however, the fabrication cost aspects of this mixing step were not investigated. The fuel-cycle costs for each of 20 yr is estimated in the code and a levelized 20-yr value is calculated. The annual capacity factor used was 80% for the first 5 yr, 75% for the next 10 yr, and 65% for the last 5 yr. The fuel-cycle cost estimate, U_3O_8 makeup, and fissile-plutonium production are given in Table XIV.

The unit costs for fabrication, shipping, and processing require more definition. A more rigorous cost model could be developed so that

[8]Cohen, K. P., and O'Neill, G. L., Safety and Economic Characteristics of a 1000-MWe Fast Sodium-cooled Reactor Design, in Proceedings of the Conference on Safety, Fuels, and Core Design in Large Fast Power Reactors held at Argonne National Laboratory, October 11-14, 1965, ANL-7120 (1965), pp. 185-204.

cost differentials between the concepts would be more meaningful. The reprocessing cost for the fast U^{235} burners was increased by 25% over the FBR cost because core and axial blanket cannot be mixed as is sometimes suggested for FBRs. Unit shipping costs also should be evaluated in terms of cask-cooling requirements for axial blanket and core materials. With expected cost disadvantages applied to the FCR, there appears to be an incentive to consider further fast converters specifically designed for U^{235} use. In addition, the technical and cost aspects of using U^{235} as the fuel in starting-up FBRs should be developed.

TABLE XIV. Estimates of Fuel-cycle Performance for Various Oxide-fueled Nuclear Power Plants[a]

Reactor Type	Fuel-cycle Cost (mills/kW)		U_3O_8 Makeup (tons/20 yr[b])	Pu_f Produced (tonne/20 yr)
	Pu_f at \$10/g	Pu_f at \$18/g		
LWR	1.48	1.31	3500	3.9
FBR with BeO	0.92	1.15	-	2.6
FBR	0.74	0.84	-	4.6
FBR U^{235}	1.92	1.44	3900	9.9
FCR	1.38	0.87	3500	10.6

[a]Based on \$8/lb U_3O_8 and \$30/kg separatory work.
[b]Does not include initial or final inventories, but only the makeup requirements.

c. Observations. Although this study was only preliminary, several observations can be made within the assumptions of the study:

1. Clearly, uranium-235 use in the fast-reactor era should be defined more rigorously.

2. On the basis of equilibrium fuel-cycle calculations, the FCR has a definite cost advantage over the other U^{235} users.

3. The FCR and LWR require about the same tonnage of U_3O_8 for fuel makeup.

4. The FCR produces about twice as much fissile plutonium as LWRs. Thus, taking design advantage of the nuclear-safety characteristics of U^{235} compared to Pu_f significantly improves fuel-cycle performance.

III. GENERAL REACTOR TECHNOLOGY

A. Applied and Reactor Physics Development

1. Extended Count-rate Capability of TREAT Fast Neutron Hodoscope

The detection system of the TREAT Fast Neutron Hodoscope has been modified to process 10^6 neutron cps. This is an improvement by a factor of eight over previous rates and was accomplished primarily by redesigning the electronic circuitry which minimizes the deadtime and saturation effects. With these electronic design changes it was not necessary to replace the Hornyak-button fast-neutron-detector phosphor.

It was realized during the early tests that the slow (microsecond) decay of ZnS:Ag phosphor used in the standard Hornyak buttons was responsible for some reduction in sensitivity of the discriminator. An effort was made to develop a new scintillator component for the Hornyak button. Several new buttons containing a P16 phosphor (which decays in a few tenths of a microsecond) have been tested, but results to date indicate that they have an inordinate sensitivity to gamma rays and result in poor resolution and signal-background criteria when used in the TREAT reactor.

Results of experimental tests are plotted in Fig. 11. After setting the discriminator level with an americium-beryllium neutron source at a value consistent with normal usage, the Hornyak-button detector was placed next to the core of the Argonne Thermal Source Reactor (ATSR). Another integral bias curve confirmed that the discriminator was set sufficiently

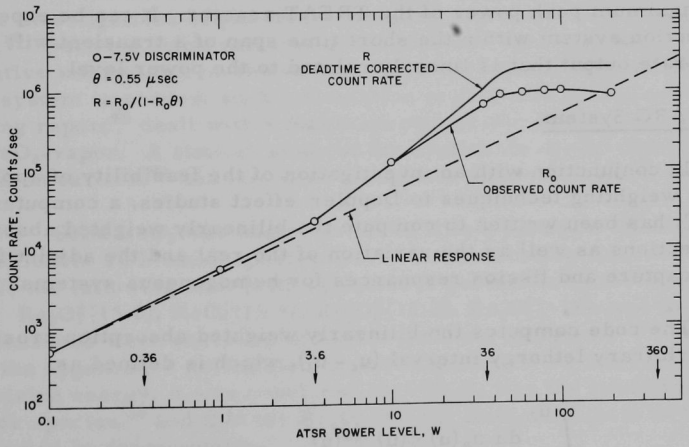

Fig. 11. Count Rate from Hodoscope Processing System at Different Reactor Power Levels

high to bias out the gammas. Starting from 0.1-W reactor power level, the count rate (of the fast digital output) of the X206 electronic processing board was followed as the reactor was brought up to and leveled off at various intermediate powers up to 200 W. The points along the curve marked R_0 are the measured count rates. The curve marked R represents the count rate corrected for the deadtime of 0.55 μsec in the digital output.

There is a noticeable departure from linearity beginning at about 3 W. This effect, previously investigated at ATSR, is due to a gain increase in the photomultiplier tube resulting from large anode currents. Such an increase would not disturb the linearity of data obtained in TREAT transients because the time required for the shift is of the order of many minutes, whereas a typical meltdown transient is completed within a second.

The deadtime-corrected curve R was computed in anticipation of the digital readout system now being designed. Because data will be stored and processed digitally, it will be possible to enter a deadtime correction during the computer-processing phase after the experiment. Thus the upper limit of count rate for the digital system is actually 2×10^6 neutron cps of recoverable data.

In summary, the latest neutron hodoscope detection system consists of a standard Hornyak button containing ZnS:Ag phosphor, an XP1110 phototube with 200-μA M503 divider string, with no bypassing, and an X206 electronic processing board having an effective deadtime of 0.55 μsec. This combination appears capable of processing 10^6 cps (equivalent to 2×10^6 cps for a digital recording system) at flux levels comparable with those produced at the maximum peak power of the TREAT reactor. It can be expected that the detection system within the short time span of a transient will provide a count-rate output that is linearly related to the power level.

2. The ARC System

In conjunction with an investigation of the feasibility of applying bilinear weighting techniques to Doppler-effect studies, a computer code, ADRIFT, has been written to compute the bilinearly weighted absorption cross sections as well as the variation of the real and the adjoint fluxes across capture and fission resonances for homogeneous systems.

The code computes the bilinearly weighted absorption cross section for an arbitrary lethargy interval $(u_2 - u_1)$, which is defined as

$$\tilde{\sigma}_a = \frac{\int_{u_1}^{u_2} du\ \sigma_a(u)\ \phi(u)\ \phi^*(u)}{\frac{1}{u_2 - u_1} \int_{u_1}^{u_2} \phi(u)\ du \int_{u_1}^{u_2} \phi^*(u)\ du}, \qquad (1)$$

where $\phi(u)$ is the real flux and $\phi^*(u)$ is the adjoint. The flux $\phi(u)$ is obtained from the solution of the slowing-down equation for energies below the range within which neutrons are born:

$$\Sigma(u)\,\phi(u) = \sum_{i=1}^{n} \int_{u-\epsilon_i}^{u} du' e^{-(u-u')}\,\Sigma_{si}(u')\,\phi(u')/(1-\alpha_i). \qquad (2)$$

The adjoint flux $\phi^*(u)$ is obtained from the solution of the integral equation resulting from the transposition of the operators in Eq. (2):

$$\Sigma(u)\,\phi^*(u) = \sum_{i=1}^{n} \left[\nu_i(u)\,\Sigma_{fi}(u) + \Sigma_{si}(u) \int_{u}^{u+\epsilon_i} du' e^{-(u'-u)}\,\phi^*(u')/(1+\alpha_i) \right]. \qquad (3)$$

The integrals in Eqs. (2) and (3) are evaluated numerically with the lethargy range of the integral divided into many, very narrow intervals at equal lethargy width. It is assumed also that the real flux is constant in lethargy above the energy range of the calculation and that the adjoint flux is constant in lethargy below the energy range of the calculation.

B. Reactor Fuels and Materials Development

1. Chemistry of Fuel Materials

a. Mass-spectrometric Study of the System Re-ReO_2-Vapor. The choice of rhenium as a container material for high-temperature thermodynamic investigations of plutonia-containing systems was discussed previously.[9a] Because some reaction of the rhenium with plutonia is expected, quantitative information on the various vapor equilibria in the rhenium-oxygen system is needed; such information is virtually nonexistent. The preceding report[9b] dealt with a mass-spectrometric study of the system ReO_2-ReO_3-vapor. A similar study of the system Re-ReO_2-vapor, briefly reported on earlier,[9a] has now been completed and is discussed below.

Solid ReO_2 was heated at ~1070°K in a platinum effusion cell within a Bendix TOF mass spectrometer. At an ionizing electron energy of 25 eV, the following ions (with appearance potentials in eV) were observed: $Re_2O_7^+$(13.0), ReO_3^+(15.9), $Re_2O_6^+$(17.2), $Re_2O_5^+$(~19), and ReO_2^+(~20). (Additional ions were observed at higher ionizing energies.) From an analysis of the appearance potentials and the variation of the ion intensity ratios with ionizing energy, it was concluded that Re_2O_7 was the predominant parent vapor species,[10] and that the Re_2O_6, Re_2O_5, ReO_2, and most of the ReO_3 were formed by fragmentation.

---

[9]Reactor Development Program Progress Report: (a) September 1966, ANL-7255, pp. 52-53; (b) February 1967, ANL-7308, pp. 52-54.

[10]This result disagrees with that of Semenov and Ovchinnikov who reported the composition ratio ReO_3/Re_2O_7 = 2 for the vapor over ReO_2 at 1043°K [J. Gen. Chem. USSR (Eng. Transl.) 35(9), 1517 (1965)].

X-ray analysis of the solid residues from similar experiments showed the presence of ReO_2 and a small amount of rhenium metal. Prolonged heating of ReO_2 at ~1070°K left residues containing rhenium as the major phase. These results together with the mass-spectrometric data indicate that the vaporization proceeds mainly according to the equation

$$7/2\ ReO_2(s) \rightarrow 3/2\ Re(s) + Re_2O_7(g), \qquad (1)$$

and that the system is univariant.

Vapor pressures were obtained by combining the results of four experiments in which $Re_2O_7^+$ intensity versus temperature was measured, with the results of three experiments in which the rate of effusion of Re_2O_7 was measured at a single temperature. The vapor phase was assumed to consist of Re_2O_7 only. The vapor pressure equation which was derived for the range 961-1082°K

$$\log P(atm) = 14.442 - (20.447/T), \qquad (2)$$

has a combined uncertainty (95% confidence level) of ±10%. Figure 12 shows a plot of this equation and the single (average) point obtained from the rate-of-effusion measurements.

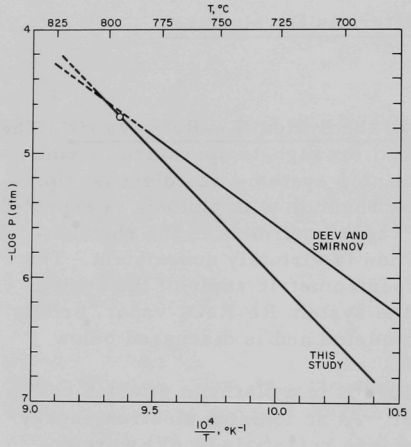

Fig. 12. Vapor Pressure over Re-ReO_2 vs. Reciprocal Temperature (O, from rate-of-effusion measurements at 1068°K)

Included in Fig. 12 is the vapor pressure curve for ReO_2 obtained by Deev and Smirnov[11] from Knudsen effusion measurements between 923 and 1058°K. As can be seen, the results of the two studies are in considerable disagreement. Our data yield the value 93.6 ± 0.4 kcal/mole of Re_2O_7 for the enthalpy of vaporization of ReO_2; from Deev and Smirnov's data, a value of 65.6 kcal/mole of Re_2O_7 is obtained. The discrepancy may be explained by the supposition that their measurements were made for the bivariant system ReO_2-vapor, which would yield higher vapor pressures and a lower enthalpy of vaporization than the univariant system. They report, and our experiments confirm, that decomposition of ReO_2 does not proceed at an appreciable rate below 1058°K, the maximum temperature of their study.

[11]Deev, V. I., and Smirnov, V. I., Dokl. Akad. Nauk. SSSR 140, 822 (1961).

b. Electron Microprobe Analysis of Irradiated Oxide Fast Reactor Fuel Pin. A portion of an EBR-II oxide fuel pin irradiated to 0.7 a/o burn-up in MTR has been examined in an unshielded electron probe microanalyzer. The fuel pin consisted of a 14.5-cm-long stack of oxide cylinders, 0.38 cm in diameter. The cylinders were contained in a Type 304 stainless steel tube of 0.396-cm inner diameter and a 0.023-cm-thick wall and in an argon atmosphere. The fuel was 93% theoretical density UO_2 with an O/U ratio of 2.001 and 13% enriched. Electron probe analysis of the unirradiated fuel material indicated that small particles (up to several microns in diameter) of stainless steel were dispersed throughout the material. Analysis of the sample on a macro scale indicated that the fuel material contained 90 ppm iron, 15 ppm chromium, and 10 ppm nickel.

The irradiated sample analyzed was a longitudinal section obtained 3 cm from the bottom of the pin, and represented a plane section parallel to the diameter and 0.025 cm from the outer edge of the fuel pin. Large, bright inclusions having a metallic luster completely filled some of the fissures that were in an area corresponding to the outer 0.015 cm of the fuel pin. These inclusions contained large amounts of iron (about 80 w/o) and lesser amounts of nickel and chromium, and were identified as stainless steel. No fission products were detected.

Numerous small inclusions up to about 3 μ in diameter were dispersed throughout the fuel matrix as in the unirradiated material. Thirty-five of these inclusions were examined with the electron probe microanalyzer; the results of these examinations may be summarized as follows:

1. All the inclusions contained at least two of the three major constituents of stainless steel, namely, iron, nickel, and chromium.

2. Seventeen of the inclusions contained at least one of the transition metal fission products, namely, molybdenum, ruthenium, technetium, rhodium, and palladium.

3. Zirconium, a major fission product, was not found in any of the inclusions and remained in the oxide phase.

4. No fission products were contained in any of the inclusions (18) examined between 0 and 0.010 cm from the outer edge of the sample.

5. No consistent ratio of fission product distribution in the inclusions was found, although molybdenum and ruthenium were the major fission products.

2. Fabrication and Evaluation

a. Irradiation of High-temperature Materials. Materials in MTR being irradiated in instrumented capsules under the high-temperature materials program were reported (see Progress Report for February 1967, ANL-7308, pp. 59-60) to include UC-20 w/o Pu, PuC, and US, each jacketed in Nb-1 w/o Zr. Electron-microscopical studies of high-burnup, vibratorily compacted UC-20 w/o PuC showed that the larger, more interconnected fission-gas bubbles in PuC_{1-x} lead to more fission-gas release than in the case of PuC_{1+x}. A shielded, electron-beam-microprobe, X-ray analyzer is to be procured for use in studying any relationship of second-phase particles to the results that have been reported. A summary of current irradiations is shown in Table XV.

TABLE XV. Status of Irradiations of Ceramic Fuel, Clad in Nb-1 w/o Zr, in MTR

Capsule or S/A No.	Specimen Number	Design Parameters: Fuel Composition (w/o)	Design Parameters: Effective Density (%)	Design Parameters: Cladding OD (in.)	Design Parameters: Cladding Thickness (in.)	Operating Conditions: Power Density (kW/cc)[a]	Operating Conditions: Max Cladding Temp (°C)	Operating Conditions: Burnup to Date: a/o (U + Pu)	Operating Conditions: Burnup to Date: fiss/cc x 10^{-20}[a]
56-11	MV-2	UC-20 PuC	79	0.281	0.012	1.2	470	7.2	18.6
56-8	MV-3	UC-20 PuC	81	0.281	0.012	1.2	715	7.7	20.4
56-8	MV-5	UC-20 PuC	80	0.281	0.012	1.2	705	7.4	19.4
56-11	MV-6	UC-20 PuC	80	0.281	0.012	1.2	480	7.7	20.2
56-13	Z-4	UC-20 PuC	79	0.174	0.015	1.2	665	2.6	6.7
56-13	Z-5	UC-20 PuC	79	0.174	0.015	1.2	585	2.6	6.7
56-13	Z-7	UC-20 PuC	79	0.174	0.015	1.2	570	2.6	6.7
56-13	C-45	PuC	84	0.174	0.009	1.4	700	2.6	7.1
56-8	S-7	US	80	0.281	0.012	1.0	535	6.0	11.6
56-8	S-8	US	89	0.281	0.012	1.0	725	8.0	17.3
56-8	S-9	US	76	0.281	0.012	1.0	750	8.0	14.7
56-8	S-10	US	91	0.281	0.012	1.0	690	8.0	17.7
56-11	S-15	US	82	0.281	0.012	1.0	380	5.1	10.1
56-11	S-16	US	90	0.281	0.012	1.0	510	7.0	15.3
56-11	S-17	US	88	0.281	0.012	1.0	500	5.7	12.1
56-11	S-18	US	77	0.281	0.012	1.0	610	7.5	14.0

[a]Based on effective density.

Preparation of instrumented capsules for irradiation of pressed and sintered pellets of UC-20 w/o US and UP is under way. These pellets are being jacketed either with 0.51-mm gauge Type 304 stainless steel or with 0.38-mm gauge Hastelloy-X tubes. The irradiation behavior of the potential fuel materials, at jacket surface temperature in the range from 650 to 800°C, will be investigated at nominal burnups of 5 and 10 a/o in the CP-5 or MTR reactors.

3. Radiation Damage to Structural Materials

a. Effect of Fast-neutron Irradiation on Jacket Materials. A total of 420 tensile-type and 103 tube-burst specimens of V-20 w/o Ti, V-15 w/o Ti-7.5 w/o Cr, AISI Type 304 stainless steel, Hastelloy-X, and Inconel 625 are being irradiated in EBR-II subassemblies XA08, XO10, XO16, XO18, and XO20 at temperatures between 500 and 650°C. The status of the specimens remained unchanged during the month because of reactor shutdown.

In February, 54 creep-rupture tensile specimens of V-20 w/o Ti that had been irradiated in sodium at 650°C to a maximum total neutron exposure of 7.5 x 10^{21} n/cm^2 were removed from their capsules. Some of the specimens were vacuum annealed one hour at 900°C, some at 1000°C, and some at 1100°C. Equivalent treatments at 850, 1100, and 1250°C were given 54 specimens of V-15 w/o Ti-7.5 w/o Cr, 27 of Type 304 stainless steel, and 18 of Hastelloy-X. Additional irradiated specimens of these alloys had been shipped for testing or were in shipment, including inner capsule tubes used for containing structural materials.

Room-temperature tensile tests were performed in March on irradiated vanadium-base alloy specimens from EBR-II subassembly XO13 as part of a study to separate the effects of exposure and irradiation temperature, as well as to provide a basis for determining to what extent recovery will effect the observed mechanical property changes during subsequent high-temperature tensile testing. The specimens were irradiated at temperatures ranging from 500 to 660°C, and were exposed to calculated total neutron exposures between 1.6 and 4.8 x 10^{21} n/cm^2. The tests were conducted at a strain rate of 2% per minute on specimens of V-20 w/o Ti alloy that had been given a one-hour anneal at 900°C prior to irradiation, and specimens of V-15 w/o Ti-7.5 w/o Cr alloy that had been given a one-hour anneal at 850°C. The values obtained were compared to those from unirradiated control specimens, some of which were annealed at 550°C for 30 days to simulate the temperature conditions during irradiation. The results are given in Table XVI.

TABLE XVI. Room-temperature Tensile Properties of Vanadium-base Alloys Irradiated in EBR-II

Material (w/o)	Condition	Exposure at Center of Specimen (n/cm^2 x 10^{21})	Irradiation Temperature (°C)	Offset Yield Strength (kg/mm^2)	Ultimate Tensile Strength (kg/mm^2)	Uniform Elongation (%)	Total Elongation (%)
V-20 Ti	Unirradiated	-	-	63.2	75.2	20.0	25.8
V-20 Ti	Unirradiated, 30 days--550°C	-	-	52.6	64.8	15.0	20.4
V-20 Ti	Irradiated	1.8	540	49.5	60.7	15.8	22.5
V-20 Ti	Irradiated	3.2	600	53.5	64.6	15.4	21.7
V-20 Ti	Irradiated	4.8	650	57.6	67.5	14.2	19.9
V-20 Ti	Irradiated	4.6	660	56.9	67.7	13.0	18.2
V-15 Ti-7.5 Cr	Unirradiated	-	-	64.4	72.3	15.0	20.6
V-15 Ti-7.5 Cr	Unirradiated, 30 days--550°C	-	-	67.2	76.3	15.0	19.9
V-15 Ti-7.5 Cr	Irradiated	1.6	500	61.3	72.2	10.4	14.8
V-15 Ti-7.5 Cr	Irradiated	3.2	570	58.1	68.9	10.0	14.2
V-15 Ti-7.5 Cr	Irradiated	4.9	610	68.5	81.8	13.6	17.8
V-15 Ti-7.5 Cr	Irradiated	4.6	630	65.6	78.3	13.6	18.3

Both the yield strength and ultimate tensile strength of the unirradiated V-20 w/o Ti alloy were decreased by approximately 14 to 17% by the 30-day 550°C anneal. Irradiation up to a total neutron exposure of

3.2×10^{21} n/cm^2 and at temperatures below 600°C did not significantly change the yield strength and tensile strength from that shown by the unirradiated control material that was annealed for 30 days at 550°C. Irradiation up to a total neutron exposure of 4.8×10^{21} n/cm^2 and 660°C increased the strength slightly above that which might be expected from the 550°C anneal.

The yield strength and the ultimate tensile strength of the V-15 w/o Ti-7.5 w/o Cr alloy were increased 4 to 6% by annealing the unirradiated alloy for 30 days at 550°C. In comparison to this annealing treatment, irradiation at temperatures from 570 to 630°C to a total neutron exposure of 4.6×10^{21} n/cm^2 did not significantly change the strength, whereas irradiation below 570°C and a total neutron exposure of 3.2×10^{21} n/cm^2 reduced the yield and tensile strength of the alloy.

The ductility of the V-20 w/o Ti alloy was decreased 25% due to the 30-day 550°C anneal, but the ductility of the V-15 w/o Ti-7.5 w/o Cr alloy was not altered significantly by the same treatment. Irradiation of the V-20 w/o Ti alloy from 1.8 to 4.8×10^{21} n/cm^2 at all temperatures and irradiation of the V-15 w/o Ti-7.5 w/o Cr alloy above 570°C and above 4.6×10^{21} n/cm^2 resulted in ductility decreases of the same order of magnitude as that which resulted from the 550°C anneal. The ductility of the V-15 w/o Ti-7.5 w/o Cr alloy was reduced up to 33% from that of the unirradiated, 550°C annealed control material at irradiation temperatures below 570°C and a total neutron exposure below 3.2×10^{21} n/cm^2.

Irradiation of V-20 w/o Ti alloy at 50°C to 1.4×10^{21} n/cm^2 ($E_n > 1$ MeV) reportedly[12] results in an increase in the room-temperature yield strength of 44% and a decrease in the room-temperature percent elongation of 90%. Testing the same material at 650°C resulted in properties similar to that of the unirradiated material. Irradiation effects, accordingly, are annealed out at the higher testing temperature.[12] Since the irradiation temperatures of the two vanadium-base alloys tested in this program were as high as 660°C and the changes in room-temperature properties were considerably less, irradiation effects apparently were annealed out at the higher irradiation temperature and the observed changes were primarily due to thermal effects.

Tensile testing of the irradiated vanadium-base alloys at 550°C is under way, to be followed by testing at 650°C. The results will be compared to those of Type 304 stainless steel and Hastelloy-X irradiated and tested under similar conditions.

---

[12] Böhm, H., et al., Irradiation Effects on the Mechanical Properties of Vanadium-base Alloys, Presented at Sixty-ninth Annual Meeting of ASTM, Atlantic City, New Jersey, June 27-July 1, 1966, Paper No. 75.

Seventeen inner capsules from subassembly XO13 are being prepared for tube-burst tests. Eight of these capsules are V-15 w/o Ti-7.5 w/o Cr, four are Inconel 625, three are Type 304 stainless steel, and two are Hastelloy-X.

During irradiation the capsules were exposed to a maximum fast-neutron flux of 7.5×10^{21} n/cm^2 and the maximum temperature was 650°C. The capsule environment was inert gas on the outside and sodium and inert gas on the inside.

The seventeen inner capsules have been cut into 4-in. sections for tube-burst tests. Eight tube-burst specimens and two metallography samples were taken from each capsule. The metallography samples were taken from the approximate location of the maximum flux. The tube-burst specimens from the eight V-15 w/o Ti-7.5 w/o Cr capsules have been put into the hot cell in preparation for testing.

4. Techniques of Fabrication and Testing

a. Argonne Three-roll Tube Reducer. Some of the parametric studies (see Progress Report for November 1966, ANL-7279, pp. 57-58) have been completed. Use of a three-roll tube reducer, developed at Argonne, was reported to simplify and improve the fabrication of tubing for fast reactor fuel jackets. Parametric studies (e.g., roll contour, feed and index rates) were then under way to establish optima both in design criteria and in operational procedures.

All roll sets have now been modified to incorporate a radius equal to one-half the starting tube outer diameter. This roll configuration used in conjunction with a 20° rotation and a reasonable feed schedule has considerably improved the chances of processing tubing alloys of limited ductility. A bonus has also been obtained in the ease of mandrel extraction or of movement over a plug, as the case may be.

Studies have been completed on the benefits of plug-reducing versus mandrel-reducing. A modified feed system has been designed to permit utilization of the plug-reducing method. Means of tube heating are being investigated for materials that require warm-reducing operations.

Studies are continuing in the area of optimum ratios of sinking and wall reduction as well as the effects of the track angle as a function of tube size and wall thickness. Presently there appear to be no problems in reduction from a 1-in.-OD x 0.125-in. wall to a 0.5-in.-OD x 0.035-in. wall by only changing roll sets and mandrels (or plugs). Some problems have been experienced in going to smaller sizes, particularly with limited-ductility materials.

b. Ultrasonic Instrument and Transducer Development. A density of less than 70% of the X-ray value was reported to be needed in porous tungsten samples made with 100 to 400 μ particles for the acoustic impedance of the tungsten to match that of lead zirconate-titanate transducer. A sample made at Argonne from 100 μ particles was reported to be 70.8% dense (see Progress Report for February 1967, ANL-7308, p. 65). Sintered specialties has made sintered samples 60, 70, and 80% dense that are of unknown particle size. These were being evaluated in February as a backing material for ultrasonic transducer probes. Evaluation of these and of lower-density samples (52% dense) that were recently received is in progress.

Lead zirconate-titanate elements from Clevite (PZT-4) have also been received. A transducer probe with a PZT-4 piezoelectric element and a 62% dense tungsten backing, which is the nearest available density to the calculated value of 63% for matching, is being fabricated.

c. Measurement of Thermal Conductivity of Irradiated Fuel as a Function of Burnup and Temperature. The checking of the high-temperature thermal-conductivity facility, which has been installed in a hot cell, was recently completed. The calibration of the system with an Armco iron conductivity standard is now in progress. This involves the measurement of Q, the amount of heat absorbed per unit area by the front surface of the standard. Knowledge of Q and the thermal diffusivity enables the conductivity to be calculated without specific heat and density values.

Preparation of three specimens from an irradiated EBR-II driver fuel pin is also in progress.

C. Engineering Development

1. Development of Master-Slave Manipulator Systems

a. An Experimental Powered Wrench for Use with Manipulators. As more complex facilities come into use, the capability of performing remote repairs and modifications on machinery will become increasingly desirable. Such work will require general-purpose tools, such as screwdrivers, wrenches, and hammers, developed specifically for use with manipulators. Nearly all tools now used in conjunction with manipulators are inefficient modifications of tools originally designed to be held by a human hand. Conventional powered tools are generally too heavy to be handled well with master-slave manipulators. They are also too bulky and tend to obscure the operator's view of the work.

An experimental powered socket wrench, which shows some promise, has been developed for use with master-slave manipulators. To keep the overall weight and size down, a small d.c. motor with relatively low torque (13 in.-lb at the socket) is used. Higher torques, generally necessary only when a bolt is cracked loose or tightened, are applied by rotating the entire wrench with the manipulator. In applying these higher torques, the manipulator operator uses the wrench as if it was unpowered. Torques up to 150 in.-lb can be applied in this way. A one-way clutch prevents the motor and gear reducer from backing up. The entire wrench weighs just under 2 lb.

The wrench was tested using a task board, originally developed by NASA, which incorporates a number of mechanical fasteners and electrical and hydraulic fittings. One of the tasks involves the unscrewing and retightening of 11 different bolts. Using an earlier powered wrench and sockets, this task took 26 min. The new wrench, which used improved sockets, cut this time to 9 min.

2. Heat Transfer and Fluid Flow

a. Niobium-1% Zirconium Loop. A facility has been built to investigate the heat transfer and two-phase flow characteristics of boiling sodium to a temperature of 2100°F and a pressure of approximately 8 atm. Among the variables to be investigated are boiling heat flux and temperature difference up to the critical-flux occurrence, boiling and adiabatic two-phase pressure losses, vapor volume fraction, boiling stability parameters, and ultimately the transient behavior of some of these same quantities.

The difficulties with the condenser shutters (see Progress Report for February 1967, ANL-7308, p. 67) have been resolved and the shutter control is performing properly. Flowmeter calibrations are continuing. Operation of the thermal-radiation heater has begun. Sodium temperatures ranging up to 1200°F and heat fluxes up to 100,000 Btu/hr/ft have been obtained.

b. Heater Experiments

(i) Electron-bombardment Heater (EBH) Experiment. As mentioned in the previous progress reports, the original tests have been terminated following satisfactory operation; further EBH tests will be conducted in the new EBH test facility that is being constructed (see Progress Report for January 1967, ANL-7302, p. 71). It will enable tests of heaters to their maximum heat-flux capabilities before they are installed in the Nb-1% Zr loop.

c. Heat Transfer in Double-pipe Heat Exchangers

(i) Countercurrent Turbulent Liquid-metal Flow. Experimentation with the second heat-exchanger test section continued. As reported previously (see Progress Report for February 1966, ANL-7308, p. 67-69), although the anomalous inlet-temperature-difference dependence found with the first test section has been eliminated with this second section, the experimentally determined fully developed overall heat-transfer coefficients are too low and reproducibility is poor.

The overall heat-transfer coefficients were low compared with values predicted by the heat-exchanger analysis. Application of the analysis requires knowledge of fully developed heat-transfer coefficients appropriate to the boundary condition of uniform heat flux. Predictions were based on use of Lyon's[13] equation for the tubeside coefficient. But if tubeside coefficients were based instead on the more recent relationship of Buleev,[14] it was found that the experimentally determined overall heat-transfer coefficients no longer appeared too low. Differences between these predictions and comparisons with experimental data are shown in Fig. 13.

Fully developed heat-transfer coefficients are determined from measurements of the temperature distribution along the outer wall of the heat exchanger. Investigations of the possible cause of the poor reproducibility of the coefficients led to the conclusion that the method of fastening the thermocouples to the outer wall of the test section needed improvement. The method used was simply to tape each thermocouple tightly to the outer wall. It now appears that when the test section was heated, the thermocouples pulled away from the wall and gave erroneous readings. The thermocouples have now been cemented in place and contact with the wall is checked periodically with a resistance meter. Recent data, obtained with the outer wall thermocouples cemented in place, are compared with previous data in Fig. 13. The improvement in reproducibility is evident.

---

[13]Lyon, R. N., Liquid Metal Heat Transfer Coefficients, Chem. Eng. Prog. 47, 75-79 (1951).

[14]Buleev, N. I., Theoretical Model of the Mechanism of Turbulent Exchange in Fluid Flow, Teplopesedacha, USSR Acad. of Sci. 64 (1962).

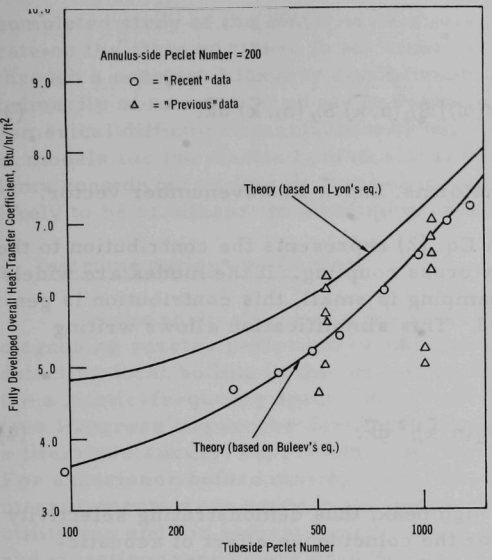

Fig. 13. Comparison of Experimental Data and Theory for Mercury-to-Mercury Counterflow Double-pipe Heat Exchanger

3. Mechanics of Materials

a. Core Structural Dynamics. The treatment of the problem of the cylinder flow-induced-vibration response as a problem in random vibration was discussed previously (see Progress Report for February 1967, ANL-7308, pp. 69-71).

To determine the mean-square values and other statistical properties of the narrow-band random response of a cylinder to a convected pressure field, a normal mode method of analysis developed by Powell,[15] will be applied.

The random response is written as a superposition of the normal modes of free vibration of the cylinder. The use of a Fourier transform representation of the spectral density of the response results in the series expansion

$$\Phi_y(\bar{x}, \omega) = \sum_n \sum_m \frac{\alpha_n(\bar{x})\, \alpha_m(\bar{x})}{|Z_n(\omega)||Z_m(\omega)|} \iint R_p[\omega, \bar{x}, \bar{x}', \tau(\omega)]\, \alpha_n(\bar{x})\, \alpha_m(\bar{x}')\, d\bar{x} d\bar{x}', \tag{1}$$

where $\Phi_y(\bar{x}, \omega)$ is the spectral density, $\alpha_n(\bar{x})$ is the nth normal mode, $Z_n(\omega)$ represents the nth modal impedance, and $R_p[\omega, \bar{x}, \bar{x}', \tau(\omega)]$ is a space-time correlation function describing the convecting random pressure field.

An objective of the experimental studies will be to determine if the convecting pressure field can be assumed homogeneous. If it can, a wavenumber decomposition of the space-time correlation function and the modal function gives the following representation of the spectral density function:

$$\Phi(\bar{x}, \omega) = \sum_n \frac{\alpha_n^2(x)}{|Z_n(\omega)|^2} C_{nn}(\omega) + \sum_{\substack{n \\ n \neq m}} \sum_m \frac{\alpha_n(\lambda)\, \alpha_m(\bar{x})}{|Z_n(\omega)||Z_m(\omega)|} C_{nm}(\omega), \tag{2}$$

---

[15] Powell, A., On the Fatigue Failure of Structures Due to Vibrations Excited by Random Pressure Fields, J. Acoust. Soc. Am. 30, 1130-1135 (1958).

where

$$C_{nm}(\omega) = \int_{-\infty}^{\infty} W_p[\omega, \bar{k}, \tau(\omega)]\, S_\alpha(n, \bar{k})\, S_\alpha(m, \bar{k})\, d\bar{k}, \tag{3}$$

W and S represent Fourier transforms, and $\bar{k}$ is wavenumber vector.

The second series in Eq. (2) represents the contribution to the response due to modal-frequency cross coupling. If the modes are widely separated in frequency and the damping is small, this contribution is generally small and can be neglected. This simplification allows writing Eq. (3) as

$$C_{nn}(\omega) = \int_{-\infty}^{\infty} W_p(\bar{k}, \omega) |S_\alpha(n, \bar{k})|^2\, d\bar{k}. \tag{4}$$

In Eq. (4), $|S_\alpha(n, \bar{k})|^2$ will have a high peak, thus demonstrating selectivity in wavenumber. This accounts for the coincidence effect of acoustic-structural coupling when the wavenumber of a structural mode matches a wavenumber associated with the spatial distribution of the pressure field. The term $|Z_n(\omega)|^2$ demonstrates a selectivity in frequency. Maximum response occurs at these coincident or resonant conditions.

Mathematical representations of the correlation functions describing convecting pressure fields will be studied.

Work has begun on the development of a small piezoelectric pressure transducer to be mounted in a cylindrical rod. The pressure transducers will be used to determine the properties of the pressure field and to construct a suitable space-time correlation function.

b. Anisotropy Studies. To provide refined analytical methods for predicting thermally induced displacements and stresses in reactor core components, study has begun of the effects introduced by (a) intrinsic anisotropic material properties of fuel elements and (b) regular substructure patterns, including how they affect the gross anisotropy of larger structural elements. Particular emphasis will be placed on the latter cause of anisotropic behavior and its possible use in developing models to describe the overall thermal deflection of fuel-element subassemblies and the entire core structure.

The analytical portion of the solution of a steady-state thermoelasticity problem for a heat-generating anisotropic cylinder has been completed and the numerical evaluation of the results has been initiated. This problem is an extension to the case of transverse isotropy of a previously

completed study of the effect of axial variations in internal heat-generation rate on the state of stress in an infinite cylinder being cooled at the surface through a constant boundary conductance. The problem as it now stands is primarily of interest as an aid in determining the degree of analytical and numerical difficulty associated with the introduction of anisotropic effects in models for the elastic behavior of fuel elements. Of the sample problems considered to date, it comes closest to containing all the features likely to be of interest in developing such models.

4. Instrumentation and Control

In the early stages of a program to develop in-core sensors for diagnosing reactor performance and detecting abnormalities, methods for detecting local boiling in the coolant are being investigated. Evaluation of the acoustic-frequency spectrum method of determining boiling continued (see Progress Report for January 1967, ANL-7302, pp. 73-74) by means of a literature survey, experiment planning, and procurement of equipment. For experience before making ultrasonic measurements, boiling spectra measurements were made in the range 1-20 kc/sec for water boiling in a utility can and for sodium boiling in a superheat experiment. Ultrasonic and vibration transducers have been selected for measuring sounds within a research reactor as well as for making out-of-pile measurements.

D. Chemistry and Chemical Separations

1. Fluoride Volatility Processes

a. Recovery of Uranium and Plutonium from Low-enrichment Fuels: Laboratory Support Work

(i) Fluorination of UO_2-PuO_2-fission Product Pellets. Development studies are being performed in a 2-in.-dia fluid-bed reactor to establish optimum conditions for the recovery of uranium and plutonium from UO_2-PuO_2 pellets containing fission products. Current emphasis in these studies is on the use of BrF_5 as a selective fluorinating agent for conversion of uranium oxides in uranium-plutonium mixtures to volatile UF_6. In this reaction, plutonium is converted to nonvolatile PuF_4. Recovery of plutonium as volatile PuF_6 is effected in a subsequent step by reaction of PuF_4 with fluorine. A recent experiment (Purse-14) was performed to evaluate the effect of high plutonium concentration in the oxide fuel on plutonium retention in the alumina bed. In this experiment, the oxide fuel pellets contained 5 w/o plutonium, whereas previous experiments were performed with UO_2-PuO_2 pellets containing nominally 0.5 w/o plutonium.

The charge to the reactor in Purse-14 consisted of 651 g of 5 w/o PuO_2-UO_2-fission product pellets and 1100 g of 48 to 100 mesh alumina

containing 0.6 g CsF, 0.15 g RbF, and 0.52 g NpO_2. The processing sequence consisted of: oxidation of the pellets for 4 hr at 450°C with 23 v/o oxygen, fluorination of the uranium to UF_6 with 9-10 v/o BrF_5 at 300°C for 2 hr, and recycle-fluorination with 90 v/o fluorine for 3 hr at 300°C, 3 hr at 350°C, 3 hr at 400°C, 2 hr at 450°C, 2 hr at 500°C, and 3 hr at 550°C.

The final alumina bed contained 0.004 w/o uranium and 0.023 w/o plutonium, which corresponds to the removal of more than 99.9% of the uranium and 99% of the plutonium. Although the plutonium concentration in the final bed was greater than that obtained in previous runs (0.007 w/o) with oxide pellets containing 0.5 w/o plutonium, the application of the volatility process to oxide fuels containing up to 5 w/o plutonium appears highly satisfactory, since the percentage of plutonium removed from the bed in the case of the high-plutonium fuel was greater than in experiments with fuel containing 0.5 w/o plutonium (see, for example, Progress Report for December 1966, ANL-7286, p. 51). Analysis of bed samples taken periodically throughout both fluorination steps indicated that most (~95%) of the neptunium was removed during the fluorination and the product appeared in both the UF_6 and PuF_6 streams.

After run Purse-14, approximately 8.5 g of fine particles were recovered from the process equipment by rapping and brushing the disengaging and filter sections of the reactor. These fine particles contained 13% plutonium or about 4% of the plutonium charged to the reactor in Purse-14. Upon disassembly of the fluid-bed reactor, an additional 25 g of fines were recovered from the internal surfaces of the vessel. These fines, which had accumulated in the reactor during 36 experiments with UO_2-PuO_2 pellets, contained 2 g plutonium. This quantity of plutonium was about 1.6% of the total quantity of plutonium charged to the reactor during these runs.

In an effort to reduce plutonium holdup in the fines which accumulate on the internal surfaces of the reactor, an experiment, run Purse-16, was performed which involved fluorination of UO_2-PuO_2 pellets in a fluid bed containing minus 100 mesh alumina (average diameter of particles 46 μ). It was expected that by providing a large concentration of fines within the system the concentration of plutonium in the fines would be diminished. The charge to the fluid-bed reactor consisted of 647 g of UO_2-PuO_2-fission product pellets (0.5 w/o plutonium) and 1100 g alumina containing 0.6 g CsF, 0.14 g RbF, and 0.5 g NpO_2. The processing sequence consisted of: oxidation of the pellets for 4 hr at 450°C with 20 v/o oxygen, fluorination with 10 v/o BrF_5 at 300°C for 2 hr, and recycle-fluorination with 90 v/o fluorine for 3 hr at 300°C, 5 hr while the temperature was increased from 300 to 550°C, and 3 hr at 550°C.

The final alumina bed from run Purse-16 contained 0.007 w/o uranium and 0.021 w/o plutonium which corresponds to the removal of >99.9% of the uranium and 92% of the plutonium in the charge. Previous experiments

with an alumina bed containing 48 to 100 mesh particles have demonstrated the removal of 97% of the plutonium under similar processing conditions (see, for example, ANL-7286, p. 51). It was observed that 31% of the original alumina bed was converted to aluminum fluoride (AlF_3), with the bulk of the reaction occurring during the final 8 hr of the recycle-fluorination period. In contrast, only 2.7 w/o of the alumina bed (48 to 100 mesh) was converted to AlF_3 in Purse-14. The high plutonium retention observed in Purse-16 may be attributed to the extensive fluorination of the bed material and the large surface area of the starting bed.

After run Purse-16, approximately 39 g of fines, containing 5.5% of the plutonium charged to the reactor, were recovered from the disengaging and filter sections of the reactor. This plutonium holdup was approximately the same as that observed in previous runs in which a coarser grade of bed material was used. On the basis of these results, it appears that the use of a bed material containing primarily minus 100 mesh particles for the fluid-bed fluorination of oxide fuel is not practical.

(ii) Purification of Plutonium Streams. In the flowsheet being studied for the volatility processing of oxide fuels, separation of plutonium is achieved by fluorination of PuF_4 to PuF_6 with fluorine. This PuF_6 stream contains uranium, neptunium, and certain fission products which form volatile fluorides, and therefore the product stream must be processed further for the preparation of a purified plutonium product. A laboratory-scale experimental program is under way to explore several processing schemes for purification of PuF_6 process streams.

One method under study involves the selective reduction of PuF_6 to PuF_4 by BrF_3. The procedure consists of contacting the fluoride mixture containing PuF_6 with liquid BrF_3 for 1 hr at 80 to 90°C. The fluorides which remain volatile are distilled from the system at 150 to 200°C. The solid residue, which is primarily PuF_4, is further purified by contact with BrF_5 for about 6 hr at 300 to 400°C. Preliminary results of two experiments involving the reduction of PuF_6 with BrF_3 from mixtures containing UF_6, NpF_6, SbF_5, NbF_5, and RuF_5 indicated that the reduction of PuF_6 was complete. The major portion of uranium, antimony, and niobium was separated from the plutonium in the distillation step. Even higher decontamination from these elements was achieved in the step in which PuF_4 was contacted with BrF_5. Essentially no decontamination from ruthenium was observed in the reduction-distillation step. The decontamination factor for ruthenium after the BrF_5-fluorination step was approximately 540. Results on the behavior of neptunium will be reported when they become available.

b. Recovery of Uranium and Plutonium from Low-enrichment Fuels: Engineering Work

(i) Engineering-scale Alpha Facility. Studies are being performed in the engineering-scale alpha facility to demonstrate handling of

PuF_6 on an engineering scale and to determine the feasibility of fluoride volatility flowsheets. Fluorine efficiencies have been calculated for the fluorination of plutonium during runs Pu-14 and Pu-15 (see Progress Reports for December 1966, ANL-7286, p. 55, and January 1967, ANL-7302, pp. 76-77). In these runs, fluid-bed material, which represented the bed after the uranium had been recovered by fluorination of oxidized UO_2-PuO_2-fission product pellets with BrF_5, was contacted with 80 v/o fluorine to recover the plutonium. Fluorine efficiencies, based on the quantity of plutonium that could be fluorinated as determined from equilibrium data and fluorine input, were high (up to 65%) at the beginning of the runs and then decreased markedly as the plutonium content of the bed decreased.

Current work in the facility involves the installation and testing of equipment which will be used in experiments with BrF_5. During the past month, the off-gas disposal system, which consists of a series of eight traps (4 in. in diameter by 5 ft long), was installed in the large glovebox.

(ii) Process Development Studies for Uranium Dioxide Fuels. Engineering-scale studies are being performed in a 3-in.-dia fluid-bed reactor facility to determine the effects of important process variables on the fluorination of UO_2 fuels with BrF_5. The current program involves a series of eight statistically designed experiments to measure the effects of six independent variables on UF_6 production rate, BrF_5 utilization, off-gas composition, and uranium removal from the fluid bed. Three experiments (runs BRF5-3, BRF5-5, and BRF5-11) have been completed. The processing conditions for these runs were: oxidation of the oxide fuel (2.2 or 4.4 kg) to U_3O_8 by reaction with 19 v/o oxygen in nitrogen at 450°C for 6 hr (run BRF5-11) or for 11 hr (runs BRF5-3 and BRF5-5), followed by fluorination of the fines with 12 to 21 v/o BrF_5 at 225 to 300°C for 3 to 6 hr.

Although complete evaluation of the results of these experiments cannot be made until all eight experiments have been completed, some general observations can be reported. In these experiments, accurate measurement was made of the thermal behavior of the system during oxidation. In all three runs, a temperature excursion within the pellet bed was observed during the oxidation step. Although the temperature of a portion of the pellet bed reached 590°C, no operational problems were encountered during oxidation of the pellets, and this behavior did not appear to affect fluorination of the oxide fines. Localized high-temperature zones of this type are not unexpected during oxidation of packed beds of pellets.

Fluorination of the U_3O_8 fines proceeded satisfactorily in all three experiments. Control of the temperature of the fluid bed within 10°C of the set point was readily achieved without employing the reactor cooling system. During run BRF5-5 (fluorination with 12 v/o BrF_5 at 225°C) a Hays oxygen analyzer was used to follow the course of the

fluorination reaction. It was observed from the concentration of oxygen in the off-gas stream that under these fluorination conditions the UF_6 production rate remained constant at 70 to 80 lb UF_6/(hr)(sq ft) until about 80% of the oxide was fluorinated, at which time the UF_6 production rate decreased markedly. A BrF_5 utilization efficiency of 50% was observed during the constant rate period.

(iii) Fluid-bed Studies with Irradiated Fuels. A series of experiments are under way in a $1\frac{1}{2}$-in.-dia fluid-bed reactor to determine the distribution of fission products during the processing of highly irradiated UO_2 fuel by the oxygen-bromine pentafluoride-fluorine process. Current work in this program has concerned investigation of methods for the removal of fission products from the plutonium product stream. Additional decontamination data have been received for run BRF-4, described in Progress Report for February 1967, ANL-7308, pp. 75-76. The plutonium purification operation involved condensing the PuF_6 stream leaving the reactor at -78°C, subliming the PuF_6 at 0°C in a nitrogen carrier gas stream, and then thermally decomposing the PuF_6 to solid PuF_4 on a bed of refractory alumina at 300°C. Decontamination factors for ruthenium and gross gamma based on the concentration of the contaminants in the fuel charge were 700 and 4000, respectively. Contact of the PuF_4 product with 10 v/o BrF_5 for 0.7 hr at 300°C increased the decontamination factor for ruthenium to 1050.

IV. ADVANCED SYSTEMS RESEARCH AND DEVELOPMENT

A. Direct Conversion

1. Liquid-metal Linear Generator

a. Effects of Interfacial Transport Processes on Film Condensation. The design of the condensing test section and loop has been completed; the loop is nearly ready to operate. Final tests on the air-water test section have been completed. Comparison of the film-conductance probes (used in air-water tests) with the needle-contact probe (to be used in condensing studies) has shown excellent agreement even in the presence of large-amplitude waves.

b. Pressure Recovery of Two-phase One-component Flow through a Diffuser. Initial experiments have been completed on a two-phase flow diffuser having an included angle of 5°. Diffuser efficiency was studied as a function of the inlet void fraction. The experiments had water and steam as working fluids, diffuser inlet pressures of 20-30 psia, and mass flow-rates of 0.3-0.6 lb/sec. The qualities of the two-phase mixture stayed in the range below 1%.

The diffuser efficiency decreased sharply as void fraction increased. For example, as void fraction was raised to 20%, efficiency dropped from 80 to 60% for an inlet at 24 psia and flow of 0.5 lb/sec.

c. Condensing Injector Studies. Condensing injector experiments have yielded improved axial-pressure distributions and cross-channel density profiles; these show with greater detail the effects of flow ratio on the axial-pressure distribution and mixing processes.

The ideal maximum discharge pressure is directly proportional to the inlet vapor-liquid momentum ratio and geometric-area contraction. In Fig. 14 are maped representative data of this investigation and other investigators[16-20] with respect to conditions at the inlet to the mixing section. The inlet vapor-liquid momentum ratio is shown for the various experimental runs at the respective velocity and flow ratios.

---

[16]Brown, G. A., An Analysis of Performance Data from the NUOS Condensuctor Test Facility with a New Theory for Variable Area Condensuctor, Report 44, Joseph Kaye and Co., Inc., Cambridge, Massachusetts, 1962.

[17]Brown, G. A., and Levy, E. K., Liquid Metal Magnetohydrodynamic Power Generation with Condensing Ejector Cycles, Paper No. SM-74/171, Proceedings International Symposium on Magnetohydrodynamic Electrical Power Generation, Salzburg, Austria, July 4-8, 1966.

[18]Platt, R. J., Jr., Investigation of a Jet Condenser for Space Power, NASA, TN D-3045, Oct 1965.

[19]Hays, L., Investigation of Condensers Applicable to Space Power Systems, Part II. Jet Condensers, Electro-Optical Systems Report 1588-Final II (Nov 1962).

[20]Rose, R. P., Steam Jet Pump Analysis and Experiments, WAPD-TM-227, Bettis Atomic Power Laboratory, June 1960.

Discharge pressures obtained in this investigation have been found to be, at best, 60% of the ideal maximum discharge pressure based on the minimum area of the injector and inlet momentum ratio.

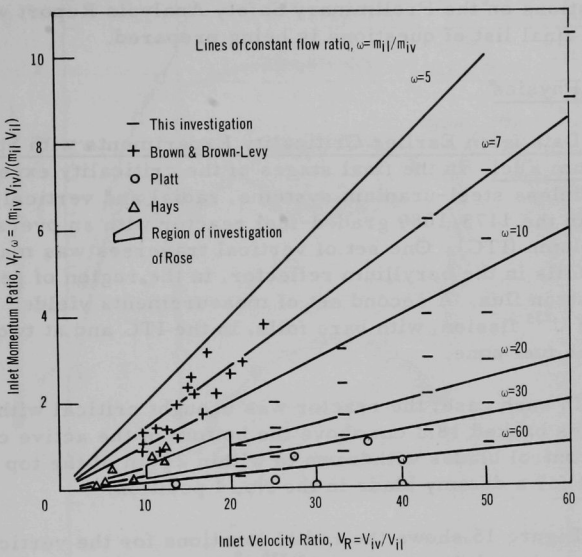

Fig. 14. Region of Investigation Based on Inlet Conditions to Mixing Section

Finally, further efforts are being made to conclude an analytical prediction of axial-pressure profile and overall performance of the test injector.

B. Argonne Advanced Research Reactor (AARR)

1. General

The architect-engineering effort is increasing as Title II work progresses. A new milestone network and detailed PERT network for Title II design and construction have been completed and are being reviewed.

The seismic consultant, Merit White, has completed initial calculations, from which design of the reactor foundation can proceed. A preliminary report on the geology work is available.

The primary heat-exchanger specifications have been sent out for bids, as were specifications for the control-rod guide assembly. The

complete control-rod guide assembly consists of the upper track and bearing assembly, lower track and bearing assembly, and lower bearing track support assembly.

Questions on the Preliminary Safety Analysis Report were reviewed with DRL; a final list of questions is being prepared.

2. Reactor Physics

a. Data from Earlier Criticality Experiments with Stainless Steel-Uranium Fuel. In the final stages of the criticality experiments program on stainless steel-uranium systems, radial and vertical traverses were made in the 1173/1089 graded-fuel reactor with an oversized Internal Thermal Column (ITC). One set of vertical traverses was made with bare manganese foils in the beryllium reflector, in the region of peak radial thermal-neutron flux. A second set of measurements yielded vertical traverses of U^{235} fission, with bare foils, in the ITC and at two radial locations in the fuel zone.

In each case, the reactor was brought critical with the in-core control blades banked 18.3 cm above the bottom of the active core and the peripheral control blades withdrawn to within $2\frac{1}{2}$ cm of the top of the active core, except for a dummy blade in the No. 4 position.

Figure 15 shows the radial locations for the vertical traverses. In Fig. 16 are plotted the results of U^{235} fission traverses normalized to

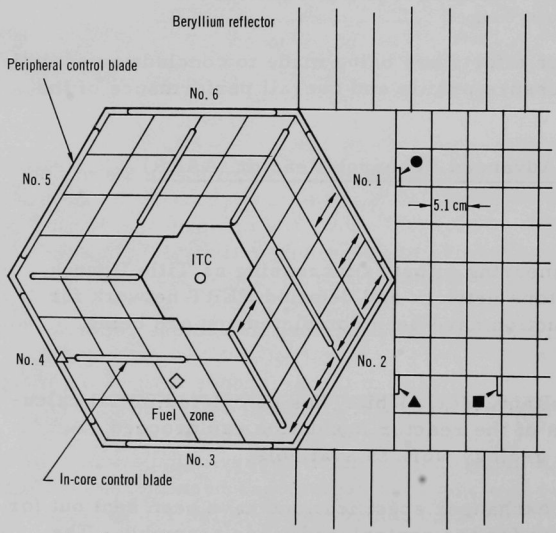

Note: The arrows in the fuel zone show the orientation of the fuel plates.

Fig. 15

Radial Locations of Foils for Vertical Traverses of Activity in 1173/1089 Graded-fuel System with Oversized ITC (simulation of previous SS-UO_2 system)

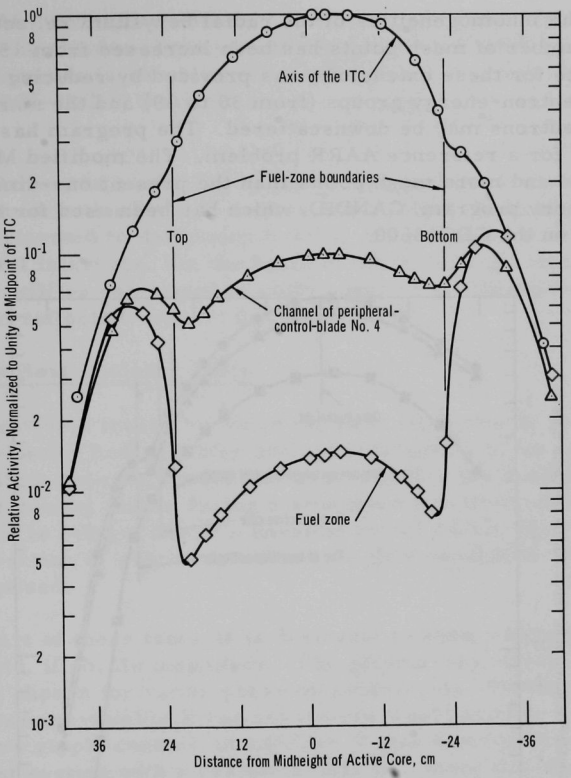

Fig. 16. Vertical Traverses of U^{235} Fission with Bare Foils (1173/1089 graded-fuel system with oversized ITC)

unit activity at the midpoint of the ITC; the flux-distortion effects of the bank of in-core control blades are evident and even the flux at the axis of the ITC is somewhat affected. Figure 17 shows the manganese-activity traverses in the beryllium normalized to peak unit activity for the traverse at a location near peripheral-blade No. 1.

The radial traverses will be described in a future report.

b. Theoretical Reactor Physics of the Reference AARR. To meet special requirements of the AARR analysis, a modified version of the MACH-1 program for the CDC-3600 computer has been prepared. The modification is on the one-dimensional diffusion-theory calculation. The maximum number of locally homogeneous regions has been increased from 20 to 35 to permit more detailed consideration of the radial fuel grading in the HFIR-type (Al-U_3O_8) core assembly, and to represent more

accurately the inhomogeneities of the radial beryllium reflector. The maximum number of mesh points has been increased from 150 to 250. The storage space for these extensions was provided by reducing the maximum number of neutron-energy groups (from 30 to 19) and the number of groups into which neutrons may be downscattered. The program has been tested successfully for a reference AARR problem. The modified MACH-1 allows more regions and more mesh points than the present one-dimensional diffusion-theory program, CANDID, which has been used for this type of computation on the CDC-3600.

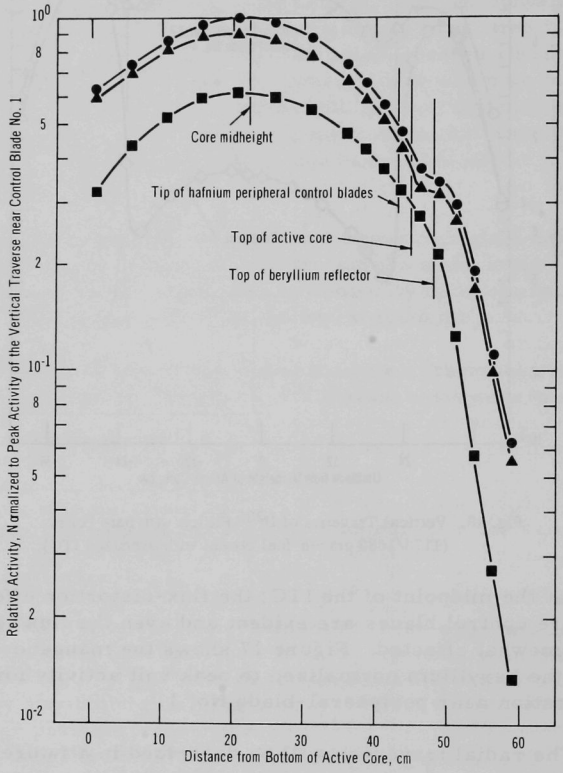

Fig. 17. Vertical Traverses with Bare Manganese Foils in the Beryllium Reflector (1173/1089 graded-fuel system with oversized ITC)

One-dimensional diffusion theory calculations of the HFIR have agreed with measured data to within ~1% in reactivity. Calculations are in progress with modified space-dependent cross sections for the thermal-neutron groups obtained from THERMOS computations. Also, two-dimensional analyses are being performed to evaluate the equivalent axial

bucklings under various conditions of neutron reflection. One such calculation will check the one-dimensional result that the fresh core assembly of two fuel elements is subcritical by ~7% when it is surrounded by water, i.e., with a 100%-H_2O ITC and with water in place of the radial beryllium reflector.

Review is continuing of the various shield-design analyses being performed in the Title-II work on the AARR. Other computations have been performed to determine heating rates in support structures for reactor-vessel internals. On the basis of these heating rates, temperature distributions will be calculated to study possible problem areas such as the aluminum reflector-support pedestal.

3. Transient Heat-transfer Tests

To provide a means by which the calculated effects that adding reactivity have on the heat transfer and hydrodynamics in the core can be compared with a physical model that approximates the behavior of a fuel plate and the cooling media during a simulated reactivity-induced power transient, use is being made of a physical model consisting of an electrically heated test section in which representative flow conditions for the AARR core are imposed.

As part of these tests, it is desirable to know whether a vapor phase is present and, if so, its magnitude. The gamma-ray attenuation technique was initially chosen for vapor-phase measurements. However, neither radioisotopes nor available X-ray generators would provide a high-intensity beam with low ripple content; in addition, it was desired to have a void-measurement system with a response time of 1 msec that would measure the density of the fluid at the test-section exit when the fluid has a minimum vapor content of 1 to 2%. Thus a special X-ray power supply with 0.1% ripple and 0.1% regulation in both high voltage and tube current will be used. An electronic stabilization system will offset X-ray and detector drifts.

All system components have been delivered and are being tested before installation on the transient heat-transfer loop. The detected X-ray beam after passage through 1/32-in. steel has a maximum ripple component of 1.5% peak-to-peak at the most unfavorable operating condition (50 kV, 30 mA). At X-ray tube conditions of 150 kV and 20 mA, the detected beam after passage through 1/4-in. copper has a ripple component of less than 0.5% peak-to-peak. When the effects of X-ray production and attenuation are considered, these values are within the specification of 0.1% rms. The tests show that the electronic stabilization system will compensate for changes in detector current common to the detector that will be used with the test section and to a reference detector by a factor of

30 to 1. Therefore, a change in X-ray beam or detector high voltage that causes a 3% change in both signals will appear as only a 0.1% change in a normalized output signal to the recorder.

4. Beam-tube Shield-plug Test Sleeve

Ten horizontal penetrations in the biological shield are required for insertion and replacement of the beam tubes. The present design requires a stepped cylindrical sleeve to provide openings in the shield. After the reactor vessel is positioned, a smaller alignment stepped cylindrical sleeve is inserted within the biological-shield stepped sleeve. The machined alignment stepped sleeve will be positioned and aligned accurately with the reactor-vessel beam-tube nozzles and then secured. The ~3.5-in. cylindrical gap between the two sleeves must be filled with high-density concrete to complete shielding requirements.

To determine the best method of placing the concrete and to evaluate the workmanship and the results of the fill, a stepped cylinder within a cylinder test sleeve has been designed and fabricated. As a test, the high-density concrete grout has been placed by hand to evaluate this method. The mix had ferrophosphorus aggregate with a maximum sieve size of 1/2 in. and concrete average density was about 232 lb/ft^3. The concrete mixture consistency was kept moist but not fluid so as to prevent the heavy aggregate from settling and the mix from spilling out of the open ends of the sleeve.

After the concrete cured, the split sleeves were separated, exposing the concrete casting, which revealed excessive voids in the heavy aggregate. Although a finer aggregate and more fluidity to the mix might have yielded a much more acceptable casting, it is apparent that this placement-by-hand method does not readily provide dense concrete that is free of voids and adequate for shielding.

The test sleeve has been modified in preparation for testing a method that involves pumping the high-density grout into the test sleeve.

5. Analysis of Flow-coastdown Dynamics

To determine the status of plant safety if utility electrical power fails, an analytical study has been made of AARR behavior after coolant pumping power is lost. The overall study involves three interrelated investigations, which have been integrated to provide preliminary instrumentation-design requirements necessary to satisfy the relevant safety criterion as stated in the AARR Preliminary Safety Analysis Report.[21] The three

[21]The applicable criterion is No. 4.4 of Preliminary Safety Analysis Report on the AARR, Approval Copy, Vol. I, March 31, 1966 (Revised December 9, 1966), which is as follows: "The core design and normal operating parameters will be such that under normal operation and under abnormal, but anticipated conditions, e.g., utility power failure, the hot-spot heat flux will not exceed that value at which the onset of local boiling occurs."

investigations, the first of which is described here, are: (a) evaluation of AARR coastdown characteristics, (b) determination of reactor core response to flow-coastdown accidents and (c) analysis of flow-sensing characteristics for instrumentation within the affected reactor-safety channels.

a. Evaluation of AARR Flow-coastdown Characteristics. This information extends that reported earlier (see Progress Report for September 1966, ANL-7255, pp. 62-63) by giving additional results and by describing the mathematical model used to calculate flow coastdown.

For a solution to the total problem, flow-coastdown dynamics were evaluated separately, then those results were used as input to a core thermal and neutronic dynamic model. Thus it is tacitly assumed that thermal conditions in the core do not significantly affect the flow in the flow range of interest.

(i) Description of Mathematical Model. In the event of a total loss of primary pumping power, coolant flow in the primary system coasts down rapidly to that supplied by the Shutdown Emergency Cooling System, which is composed of d.c. series-wound battery-powered "pony" motors. To provide a means for calculating the flow-time history subsequent to loss of utility electrical power, a general but simple coastdown model suitable for programming on the analog computer was derived. The model includes the effects of system head losses, pump-developed head, pump-load torque, shaft and water inertias, and pony-motor characteristics. Although the present model can evaluate flow response only for the case of two pump motors tripping off simultaneously, it can easily be adjusted to describe cases involving one pump tripout, sequential pump tripout, pump startup, etc.

For the purposes of this analysis, the primary system was subdivided into the following groups of components, each of which contributes the indicated estimated head loss for normal (full-flow) operation:

Component	Head Loss (ft)
Reactor (vessel and internals)	298
Heat-exchanger complex	58
Pump complex	15
Main piping	35
Strainer	20
Total system	426

The heat-exchanger and pump complexes include their associated inlet and outlet piping as well as inlet and/or outlet valves. A schematic diagram of the basic system analyzed is shown in Fig. 18.

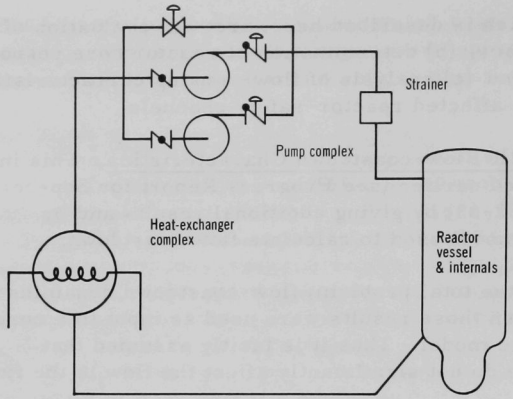

Fig. 18
Schematic Diagram of AARR Primary System for Flow-coastdown Analysis

The estimated total system loss is based on a core pressure drop of 110 psi (259 ft) at a total pump flow of 19,000 gpm. The core loss was assumed to obey a flow ratio law with an exponent of 1.8; for the remainder of the system an exponent of 1.9 was used. This yields an expression for the total system head loss:

$$\Delta H_T = 259(Q/Q_0)^{1.8} + 167(Q/Q_0)^{1.9}. \quad (1)$$

Pump-head and horsepower requirements used in the analysis are consistent with a developed head of 426 ft with each of two pumps delivering 9,500 gpm. Head-versus-capacity curves for typical centrifugal pumps were obtained for a range of design head and flow values, from which one curve, typical for AARR application, was chosen for this study. Horsepower and torque relationships were obtained directly from the head and efficiency curves as

$$HP = \frac{\rho}{(7.48)(33,000)}\left(\frac{Q\Delta H_p}{\eta}\right) \quad (2)$$

and

$$\text{Torque} = \left(\frac{33,000}{2\pi}\right)\frac{HP}{N}, \quad (3)$$

where ρ is fluid density, ΔH_p pump head, N pump speed, Q volumetric flowrate, and η the pump efficiency.

It was assumed that the pony motors on the AARR primary pumps would be similar to those used at ORNL for the HFIR (i.e., battery-powered, d.c. series wound), mounted on the main pump-motor shaft. The essential criterion used for establishing pony-motor size was that each

motor, when operating singly, must deliver at least 10% of full rated AARR flow, or 1900 gpm. Thus, a torque versus speed characteristic was obtained for such a typical motor in the range 2-6 hp, and this characteristic was used in the coastdown model.

To complete the model used to describe AARR flow-coastdown dynamics, it was necessary to determine values for pump-shaft (rotary) inertia and loop (water) inertia. The total shaft inertia was evaluated by adding the contributions of the motor, pump, and water rotating within the pump. Data were obtained for inertias corresponding to a series of motor and centrifugal pump combinations for various sizes. From these, one was selected for which the total shaft inertia (I'_p, or Wk^2) was found to be 1040 lb_m-ft^2.

The loop inertia was evaluated by subdividing the primary loop into a series of blocks, each of which was described by an effective length $\bar{L}$ and cross-sectional area $\bar{A}$. The summation of ratios of these quantities is used to obtain the loop inertia I'_w:

$$I'_w\left(\frac{lb_f\text{-}sec^2}{lb_m\text{-}in.^2}\right) = \frac{1}{144g_0}\sum_i\left(\frac{\bar{L}}{\bar{A}}\right)_i.$$

The value of $\sum_i (\bar{L}/\bar{A})_i$ was found to be 87 ft^{-1}; thus $I_w = 0.0187$.

The foregoing parameters and relationships were then used to derive the final equations representing flow-coastdown conditions in the AARR. The basic assumptions made in this derivation are: (a) the transient is sufficiently slow so that compressibility effects are negligible; (b) steady-state pump-head and torque equations hold during the coastdown transient; (c) each of the two parallel pump-motor units acts identically, i.e., together as a single unit.

The coastdown dynamics are then defined by a pair of first-order, nonlinear differential equations describing the pump speed and flow dynamics:

Flow Dynamics:

$$\frac{dw}{dt} = \frac{1}{I_w}(\Delta H_p - \Delta H_T). \tag{4}$$

Pump-speed Dynamics:

$$\frac{dn}{dt} = \frac{1}{I_p}(T_M - T_p), \tag{5}$$

where

Pump Head:

$$\Delta H_p = P_n n^2 + P_c nw + P_w w^2, \tag{6}$$

System Loss:

$$\Delta H_T \cong \Delta H_{T_0} w^{1.85}, \tag{7}$$

Motor Torque:

$$T_M = T(t) + T_{pM}(n) \tag{8}$$

where $T(t)$ is the main motor torque and T_{pM} the pony motor torque,

Pump Torque:

$$T_p = K_p \Delta H_p + K_c nw, \tag{9}$$

Normalized Pump Speed and Volumetric Flowrate:

$$\begin{aligned} n &= N/N_0, \\ w &= Q/Q_0. \end{aligned} \tag{10}$$

Also,

$$I_p(\text{ft-lb}_f\text{-sec}) = \frac{\pi N_0 I_p'}{30 g_0}$$

and

$$I_w\left(\frac{\text{ft-lb}_f\text{-sec}}{\text{lb}_m}\right) = \frac{Q_0}{(7.48)(60)g_0} \sum_i \left(\frac{\bar{L}}{\bar{A}}\right)_i.$$

(ii) Calculated Results for the AARR. An analog computer program was developed to solve these equations and to calculate theoretical coastdown for AARR. The calculations consisted primarily of evaluating three cases of flow versus time following simultaneous loss of power from both main pump motors. The three cases show the effect of pony motors on the coastdown dynamics. In addition, a limited analysis was done showing the effect of flywheels mounted on the pump-motor shafts.

Flow coastdown was evaluated without flywheels for three cases: (1) no pony motors operating, (2) one pony motor operating, and (3) two pony motors operating.

To illustrate the calculated results, Fig. 19 depicts normalized pump speed and flowrate versus time for Case 2. Similar graphical results were obtained for all cases studied. The results show that in all three cases, 50% of initial pump speed occurs at 1.76 sec and 50% flow occurs at 1.80 sec. Thus, the effect of pony motors is negligible during the early phase of the transient. During the latter stages, however, the difference is large since flow goes to zero without pony motor(s).

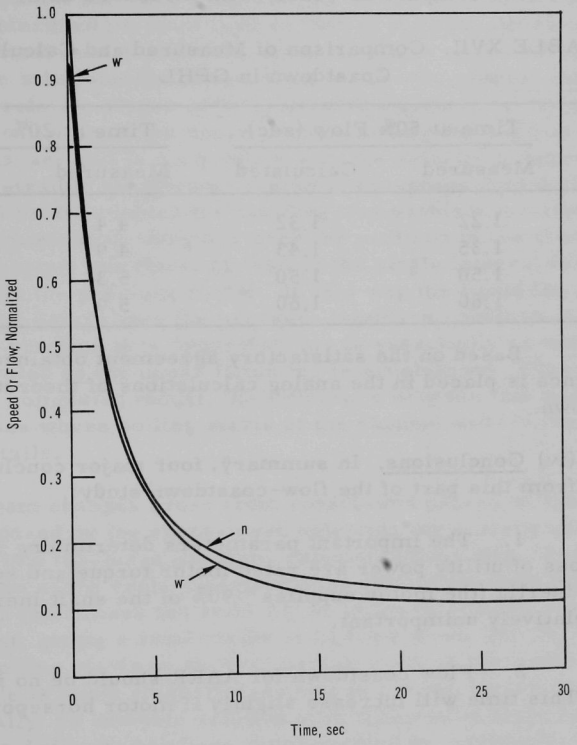

Fig. 19. AARR Flow Coastdown with One Pony Motor Operating

As expected, flywheels were found to increase the coastdown time in nearly exact proportion to the total rotary inertia, i.e., doubling the shaft inertia doubles the time at which a 50% flow reduction occurs. This study showed that the important parameters determining rate of coastdown for AARR are the rotary inertia I_p', rated motor speed N, and the rated motor torque T_p. The effect of water inertia is small.

(iii) Experimental Verification of Mathematical Model. Verification of the theoretical model described above and confidence in results

obtained therefrom has been accomplished by comparison of analog calculations with measured coastdown data. These data were obtained from a series of coastdown experiments conducted on the ANL General Purpose Hydraulics Loop (GPHL) and the CP-5 reactor. Basic analog input information was obtained for both the GPHL and CP-5, as required in Eqs. (4-9).

For both systems data in Table XVII are illustrative. The analog calculations compare favorably with measured data.

TABLE XVII. Comparison of Measured and Calculated Coastdown in GPHL

Q_0, (gal/min)	Time at 50% Flow (sec)		Time at 20% Flow (sec)	
	Measured	Calculated	Measured	Calculated
1200	1.22	1.32	4.4	5.4
1000	1.35	1.43	4.9	5.7
800	1.50	1.50	5.3	6.0
600	1.60	1.60	5.9	6.4

Based on the satisfactory agreement obtained, considerable confidence is placed in the analog calculations of theoretical AARR flow coastdown.

(iv) Conclusions. In summary, four major conclusions have been drawn from this part of the flow-coastdown study:

1. The important parameters determining rate of coastdown upon loss of utility power are rated motor torque and speed, and the total rotary inertia (the motor supplies >90% of the shaft inertia); water inertia is relatively unimportant.

2. Flow coastdown for AARR should be no faster than 50% in 1.8 sec. This time will increase slightly if motor horsepower is increased.

3. Rate of coastdown is not affected by pony motors during the initial stages of the transient (i.e., up to 2.5 sec). Later, of course, the difference is large because flow goes to zero without pony motors.

4. Analytical versus experimental comparisons on the GPHL and CP-5 were judged to be satisfactory (disagreement on GPHL was 0-10% and on CP-5 was 6-14%).

V. NUCLEAR SAFETY

A. Accident Analysis

1. Calculations on Transient Sodium Boiling

A calculational model which allows boiling to start at an arbitrary point in the channel has been programmed for the computer. When boiling starts at an intermediate point (rather than at the exit end as in previous work,[22] the lowest (nearest channel inlet) interface of the sodium and sodium vapor mixture subsequently moves down toward the channel inlet as determined by the relative slopes of the coolant and saturation-temperature profiles. At the same time, the upper interface of the bubble moves upward toward the channel exit in accordance with the velocity of expelling coolant, thus giving a steadily lengthening region of two-phase flow with time. The computational model adopted for handling this problem involved the use of two separate momentum integrals over the portions of the channel above and below the upper interface, instead of the single integral for the whole channel used in the previous model. In this way the liquid leg above the upper interface determines the pressure boundary condition at the upper interface. In practice it is found that this is essentially as inertial pressure loading generated as the upper liquid leg is accelerated. Other than this change in the computing model, the difference between this and the previous work (for cases where boiling starts at the channel exit) is mainly in programming details.

Program changes arose from constraints placed on the minimum time step imposed by the space-mesh selection for a particular problem, and resulted in a too-large program-calculated time step. In the previous work, the slope of the coolant-temperature profile adjacent to the boiling region (which determines the ratio $\Delta t/\Delta z$ in the two-phase region) tended to be quite flat, giving a small value of Δt for a given Δz. On the other hand, when boiling starts at an intermediate point in the channel, this coolant profile is much steeper, resulting in a much larger Δt for a given Δz, and, usually, an unstable solution after a few time steps after boiling started. This difficulty has been circumvented by introduction of a revised algorithm which has been demonstrated to have good computational stability characteristics for a wide range of problem parameters.

B. Coolant Dynamics

1. Sodium Expulsion

This experiment, in which it is planned to investigate the mechanism of coolant expulsion in a simulated reactor environment, includes measurement of the void distribution, expulsion velocities, pressure transients, and liquid superheats during coolant expulsion.

[22] MacFarlane, D. R., An Analytic Study of the Transient Boiling of Sodium in Reactor Coolant Channels, ANL-7222.

The eddy-current coils are being fabricated; they will be used to measure the expulsion velocity and perhaps the void fraction of the two-phase mixture during expulsion. Coil operation is being analyzed to determine the optimum excitation voltage and frequency for obtaining linear output and response as well as stability. Several other techniques for measuring expulsion velocity are also being studied. The electron-bombardment heater is expected to be delivered within the next few months.

2. Superheat

To determine the amount of liquid superheat required to initiate nucleate boiling in sodium under various conditions simulating a reactor environment, this experiment measures the independent and combined effects of pressure, dissolved gas, heat flux, surface characteristics, and the pressure-temperature history of the system.

A thermal-radiation heater is being installed to extend the range of heat flux. The superheat data obtained from previous test runs are being reduced.

3. Critical Flow

Calculations indicate that critical flow may occur in the core of a sodium-cooled reactor during an accidental power surge. Critical flow could lead to detrimental effects such as voidage of the coolant channel, shock phenomena, and pressure buildup. To investigate these effects, a sodium loop has been operated successfully up to 1600°F; measurements include critical pressure, critical flowrate, stagnation temperature and pressure, and axial temperature profile in the test section. Similar data are being collected for steam-water mixtures using the subatmospheric water loop. Data reduction and analysis are under way; quantitative comparisons between liquid sodium-vapor and steam-water critical-flow data will be available soon.

4. Electron-bombardment Heater Tests

The operation of various electron-bombardment heaters (EBH), which will be used to simulate in-pile experiments pertaining to reactor safety, is being examined in a large evacuated vessel. Both single-pin heaters and multipin heaters will be built and tested.

The EBH test vessel and the ion pump have been ordered, and fabrication of the first EBH section is progressing satisfactorily.

5. Convective Instability

After some delivery delays, the experimental apparatus is being constructed, and checked for leaks and design flaws.

Analytically, the second approximation for the method of integral relations has been formulated and solved. It seems to give an added correction to the previous solution; if a third term is taken in the complete set of functions, apparently the solution to the problem will be attained to within a few percent. This will be attempted next month.

6. Component Dynamics

This work, which was reported under the present heading the last two months (see Progress Reports for January 1967, ANL-7302, pp. 88-90, and for February 1967, ANL-7308, pp. 84-85) was reported previously under the heading, "Effect of Rapid Heating of Reactor Components" (see Progress Reports for October 1966, ANL-7267, pp. 74-75, and for December 1966, ANL-7286, pp. 69-70).

In the initial phase of the component-dynamics studies, a qualitative classification of coolant-structure systems was proposed (see Progress Report for October 1966, ANL-7267, p. 75). Such an investigation is an obvious part of any study to examine various energy-partition mechanisms for their sensitivity to variations in the parameters within the region of interest for in-core structures.

An example problem is that of determining parameter relations defining conditions under which particular frequency components of a pressure-pulse may be transmitted unreflected through the bounding structure. Energy lost in this way is not available for doing work on the coolant.

This problem was investigated by considering the one-dimensional model consisting of a slab of solid material (shell) bounded by the same homogeneous fluid medium (coolant) on each side. The slab of material is of thickness b and the planes forming the two interfaces are $x = 0$ and $x = b$. The wave equation, assumed to govern the propagation of waves in the two media, has a solution for the plane wave, represented by the velocity potential

$$\phi_0(x, t) = A_0 \exp\left[i\omega\left(t - \frac{x}{C_1}\right)\right], \tag{1}$$

where A_0, ω, and C_1 represent amplitude, frequency, and the velocity of sound in the coolant, respectively. This wave could represent a particular frequency (ω) component of a pressure pulse originating within an in-pile loop.

The condition satisfying the requirement of no reflected wave, for normal incidence on a plane interface, is[23]

$$C_1\rho_1 = C_2\rho_2, \quad \text{if } \sin\left(\frac{\omega b}{C_2}\right) \neq 0 \tag{2}$$

[23] Bateman, H., Partial Differential Equations of Mathematical Physics, Cambridge University Press, pp. 333-336 (1959).

or

$$\sin\left(\frac{\omega b}{C_2}\right) = 0 \rightarrow \frac{\omega b}{C_2} = n\pi, \qquad n = 1, 2, 3, \ldots . \tag{3}$$

In these equations, ρ is the density and subscripts 1 and 2 refer to the fluid and solid, respectively. The case in Eq. (2) involves acoustical impedance matching and is somewhat special in that the requirement for no reflection is independent of the thickness of the structural medium. The second case [Eq. (3)] implies that no reflection occurs if the structural thickness is an integral multiple of one-half the wave length of the sound wave in the solid, i.e., $b = n(\lambda_2/2)$, where $\lambda_2 = (2\pi C_2/\omega)$.

If the structural natural frequency corresponds to the frequency associated with complete transmission, a frequency component which would otherwise be transmitted unreflected might possibly be attenuated due to resultant structural coupling. The free-vibration natural frequencies of an elastic circular shell can be estimated as

$$\omega_1 = \frac{1}{r}\sqrt{\frac{E}{\rho}} \tag{4}$$

for extensional vibrations, or as

$$\omega_m = \frac{m(m^2 - 1)}{(1 + m^2)^{1/2}} \sqrt{\frac{Eb^2}{12\rho r^4}}, \qquad m = 2, 3, 4, \ldots \tag{5}$$

for bending vibrations. In these frequency equations, r is the radius of the shell, b is the thickness, ρ is the mass density of the material, and m the number of full sine waves along the circumference. The thickness-to-radius ratio of the shell having a natural frequency equal to the frequency of a sound wave which will be transmitted unreflected can be computed by equating Eq. (3) to Eqs. (4) and (5), and noting $C_2 = \sqrt{E/\rho_2}$. The results are

$$\left(\frac{b}{r}\right) = n\pi, \qquad n = 1, 2, 3, \ldots \tag{6}$$

for extensional vibrations, or

$$\left(\frac{b}{r}\right) = [12(1 + m^2)]^{1/4}\left[\frac{n\pi}{m(m^2 - 1)}\right]^{1/2}, \qquad \begin{matrix} n = 1, 2, 3, \ldots \\ m = 2, 3, 4, \ldots \end{matrix} \tag{7}$$

for bending vibrations. Equation (7), for the lowest-frequency sound wave that will be transmitted unreflected ($n = 1$), gives the following values for the thickness-to-radius ratio corresponding to the various vibrational modes:

m =	1	2	3	4	5
b/r =	3.14	2.02	1.19	0.847	0.676.

For large m, say $m > 5$, Eq. (7) can be approximated as

$$\left(\frac{b}{r}\right) \approx \frac{(12\pi^2)^{1/4}}{m} = \frac{3.3}{m}. \tag{8}$$

The thickness-to-radius ratios given above are of such magnitude that the thin-shell assumptions tacitly implied in Eqs. (4) and (5) are violated. However, since the thickness-to-radius ratio of typical in-pile loops is in the range from 0.05 to 0.25, these results do lead to the conclusion that a structural-coupling phenomenon, which might give rise to a dissipation of energy in the frequency component which would otherwise be totally transmitted, cannot be expected for practical in-pile loop geometries.

C. Fuel Meltdown Studies with TREAT

1. Defected Elements

Nineteen fuel elements are being fabricated for irradiation in EBR-II followed by destructive testing in TREAT. The elements are being made to fit a standard B-37 irradiation assembly in EBR-II. Each element has an 18-in.-long fuel section that can be cut out and used in TREAT following irradiation in EBR-II.

Each fuel section consists of an 11-in. column of 0.246-in.-dia $(U_{0.8}Pu_{0.2})O_2$ pellets inside a 0.250-in.-ID stainless steel-jacketed tube. One end of each tube is spread open to 0.260 in. to provide sufficient clearance between the tube ID and the pellet OD for a loading funnel. Each jacket tube is covered with shrinkable electrical insulation that prevents contamination of the external portions of the tube while loading. The pellets, which were purchased from a commercial fabricator, are loaded into the jacket tubes by means of an inclined, vibrating feeder. The plastic insulation is removed in a low-contamination area and the bared assembly is moved into a clean glovebox. The top is reformed to a diameter of 0.250 in. and a top plug is inserted and welded in place. Each fuel section is inspected and joined to a top and bottom section by welding.

Progress to date consists of the following accomplishments: (1) the design of the element has been completed, (2) all hardware has been fabricated and inspected, and (3) four fuel sections have been fabricated and inspected. The idea of spreading the tube mouth to accommodate a loading funnel has proven successful as has the idea of protecting the jacket tube with plastic while it is in the glovebox.

2. Advanced Sodium Loop Development for TREAT

Fast reactor safety experiments on the transient behavior of fuel and coolant performed in the TREAT reactor require specially designed sodium loops. Development of a Mark-II integral sodium loop is underway to provide improved capabilities in containment, remote handling and instrumentation over the Mark-I loops used for the TREAT sodium loop experiments performed to date.

a. Prototype Annular Linear Induction Pumps. The Mark-II loop design includes an annular linear induction pump (ALIP) as replacement for the thin-walled Faraday-type electromagnetic sodium pumps used in the Mark-I loops. This change was dictated by establishment of a design pressure rating for Mark II of an order of magnitude greater than the pressure rating for the older loop design.

All of the components required for the assembly of prototype 4-pole and 5-pole ALIP have been received. Bench assembly and outfitting of the units is well underway. The 5-pole pump has been finished and given an electrical bench test. A 4-pole version of the ALIP is in the final stages of construction. Pumps will be flow tested using the new component test loop.

b. The Mark-II Integral Sodium TREAT Loop. The Mark-II Integral Sodium TREAT Loop was designed for a reference containment pressure and temperature of 340 atm and 538°C, in accordance with the ASME Boiler and Pressure Vessel Code, for a Class A Nuclear Vessel. The code requires conformation in material composition, weld continuity, strict inspection criteria at all stages of fabrication, and tabulated maximum allowable design stresses for the T316 stainless steel used in the loops.

Loop bends which would meet the full specification of 340 atm have not yet been obtained because of the difficulty in procuring heavy-walled tubing bent into the small-radius curves required by the narrow geometry of an integral loop. All other components of the loop assembly have been finished, and the loop fabrication must await the receipt of the finished bends for inlet and return tubing.

A supply of inlet and return bends having walls thinned beyond specifications during the bending process have been received. Although unsuited for the reference design pressure, these bends have a wall thickness capable of meeting the code requirements for half of the reference pressure (i.e., 170 atm) and are well suited for use in a lower-pressure loop in which only experiments on metallic fuel would be performed.

The original reference design loop is designated "Mark IIA," and the lower capability loop is designated "Mark IIB." In order to avoid

possible mixing of the two kinds of Mark-II loop, the Mark IIB has been designed with a top closure flange (used to insert the sample) that is different from the closure of the Mark IIA. The two closure flanges are not interchangeable.

In addition to providing experimental capabilities beyond those of the first-generation TREAT integral loop well in advance of the time that the 340-atm Mark-IIA loops would be available, the Mark-IIB loops will permit an early checkout of assembly and alignment procedures. Final assembly of three Mark-IIIB loops has begun.

D. Materials Behavior, Equation of State, and Energy Transfer

1. Physical Properties and Equations of State

The coefficients of thermal expansion and compressibility of liquid sodium are of interest for reactor safety, the former for natural convection heat transfer and the temperature coefficient of reactivity studies, whereas the latter is of interest for the bursting of fuel pins utilizing a sodium bond or for the propagation of pressure pulses in a reactor accident.

The thermal-expansion coefficient α is defined as

$$\alpha = \frac{1}{V}\left(\frac{\partial V}{\partial T}\right)_P = -\frac{1}{\rho}\left(\frac{\partial \rho}{\partial T}\right)_P , \qquad (1)$$

where V is the specific volume, T is the temperature, P is the pressure, and ρ is the density. Recent experimental determinations of the density of sodium at high temperatures[24] along the saturation curve were used to fit an equation to the best published values from the melting point to 1300°C.

At higher temperatures, the density-temperature relation suggested by the lattice-gas model[25] of the thermodynamic critical point was used:

$$\rho/\rho_c = 1 + A[1 - (T/T_c)]^b \text{ for } T/T_c > 0.65, \qquad (2)$$

where the temperatures are on the absolute scale and the subscript c indicates the critical condition. Best values of these constants have been found in another study[26] as

$T_c = 2923°K;$

$\rho_c = 0.1591 \text{ g/cm}^3;$

$A = 5.078;$

$b = 0.669.$

---

[24] Stone, J. P., et al., J. Chem. Eng. Data 11, 320 (1966).

[25] Fisher, M. E., J. Math. Phys. 5, 944 (1964).

[26] Muter, D., Cohen, A. B., and Dickerman, C. E., unpublished.

These values might be subject to small changes which, however, should not significantly affect the results.

Values calculated from Eqs. (1) and (2) are plotted in Fig. 20. The dotted curve represents an interpolation between the two regions of temperature.

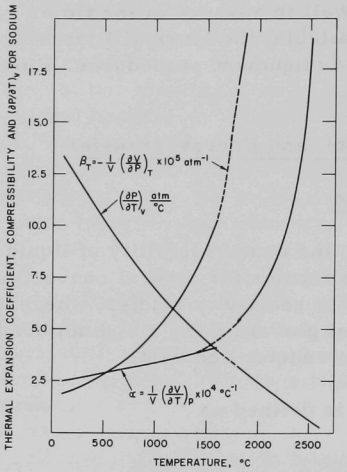

Fig. 20. Expansion Coefficients of Sodium as a Function of Temperature

The isothermal compressibility β_T is defined as

$$\beta_T = -\frac{1}{V}\left(\frac{\partial V}{\partial P}\right)_T = \frac{1}{\rho}\left(\frac{\partial \rho}{\partial P}\right)_T$$

and is related to the adiabatic compressibility β_S by

$$\beta_T = \frac{C_P}{C_V}\beta_S = \beta_S + \frac{T\alpha^2}{\rho C_P},$$

where C_P and C_V are the heat capacities at constant pressure and volume, respectively.

The isothermal compressibility has been measured for sodium just above the melting point but not over wide enough range for extrapolation.

The velocity of sound C can be related to the adiabatic compressibility by

$$\beta_S = 1/C^2\rho.$$

Sonic velocities have been measured in sodium by a number of investigators, who also established the temperature variation.[27] The work of Trelin and Vasil'ev covered the widest temperature range but gave a value for the velocity at the melting point which disagreed with that found by other investigators. An equation fitted to the work of Pochapsky, which has been corroborated by others, was used extrapolated far beyond the experimental limits, since the unavailable work of Trelin and Vasil'ev indicated a linear behavior over a wide range of temperature. Also extrapolated was the heat capacity relation,[28] although this extrapolation has some experimental confirmation.

---

[27]Pochapsky, T. E., Phys. Rev. 84, 553 (1951); Abowitz, G., and Gordon, R. B., J. Chem. Phys. 37, 125 (1962); Trelin, Yu S., and Vasil'ev, I. V., MOPI, No. 13, p. 3 (1961) (in Russian).

[28]Ginnings, D. C., Douglas, T. B., and Hall, A. F., T. Research (NBS) 45, 23 (1950).

Values of the isothermal compressibility plotted in Fig. 20 interpolate smoothly between the two temperature regions of interest. Also calculated was the constant volume change of pressure with temperature, which can be related to α and β_T by the equation

$$\left(\frac{\partial P}{\partial T}\right)_V = \frac{\alpha}{\beta_T}.$$

This quantity is also plotted in Fig. 20 and also varies smoothly from the region where experimental data is available to a small value near the critical point. Integration of this curve for a given initial pressure and temperature would give the total pressure in a confined volume of sodium, i.e., that to burst a cladding. That pressure would be achieved as long as the average density of the sodium in the volume available to it was greater than the liquid density on the saturation curve. Otherwise the pressure would correspond to the vapor pressure of the sodium.

E. TREAT Operations

Prototype digital readout equipment for the fast neutron hodoscope system was installed. Radiofrequency noise generated by the digital equipment interfered with the low-level amplifier circuits connected to the neutron detectors. Work required to suppress this noise sufficiently to permit operational testing of the system has delayed testing of the system during fuel-element-meltdown experiments.

The following results were obtained during initial testing of the out-of-pile portion of the large TREAT sodium loop:

1. The main electromagnetic (EM) pump and associated rectifier and control system operated satisfactorily.

2. The system flow, temperature, level, and pressure instruments operated satisfactorily.

3. Gas was trapped in the plugging-meter circuit during filling of the loop. It was necessary to evacuate part of the system to remove this gas before the EM pump in the plugging-meter circuit would operate. Temperature sensitivity of the EM flowmeter in the plugging-meter circuit has prevented satisfactory operation of the plugging meter. The original Type 347 stainless steel electrodes on the flowmeter were replaced with Type 304 stainless steel electrodes, and preliminary data indicate that the temperature sensitivity of the flowmeter has been greatly reduced.

4. The five main, bellows-sealed sodium valves operated satisfactorily most of the time, but the valves that are spring-loaded to open have occasionally stuck in the closed position. This sticking is apparently

caused by excessive friction between the secondary seal packing and operator shaft. Lubrication of the shaft with dry lubricants and loosening the packing retainer has not solved this problem. Since these valves may operate normally for a considerable period of time, it is very difficult to determine the effectiveness of any action taken to correct this problem.

5. The valve between the sodium-storage tank and the dump tank leaks at a rate of about 1 gpm with a 3-psi head at a temperature of 200°C. Adjustments in valve operation position recommended by the valve manufacturer did not change this leak rate. Radiographs of the valve did not reveal any reason for the leakage. If the leak rate does not increase appreciably at the normal operating temperature of 500°C, it may be possible to operate without removing the valve for repairs.

6. A leak developed in a safety head flange and a small amount of sodium burned in the area around the flange. Following the fire, six of the eight studs in the flange were found broken. It is not known whether the studs broke prior to the fire and caused the leak, or if they broke during the fire. In either case, it is not clear why the bolts failed. Tests on one of the bolts which failed showed that the material remained ductile, had about the specified yield strength, and had not experienced a measurable reduction in diameter adjacent to the break which occurred where the stud entered the nut. This matter is being investigated further, and the operating temperature of this flange has been limited to 200°C during the testing which followed the leak.

Testing of the out-of-pile portion of the loop is continuing with the primary purpose of identifying problem areas so repairs and/or modifications can be made prior to the time that the loop is needed for in-pile experiments.

F. Chemical and Associated Energy Problems (Thermal)

1. Studies of Fuel Migration

Segregation of uranium and plutonium within a fast reactor fuel during its in-pile lifetime could have significant effects on the chemical and physical properties of the fuel with regard to operational safety. Axial or radial redistribution of plutonium in $(U, Pu)O_2$ fuels might result in melting of plutonium-rich areas at temperatures below that of the originally homogeneous fuel. Such an occurrence could materially affect the integrity of the cladding. Changes in physical and chemical properties may occur in regions where significant fuel redistribution has taken place. An experimental program for fast reactor ceramic fuels is under way to study the potential segregation of plutonium and uranium in a thermal gradient in order to evaluate the extent of such migration and to try to understand its

mechanism. The data will also be evaluated relative to changes in the Doppler coefficient, fuel melting point, thermal conductivity, emissivity, vapor pressure, and other significant changes that relate to reactor safety. Initial studies are being conducted with $(U, Pu)O_2$ fuels.

Development of the thermal-gradient furnace for use in the migration studies has been previously described and three preliminary experiments using UO_2-CeO_2 pellets reported (see Progress Report for September 1966, ANL-7255, p. 87). In a continuation of these preliminary studies, UO_2-CeO_2 solid-solution pellets were heated for extended periods (up to approximately 500 hr). Although these initial experiments were performed primarily to test the equipment, the possible migration of cerium in the heated pellets was also of interest. These experiments were performed by heating one end of the pellet to about 2000°C by means of radiation from a resistance-heated tungsten foil; the other end of the pellet was cooled to obtain a gradient. The system was maintained under an argon pressure of several hundred Torr during the experiments. Analyses for cerium and uranium were carried out by scanning longitudinal sections of the pellets along the centerline, using an electron microprobe analyzer. In addition, the sectioned pellets were examined ceramographically.

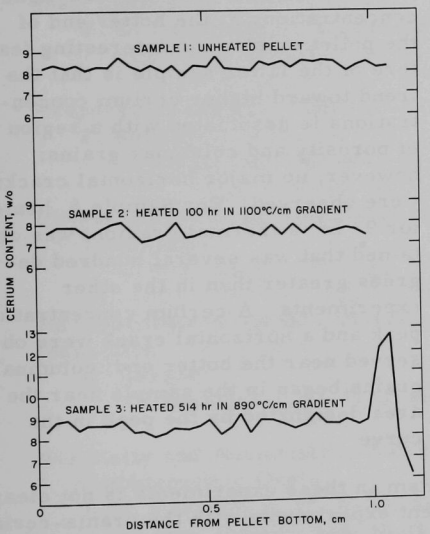

Fig. 21. Cerium Distribution in $(U, Ce)O_2$ Pellets after Heating in Thermal Gradient Furnace. [Initial Cerium Content: 8.4 w/o and Pellet Dimensions: 3/8 in. (0.95 cm) dia by 1/2 in. (1.27 cm) long.]

The Ce/U counting ratios obtained from the electron microprobe scans were used to calculate cerium and uranium concentration profiles as a function of distance from the cool end of the pellet; an example of a profile is presented in Fig. 21. It should be noted that the pellets used in these experiments were not prepared from coprecipitated oxides, but rather from a mechanical mixture. Hence, some inhomogeneity existed initially throughout each pellet's length. The degree of inhomogeneity is demonstrated in Fig. 21 by the variation in cerium composition for an unheated pellet (Sample 1). Minor composition changes (~0.5 w/o cerium) due to migration could thus be masked by this initial inhomogeneity.

A comparison of cerium concentration profiles for two heated pellets, initially containing 8.4 w/o cerium, is included in Fig. 21.

Sample 2, heated for 100 hr, showed no distinguishable migration, whereas Sample 3, heated for 514 hr, showed a maximum in cerium concentration at the hotter (upper) end of the pellet. Ceramographic examination of Sample 3 revealed a horizontal crack near the upper end, and a porous region followed by a columnar grain region in the vicinity of the cerium maximum.

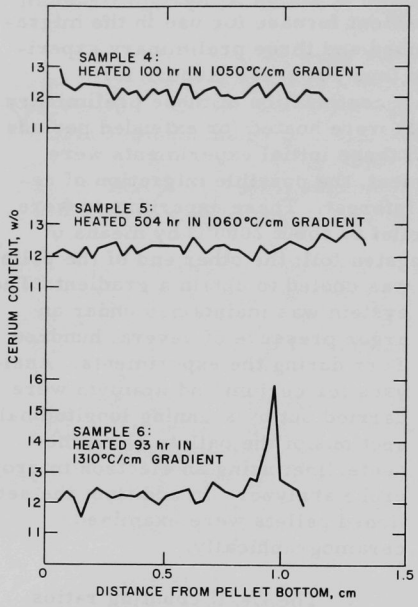

Fig. 22. Cerium Distribution in $(U,Ce)O_2$ Pellets after Heating in Thermal Gradient Furnace. [Initial Cerium Content: 12.4 w/o and Pellet Dimensions: 3/8 in. (0.95 cm) dia by 1/2 in. (1.27 cm) long.]

A comparison of cerium concentration profiles for three heated pellets, initially containing 12.4 w/o cerium, is presented in Fig. 22. For Sample 4, heated 100 hr, no migration was evident. Sample 5, heated 500 hr, exhibited no cerium concentration peaks although a trend toward higher concentrations at the hotter end of the pellet exists. An interesting feature of the latter sample is that the trend toward higher cerium concentrations is associated with a region of porosity and columnar grains; however, no major horizontal cracks were observed. For Sample 6, heated for 93 hr, a thermal gradient was obtained that was several hundred degrees greater than in the other experiments. A cerium concentration peak and a horizontal crack were observed near the hotter end; columnar grains began in the sample near the area designated by the peak in the curve.

The cerium-transport mechanism in these experiments is not clear at this time. In recent thermal-gradient experiments with the urania-ceria system, Beisswenger et al.[29] also observed ceria migration to the hotter end of pellets. They attributed this migration to thermal diffusion. In our experiments, another possible transport mechanism for migration of cerium to the hotter end of the pellet could be via pore sweeping under the influence of the impressed temperature gradient. The general occurrence of cracks, pores, and columnar grains, in association with the observed maxima for the cerium concentration, implies that such a mechanism is in operation.

Upon completion of the above preliminary experiments, the thermal-gradient furnace and auxiliary equipment were moved into a plutonium glovebox. Experiments involving the use of $(U_{0.8}Pu_{0.2})O_2$ pellets are currently under way.

[29] Beisswenger, H., Bober, M., and Schumacher, G., J. Nucl. Mater. 21, 36 (1967).

VI. PUBLICATIONS

Papers

Extraction of Plutonium from Uranium-Plutonium Alloy with Uranium Trichloride
N. R. Chellew and R. K. Steunenberg
Nucl. Appl. 3, 142-146 (March 1967)

Intermetallic Phases in the Systems of Zinc with Lanthanum, Cerium, Praseodymium, Neodymium, and Yttrium
E. Veleckis, R. V. Schablaske, I. Johnson, and H. M. Feder
Trans. Met. Soc. AIME 239, 58-63 (January 1967)

Inelastic Scattering Measurements in a Fast Reactor by the Spherical Shell Method
W. G. Davey and P. I. Amundson
Nucl. Sci. Eng. 28, 111-123 (April 1967)

Preparation and Properties of Uranium Metaphosphate, $U(PO_3)_4$
Y. Baskin
J. Inorg. Nucl. Chem. 29(2), 383-391 (February 1967)

Phase Studies in the Pseudobinary System UN-UP
Y. Baskin
J. Am. Ceram. Soc. 50, 74-76 (February 1967)

An Ultrasonic Imaging, Lamb Wave System for Reactor Fuel Plate Inspection
H. Berger
Ultrasonics 5, 39-41 (January 1967)

Elasticity and Anelasticity of Uranium Oxides at Room Temperature. I. Stoichiometric Oxide
R. J. Forlano, A. W. Allen, and R. J. Beals
J. Am. Ceram. Soc. 50, 93-96 (February 1967)

Electrical Properties and Electronic Configuration of the Monocarbide, Monophosphide, and Monosulfide of Plutonium
O. L. Kruger and J. B. Moser
J. Chem. Phys. 46, 891-900 (February 1, 1967)

Computer Program for Determining Specimen and Irradiation Capsule Component Temperature Distribution
C. F. Reinke
Intern. Symp. on Developments in Irradiation Capsule Technology, Pleasanton, California, May 3-5, 1966. USAEC Report CONF-660511, pp. 2.1.1-2.1.10

Comments on the Optimal Shutdown Control
J. J. Roberts
Nucl. Sci. Eng. 28, 156 (April 1967) Letter

A Method for Identifying and Evaluating Linear Damping Models in Beam Vibrations
M. W. Wambsganss, B. L. Boers, and G. S. Rosenberg
36th Shock and Vibration Bull., Proc. Symp., Los Angeles, October 18-20, 1966. Shock and Vibration Information Center, Naval Research Laboratory, Washington, D.C., Part 4, pp. 65-74

A Modified Cascode Preamplifier for Proportional Counters
E. F. Bennett
Nucl. Instr. Methods 48(2), 170 (1967)

Energy Dependence of $\bar{\nu}_p$ for Neutron-Induced Fission of U^{235} below 1.0 MeV
J. W. Meadows and J. F. Whalen
J. Nucl. Energy 21, 157-170 (February 1967)

On the Synthesis of Space Dependent Transfer Functions
C. K. Sanathanan
IEEE Trans. AC-11(4), 724-729 (October 1966)

The Application of a Hybrid Computer to the Analysis of Transient Phenomena in a Fast Reactor Core
C. K. Sanathanan, J. C. Carter, L. T. Bryant, and L. W. Amiot
Nucl. Sci. Eng. 28, 82-92 (April 1967)

ANL Reports

ANL-7212 AN EXPERIMENTAL BOILING-LIQUID-METAL FAST REACTOR
R. H. Armstrong and J. C. Carter

ANL-7229 CONSTRUCTION OF A GLOVEBOX THERMOGRAVIMETRIC ANALYSIS APPARATUS: LANGMUIR AND KNUDSEN EXPERIMENTS ON THE EVAPORATION OF Gd_2O_3 FROM 2140 TO 2600°K
Donald R. Messier

ANL-7262 TESTS OF COMMUTATING BRUSHES FOR USE IN D.C. MOTORS OPERATING IN A DRY ARGON ATMOSPHERE
M. A. Slawecki, G. J. Bernstein, and L. F. Coleman

ANL-7263 ON THE STEADY-STATE THERMAL STRESSES IN CYLINDRICAL FUEL PINS DUE TO AXIAL VARIATIONS IN THEIR HEAT-GENERATION RATE
Richard A. Valentin

ANL-7269 COMPARISON AND ANALYSIS OF THEORETICAL DOPPLER-COEFFICIENT RESULTS FOR FAST REACTORS
R. N. Hwang and K. Ott